INSTITUTO SUPERIOR DE ENGENHARIA DO PORTO
MESTRADO EM ENGENHARIA ELECTROTÉCNICA E DE COMPUTADORES

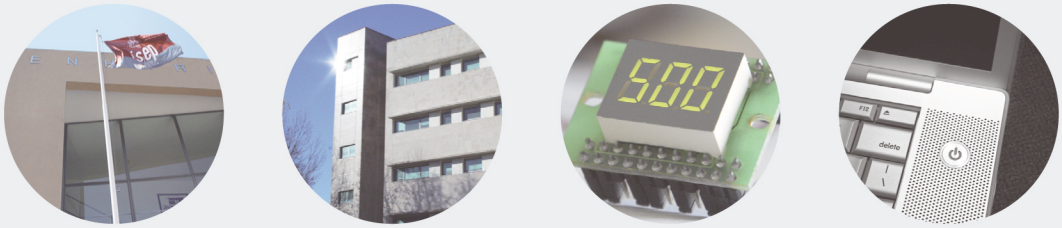

Towards the industrialized AGVS with stringent safety requirements for the cooperative setting

PEDRO ALEXANDRE AFONSO NETO
julho de 2022

POLITÉCNICO
DO PORTO

INSTITUTO SUPERIOR DE ENGENHARIA DO PORTO
MESTRADO EM ENGENHARIA ELECTROTÉCNICA E DE COMPUTADORES

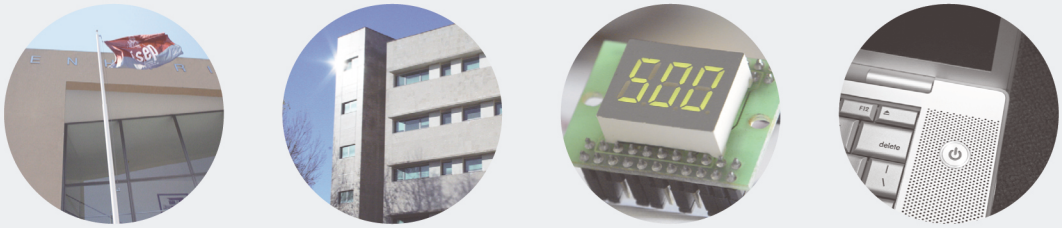

Towards the industrialized AGVS with stringent safety requirements for the cooperative setting

PEDRO ALEXANDRE AFONSO NETO
Maio de 2022

POLITÉCNICO
DO PORTO

Politécnico do Porto
Instituto Superior de Engenharia do Porto

Towards the industrialized AGVS with stringent safety requirements for the cooperative setting

Pedro Alexandre Afonso Neto

Master in Electrical and Computer Engineering
Specialization Area of Automation and Systems

Departamento de Engenharia Eletrotécnica
Instituto Superior de Engenharia do Porto

July, 2022

This dissertation partially satisfies the requirements of the Thesis/Dissertation course of the Master in Electrical and Computer Engineering, Specialization Area of Automation and Systems.

Candidate: Pedro Alexandre Afonso Neto, No. 1150386,
1150386@isep.ipp.pt

Scientific Guidance: Manuel Fernando dos Santos Silva, mss@isep.ipp.pt

Company: Gislotica - Mechanical Solutions, Lda.

Advisor: Humberto Joaquim Ramos Mendonça,
humberto.ramos@gislotica.pt

Departamento de Engenharia Eletrotécnica
Instituto Superior de Engenharia do Porto
Rua Dr. António Bernardino de Almeida, 431, 4200–072 Porto

July, 2022

To my grandparents António and Inocência, and to my dad Paquito, until that promised sunny day.

Abstract

As efficiency and flexibility dictate the sustainability of the manufacturing industry, evermore, automation is becoming a requirement rather than a benefit. The Autonomous Guided Vehicle (AGV) proposes a flexible and scalable approach for automating the intralogistics of a manufacturing process. However, the solution entails safety concerns resulting from the shared space between people and the machine. The cooperative setting requires stringent protective measures to enable the AGV for industrial applications.

With the intent to introduce AGV in their applications, Gislotica prompted the subject of this thesis: research the safety challenges for industrial AGV applications; and, design and validate an AGV safety system for a creel application.

Following established standards and regulatory AGV requirements, the project sought to devise the methodology to achieve functional safety in AGV applications. Preventing collisions with personnel in the cooperative setting is arguably the most critical role of these safety systems. Accordingly, the personnel detection and drive-based safety functions were integrated under the safety system to provide personnel protection while not compromising the natural navigation system. Notably, for devising the protection fields that project the braking space of the AGV, the thesis relied on the simulation of the modelled vehicle braking kinematics.

The resulting safety system, designed and implemented for a creel application, was able to validate the methodology and raise findings regarding the characteristics of an AGV safety system. A major takeaway from this thesis is the need to analyse the full range of vehicle kinematics when devising the personnel detection system. Moreover, based on the thesis findings, it was possible to identify shortcomings with the current standardization and alternative methodology for devising personnel detection systems.

The thesis was able to contribute to the knowledge base and available methodology in the context of AGV safety with a case study set in a real industrial application.

Keywords: Industrial AGVS, Safety systems, Personnel detection system, Drive-based functional safety.

Resumo

A automação apresenta cada vez mais uma necessidade e não apenas uma vantagem, onde a eficiência e produtividade determinam a sustentabilidade da industria fabril. O *Autonomous Guided Vehicle* (AGV) apresenta uma abordagem flexível e modular para automatizar sistemas intralogísticos na Indústria. No entanto, esta solução implica questões de segurança consequentes do espaço partilhado entre pessoas e a máquina. O ambiente de produção cooperativo requer medidas de proteção robustas de forma a viabilizar o AGV para aplicações industriais.

Com o propósito de introduzir o AGV nas suas soluções, a Gislótica propôs a tese: investigar os desafios para a segurança dos AGV em ambiente industrial; e, desenvolver e validar um sistema de segurança para um AGV de um sistema *creel*.

De acordo com as normas e leis que especificam os AGV, este projeto procurou desenvolver a metodologia que garanta o funcionamento seguro em aplicações de AGV. Pode-se afirmar que a prevenir colisões com os trabalhadores no ambiente cooperativo é o principal papel da segurança num AGV. Com base nisso, a segurança do AGV integra um sistema de deteção de pessoas com funções de segurança de *drive*, de forma a garantir a proteção de pessoas no ambiente, considerando a viabilidade do sistema de navegação natural. Em particular, para definir os campos de proteção que cobrem o espaço de travagem do AGV, a tese recorreu à simulação do modelo cinemático do veículo em travagem.

O sistema de segurança final, dimensionado e implementado para uma solução *creel*, permitiu validar a metodologia proposta e caraterizar as particularidades de um sistema de segurança de um AGV. Uma das principais conclusões desta tese é a necessidade de avaliar todas as possíveis trajetórias do veículo para o correto dimensionamento do sistema de deteção de pessoas. Ainda, com base nos resultados da tese, foram identificadas algumas limitações com as normas disponíveis e com a metodologia pré-existente para implementar um sistema de deteção de pessoas.

Esta tese aprofundou conhecimentos e desenvolveu novas metodologias no ramo da segurança dos AGV, com base em um caso prático de uma aplicação industrial.

Palavras-Chave: AGVS industrial, Sistemas de segurança, Sistema de deteção de pessoas, Segurança baseada em *drives*

Ancerradeiro

L'outomaçon trai cada beç mais ũa necidade i nun solo un porbeito, adonde la eificéncia i la pordutebidade ban a detreminar la sustentabelidade de l'andústria fabril. L *Autonomous Guided Vehicle* (AGV) apersenta ũa abordaige flexible i modular para outomatizar ls sistemas antralogísticos de l'andústria. Por outra bia, este remédio alhebanta preguntas de siguránçia resultantes de l spácio que las pessonas i las máquinas partilhan. L'ambiente de porduçon coperatiba percisa de medidas de porteçon fuortes de modo a biabelizar l AGV para aplicaçones andustriales.

Cun l perpósito de meter l AGV ne ls sous perdutos, ne ls sous perdutos, Gislótica porpuso la tese: Ambestigar ls zafius ne ls sistemas de siguránçia an aplicaçones andustriales; I, zambolber i balidar un sistema de siguránçia dũa aplicaçon creel cun *creel* cun AGV.

Cunsante seia cun las normas i leis que specifícan ls AGV, este porjeto precurou zambolber la metodologie que garanta l funcionamente siguro de las aplicaçones AGV. Puode-se dezir que la prebençon de colisones cun ls trabalhadores ne l ambiente coperatibo ye l percipal papel de la siguránçia nun AGV. Cun l studo nisso, la siguránçia de l AGV antegra un sistema de deteçon de pessonas cun funçones de siguránçia de las *drives*, de maneira a garantir la proteçon de pessonas ne l spácio, cunsiderando la possiblidade de l sistema de nabegaçon natural. An particular, para ajustar ls campos de proteçon que ban a cubrir ls spácio de trabaige de l AGV, l studo simulou l modelo cinemático de l beiclo quando frena.

L sistema de siguránçia resultante, purparado i amplementado para ũa aplicaçon *creel*, fizo balidar la metodologie perpuosta i caraterizar ls calatrizes de ls sistema de seguránçia dun AGV. Ũa de las percipales cunclusones deste studo, ye la necessidade de abaluar todos ls possibles caminos de l beículo para poder pensar bien l sistema de deteçon de pessonas. cumo punto de salida ne ls resultados de l studo, fúrun ancuntradas alguas fraquezas cun las normas i las metodologies çponibles para poner ls sistemas de deteçon de pessonas.

Esta tese aperfundou l coincimiento i zambolbiu nuobas metodologies ne l ramo de siguránçia de ls AGV, cun studo nun causo prático dũa aplicaçon andustrial.

Palabras-Chabe: AGVS andustriales, Sistemas de siguránçia, Sistemas de deteçon de pessonas, Siguránçia baseada an *drives*

Contents

List of Figures

List of Tables

List of Acronyms

2NC	Dual-Channel Normally-Closed
AC	Alternating Current
AGV	Autonomous Guided Vehicle
AGVS	Autonomous Guided Vehicle System
CCF	Common Cause Failure
DC	Direct Current
DCO	Diagnostic Coverage
EC	European Commission
EFI-Pro	Enhanced Function Interface Protocol
ESPE	Electro-Sensitive Protective Equipment
Ethernet/IP	EtherNet Industrial Protocol
EU	European Union
FMS	Flexible Manufacturing System
GNSS	Global Navigation Satellite System
HTL	High Threshold Logic
ICC	Instantaneous Center of Curvature
IPC	Industrial Personal Computer
ISO	International Organization for Standardization
LiDAR	Light Detection and Ranging
LPR	Local Positioning Radar
MHS	Material Handling System
$MTTF_d$	Mean Time To dangerous Failure

PFH_d	Probability of a dangerous Failure per Hour
PL	Performance Level
PL_r	PL requirement
PLC	Programmable Logic Controller
PMSM	Permanent Magnet Synchronous Motor
PSPE	Pressure-Sensitive Protective Equipment
RPM	Revolutions per Minute
SBC	Safe Brake Control
SDI	Safe Direction
SIL	Safety Integrity Level
SLAM	Simultaneous Localisation and Mapping
SLS	Safely Limited Speed
SMS	Safe Maximum Speed
SS0	Safe Stop 0
SS1	Safe Stop 1
SS2	Safe Stop 2
SSM	Safe Speed Monitor
STO	Safe Torque Off
TTL	Transistor-Transistor Logic

Chapter 1

Introduction

1.1 Background

In the face of an ever-growing need for automation and digitalisation, driven by shortening product life cycles and increasing market competition, industries seek to increase productivity, flexibility and efficiency of their operations. The introduction of autonomous and "smart" machines in manufacturing provides the ability to collect and process data to be used in the decision making and control of the industrial process, leading to the production of higher quality goods at a lower cost [1].

Improving efficiency in the manufacturing process is a cost-effective way to improve competitiveness, which may determine the economic sustainability of a company [2]. Moreover, a campaign by the United Nations prompted the Industry sector to "audit the energy use and resource efficiency of their operations to identify cost-effective high-impact reductions", among the major long-term measures to fight climate change [3, 4]. The highly competitive market and the growing regulation to address climate change pressure the Industry to adopt the autonomous paradigm throughout the entire production process.

The intralogistics that drive a manufacturing process, namely the transport and handling of goods, require a flexible and reactive system to meet the dynamic and unpredictable production demand [5]. The Autonomous Guided Vehicle System (AGVS), founded on "unmanned" vehicles that navigate the manufacturing layout hauling goods according to production needs, emerges as the key solution for tackling modern logistics [6]. AGVS provide a flexible and scalable solution suited for large

area layouts and volatile production applications while requiring minimal support infrastructure [1].

Although the AGVS is an effective tool to improve the efficiency of intralogistics, challenges remain when deploying the solution in the industrial setting. In particular, as the Industry matures towards a standardized approach to Autonomous Guided Vehicle (AGV) safety, the complexity of control and associated safety system may discourage industries from adopting the solution [7, 8]. The cooperative nature of AGVS applications, where the autonomous machine must coexist with humans, raises dangerous conditions for working personnel. Due to operating at high speeds and exerting strong forces, autonomous machines and robots are commonly constricted with safety dividers to ensure the safety of any passerby. However, AGVS tasks involve operating in the unrestricted presence of personnel, presenting a persistent hazard that cannot be contained behind physical barriers. Hence, integrating AGVS in intralogistics systems entails stringent requirements to ensure a safe operation to personnel, raising the need for a complex safety system [9]. Nevertheless, studies reveal that the integration of safety measures in industrial machines reduce costs in the long run [10], which, in addition to the efficiency brought by AGVS to the Industry, strongly justifies the additional engineering efforts.

1.2 Motivation

The benefits of AGVS to intralogistics and the importance of the technology in the evolving Industry greatly encourage further research of the remaining challenges that hinder the adoption of these systems in industrial applications.

1.2.1 AGVS Market Analysis

Emerging technologies, namely Artificial Intelligence, the Internet of Things and Robotics, bringing new challenges to safety legislation, prompted the European Commission (EC) to perform, in april 2021, an impact assessment of the new advents in the Industry [11]. In particular, the study reviewed the emergence of self-driving robots. A market research commissioned by the study, forecasting the mobile robotics presence in the Industry, predicted that the market will endure a continuous growth throughout the next 5 years (until 2026), at an expected rate ranging between 12.9% and 21.5% per year. Another 2018 EC survey regarding enterprises with at least 10 employees in the European Union (EU) recorded that 22% had introduced mobile robots for the transportation of people and goods [12]. Moreover, an independent study published in january 2021 [13], surveying over 600 enterprises involved in the global AGV market, claims the figures of €2 billion in sales with 60,000 mobile robots shipped in 2020. Furthermore, the study projects

a yearly growth of 35%, reaching over €10 billion market value and 1.5 million installed units by 2026. The major driver of this development was identified as the growth in e-commerce and the ensuing demand for warehouse automation.

The precise figures of the market volume and adoption rate of self-driving vehicles by the Industry are, however, reportedly not attainable due to it being a rapidly evolving market [12].

1.2.2 Thesis Context

Gislotica Mechanical Solutions Lda. is an engineering company focused on the design, fabrication and automation of machines for industrial manufacturing and specialises in integrated solutions for the tyre manufacturing Industry [14]. Following the company's values of innovation, creativity and competitiveness, Gislotica aims to introduce the AGVS to its product line with the goal of improving the flexibility and autonomy of its solutions.

Prior to this thesis, the company developed a prototype [15] to flesh out an AGV architecture regarding their mechanical, power and control designs, with an emphasis on defining the navigation approach. Accordingly, a natural navigation based AGVS was developed and validated.

Among the automation solutions by Gislotica are logistics systems for the transportation, handling and manipulation of tyres and materials used throughout the manufacturing process of tyres. One of the company's products is the automated creel room, a crucial system for automating and expediting the manufacturing of tyre beads.

Following the functional prototype, the remaining challenge of Gislotica for introducing AGVS in its solutions is the industrialisation of the machine. In order to integrate industrial applications, the AGVS must achieve the required safety levels and oblige by decreed safety norms. In the light of this problem, Gislotica prompted the subject of this thesis: the integration of an AGVS solution for the supply logistics of a creel system.

1.3 Goals and Requirements

The overall purpose of this thesis is to investigate and address the challenges set to the industrialisation of AGVS application. In particular, the main objective is to identify and examine an approach to solve the cooperative safety concerns of AGVS applications in an effort towards enabling the technology for the industrial setting.

The established problem is to be addressed with the implementation of an AGVS so as to both evaluate the proposed approach and avoid disregarding its feasibility and effectiveness. The implementation must then focus on the design, integration and validation of the AGV safety system in the context of a creel system application.

The system must accomplish a reliable AGV operation that ensures personnel safety and fully adheres to the existing regulations without compromising the flexibility and feasibility of the AGVS concept.

Beforehand, the project first requires a review of the safety concepts and challenges prevalent in AGV applications as well as the standing regulation and standards that define their safety systems to define the approach to be employed in this thesis. The AGVS implementation mission, as stated, is focused on the design and implementation of the safety system, highlighting the selection and integration of the protection measures that will fulfil the identified requirements. However, safety cannot be addressed independently from the other AGVS elements, particularly from the navigation system [16]. Therefore, the implementation will encompass the integration of the navigation solution and powertrain modules, focusing on the functionality that impacts the safety system.

Ultimately, this thesis seeks to identify, implement and validate an AGVS safety system that will enable the autonomous machine for the industrial setting.

1.4 Document Structure

This dissertation is composed of 7 chapters, including the current one. The subsequent chapters are organised as follows:

Chapter 2 overviews the AGVS concept and its enabling technologies, as well as the impact of these systems in the Industrial context;

Chapter 3 surveys the safety concepts for overall industrial machines and the methodology specific to AGVS, followed by a review of the current regulation and standardization to consider in the design of the safety system;

Chapter 4 introduces the targeted industrial application, presents the ensuing AGVS design and outlines the approach for the implementation of the protection measures of the safety system;

Chapter 5 details the full undergone implementation of the AGVS in the context of this thesis. The chapter describes the integration and configuration of the protection measures for the safety system as well as the integration of the safety pertinent subsystems, namely the navigation and powertrain systems;

Chapter 6 analyses the resulting implementation of the AGVS so as to assess the validity and effectiveness of the devised approach. In addition, comparing to the thesis results, the chapter evaluates alternative approaches and standardized requirements of personnel detection systems;

The dissertation concludes with Chapter 7, which summarises the project and draws conclusions on the thesis, assessing the attained outcome and how it realises the set thesis goals. Furthermore, the chapter raises future work that shares a goal

with this thesis, namely regarding the remnant safety challenges that the AGVS face to enable industrial applications.

Chapter 2

The Autonomous Guided Vehicle

This chapter aims to introduce the underlying concept of the AGV from an Industry perspective, seeking further automation by entrusting the technology. Moreover, here are presented the commonplace applications targeting automation via AGVS, as well as the different technologies and solutions driving these systems, as have been proposed and deployed by both Industry and scientific community.

2.1 The AGVS Concept for Automation

The Autonomous Guided Vehicle System (AGVS) concept enables the Industry to reach towards a full automation and maximized efficiency of the production process. The technology is built upon one or more "driverless" vehicles, the Autonomous Guided Vehicle (AGV), and is largely employed in intralogistics applications. These encompass the roles of managing, executing and simplifying the transport, as well as handling logistics of materials and goods, both directly in manufacturing floor and warehouses [7].

The classic conveyor belts, which often share the automation target with AGVS, entail high costs in infrastructure and shop floor space, as well as additional handling support so as to meet the same automation level. The AGVS proposes not

only a less expensive approach, in terms of money, time and space, derived from installation and maintenance, but also a more flexible one when compared to the previous technology [1]. As goods flow paths can easily be reconfigured, and in some navigation approaches, without any infrastructure changes, the solution presents an increase in flexibility over fixed conveyors for the Material Handling System (MHS) of a production line [17].

Opting for an AGVS implementation results in an MHS with improved performance and reliability, and consequently, competitiveness [18]. Market volatility driven by shortening product life cycles, technological advancements and demand for high-quality products at a lower cost, highlights the paramount importance of flexibility on a production line. To respond to the challenge, the Industry then introduced the Flexible Manufacturing System (FMS) concept, consisting of semi-independent manufacturing cells connected by an automated MHS and storage, highly reliant on AGV. The AGVS, now decisive in certain products profitability, provides the necessary adaptability required by FMS to address the dynamic and unpredictable changes in production demand throughout an entire product line [5].

Furthermore, as well as providing a flexible automation solution for intralogistics, the AGVS establishes an increased safety in the process. The safety improvements resulting from AGVS, one of the main drives for automation, are associated with reducing operators involvement, as well as the increased determinism (with consistent and predictable behaviour) and accuracy when the process is computerized [19, 20]. Additionally, collaboration capabilities are required, as the AGV often must be able to interact or at least coexist with human operators in a shared work environment.

Personnel safety is strictly regulated and enforced by lawmakers, via standards and norms, in order to minimize potential harm to workers. These policies involve regulations for the AGV to include added sensing functionalities to ensure collision avoidance with people, environment elements or other AGV [21]. These commonly entail scanners to survey the environment for clearance to operate safely and are often combined with protection zoning to regulate the vehicle speed and preserve safety [16, 22, 23].

2.1.1 The Advent of the Modern AGV

The invention of the AGV is widely credited to Arthur Barrett when, in 1954, the co-founder of Barrett-Cravens Co. (Illinois, USA) modified a trailer towing tractor to autonomously drive following a guiding strip embedded in the floor. The vehicle, trademarked as “GUIDE-O-MATIC”, would detect the electromagnetic field induced on the conductive wire, allowing the tractor to maintain alignment with the strip and transport the connected trailers goods alongside a structured route. At selected locations along the path, each emitting distinct patterns coded with magnets would

signal the AGVS the relevant service stops, hereby automating the transport role of the process.

The safety system on this AGV was limited to a passive safety implementation, relying on bumpers installed on the tractors. Upon collision with an obstacle, the bumpers would detect the incident and signal the vehicle controller to stop, hereby minimizing further damages. However, this approach did not fully safeguard any bystander's integrity [24, 25, 26].

Although not up to today's safety standards, this unrefined first implementation was able to prove the feasibility of an AGVS and showcased the intended benefits of applying the technology. As a result, the AGVS concept spread across industries during the following decades, relying on a similar path guided navigation solution.

The first AGV were, however, overall impractical and expensive, as, at the time, the attainable "control systems were bulky and possessed a limiting load capacity" [27]. However, the advent of microelectronics allowed for further compact and improved controls, as well as increased functional robustness, with more reliable vehicles for the applications. With this breakthrough, alongside the maturing of navigation methods, the AGVS was able to meet the flexibility, reliability and affordability demanded by the Industry in order to drive their intralogistics systems [28].

2.2 Current Applications and Technologies

The repetitive and predictable operations, commonly targeted by automation, are, likewise, the target of an AGVS implementation. The loading and unloading of goods is a uniform and recurrent process and inherent to most industrial manufacturing. From providing raw materials and supplies commissioned to workstations, transferring work-in-process goods between them, down to transporting final products to be shipped, opportune scenarios are presented to AGV.

In addition to cargo, an AGVS conveys information, another key good for the manufacturing process. When reporting the inventory and material flow, throughput times and availability of workstations in real-time, the technology provides a critical quality service when managing a production system. With the acquired data, the management system, in turn, employs the AGVS to regulate stock levels of materials and supplies, by streamlining the balancing of assembly lines with supply priorities, in order to optimize lot sizes and production capacity [6].

2.2.1 Popular AGV Designs

The aforementioned intralogistics roles which employ AGVS are present across different operations of the broad manufacturing process. These applications have divergent requirements, namely the distance and condition specifications to transport

the goods, as well as load weight, shape and handling considerations. AGV manufacturers were therefore driven to specialize the autonomous solution into different AGV types. Not being standardized, the names of the different design types vary across both Industry and scientific communities, but, based on their shared features, fall into the following categories ([21, 28, 29]):

- The Forklift AGV, designed to move fairly high loads, opportunely inherits the classical forklift trucks tasks. Taking over the handling of "palletized" objects, already standardized and prevalent in intralogistics, this AGV facilitates the introduction of the vehicle in conventional manufacturing processes. Moreover, as forklifts present a common source of the registered severe accidents in factories, automating the operation directly improves safety levels in the manufacturing process [30, 31].

- The Tow, Train or a Tugger AGV consists of a "driverless" towing vehicle, capable of pulling along a train of carts, often bearing an automatic hitch to automate the coupling and decoupling of each trailer in function of the process. This model stands out to applications which involve large batches to be transported over long distances, although with compromised mobility, due to the train length. The reduction of the transit time by transporting multiple carts can be further improved in the loading and unloading processes. To optimize these procedures, train carts can be equipped with powered roller conveyors for a simultaneous material transfer (horizontal transport) [32, 33].

- The Unit Load or Platform AGV, with a compact minimalist build, provides a practical surface base above the vehicle structure, compatible with diverse load formats. This design provides increased manoeuvrability around a restrictive factory floor and through confined spaces, as well as being less intrusive in the process. This AGV format supports pallets, much like the Forklift variant, however offering higher payload compatibility, as it can transport different box or carrier shapes that better suit the application. Furthermore, the base can be adapted to hold specific items or tools, being able to directly intervene in assembly stages, where the transporting goods are being processed while in the vehicle, often contextually named as the Assembly AGV [16]. The loading process can also be automated for these AGV types, and such is the case of the Underride AGV. These vehicles position themselves under the load to be collected and, via a lifting base, may autonomously collect and unload the payload [34].

2.2.2 Navigation Technology Systems

The AGV, by definition, has self orienting capabilities without any direct control by an operator. The guidance aspect is to be provided by the interaction with the

surrounding environment through the means of a closed-loop system anchored on sensor enabling instruments. The employed navigation technology, a centrepiece of an AGVS, is highly dependant on the application needs and the set environment. AGVS applications require varying degrees of flexibility, robustness and infrastructure. Consequently, presented below, different approaches have been proposed to address the AGVS navigation challenge [28].

Fixed Path Navigation

On a Physical Guideline based system, the AGV strictly navigates the environment along fixed guidelines, offering reduced flexibility in exchange for higher robustness when compared with other navigation approaches.

The physical properties of magnetic fields can be leveraged to create a guiding path for an AGVS. In a passively inductive guidance track, the vehicle makes use of magnetic field sensors, capable of detecting the magnetic strips that constitute the track, which, by sensing the magnetic field fluctuation, the AGV is able to steer and follow the defined path [35]. With a similar principle, relying on an actively inductive guidance track, the vehicle follows electrically conducting wires which mark a path. The Alternating Current (AC), present in the wire, will induce a current on two sensing coils mounted on opposite sides of the AGV angled at the floor wire. The current differential measured between the two sensors is proportional to the deviation from the path, which is used to maintain the vehicle on course [16].

Alternatively, relying on optical guidance, the AGV follows a coloured strip, with a high colour contrast against the floor for improved reading accuracy by optical sensors. Sulaiman Sabikan, *et. al.*, in an incremental approach in [36], proposed an optical guidance system which relies on an image processing algorithm for the detection of track lines and motion symbols. The system, based on a camera sensor mounted under the vehicle, is capable of detecting the edge of the strip, allowing the vehicle steering to follow a line, as well as symbols to aid in the decision making of the AGV navigation.

Anchoring Points Navigation

The Anchored or inertial navigation is based on the principle of dead reckoning navigation, also known as odometry. This method estimates the current position by relying on previously acquired values for reference and, subsequently, updates the vehicle position using the measured value of the wheel angle, speed and acceleration. The reference values are based on an anchor setup, and, to further improve the precision of the dead reckoning navigation, the actuated inertial parameters can be compared with the measurements of a gyroscopic compass (inertial sensor). The anchor system disposition can be based on a grid setup, whose points are set

a distance apart defined by the AGV specifications, or, alternatively, the system navigates through a series of points that connect through a virtual line [16].

GNSS and LPR

Satellite navigation technology, used for localization in various applications, may also be employed by an AGV navigation system. In large areas, the usage of physical guidelines or anchor markers becomes increasingly expensive and unreliable as means for navigation. For these scenarios, a Global Navigation Satellite System (GNSS) solution, otherwise considered too expensive and impractical, arises as an adequate alternative. However, the approach is restricted for usage in outdoor areas with an unobstructed path to the satellites. For indoor usage, the Local Positioning Radar (LPR) can be deployed for an AGVS navigation method. Deriving from the GNSS principle, the LPR relies on fixed radio beacons to attain the vehicle position via trilateration, based on the measured time the signal takes from the AGV mounted antenna to the strategically positioned beacons. An LPR implementation, although inexpensive compared to the GNSS, provides a less practical positioning system while also requiring an unobstructed area to function properly. Therefore, the beacons must be carefully positioned to guarantee full coverage for the operation. Hence, this approach might not be feasible for applications set in cluttered environments [28].

Artificial Landmarks

By using artificial landmarks installed in the environment, an AGVS is able to determine its position in the workspace and navigate the environment.

An artificial laser navigation system relies on reflective markers, which function as fixed landmarks known to the AGVS. In typical applications, the markers utilize retro-reflecting foils and are installed high above the operators' height to ensure a constant clear line of sight to a laser mounted on the vehicle. The reflected laser beams, based on the time of flight principle, allow an AGVS to derive its absolute position from the known coordinates of each reflector [21], similarly to the LPR approach. This approach, however, given the lasers are required to be mounted high, involves adapting both the environment and AGV, leading to added infrastructure cost, as well as a decrease in flexibility.

Furthermore, artificial landmarks can enable AGV applications without the need for absolute localization functionality. In [37], based on a vision-guided navigation system, the AGVS relied on different coloured symbols, as known landmarks, in order to acquire its relative position. With a mounted webcam, the AGVS image processing algorithm was able to discern between the symbols and navigate the vehicle towards the desired landmark.

Natural Navigation

Natural navigation, or contour navigation, makes use of the natural features of the environment, having the AGV recognize the built-in walls, pillars and any static elements to serve as landmarks for localization. Requiring no changes to the environment, this solution provides the highest flexibility to an AGVS of the presented approaches, and, similarly to the artificial landmarks, natural navigation can rely on either laser or vision-based navigation, provided they possess depth perception, with technologies such as Light Detection and Ranging (LiDAR) or 3D vision.

Instead of a guideline, anchors or artificial landmarks for localization, natural navigation relies on a map of the environment to pinpoint the encountered landmarks during navigation. Being able to recognize the natural landmarks, and based on the measured relative distance from the vehicle to each of them, the AGV is then able the locate itself in the environment, and enable autonomous navigation.

A static map of the environment, however, presents a challenge to the precision and reliability of the natural navigation system. Unexpected elements in the environment can result in miss identified landmarks and localization errors, compromising the navigation system. In dynamic environments such as warehouses or the factory floor, the flow of materials, boxes, and even operators, often prompts changes to the perceived space by the AGV.

A solution to natural navigation set in dynamic layouts is to constantly update the environment map. The approach requires the AGVS to continuously update the map, including features positions, based on the instant localization coordinates of the AGV. This presents one fundamental challenge in mobile robotics, as localization is derived from the known map, and, in turn, the map is derived from the localization. This origin paradox is known as the Simultaneous Localisation and Mapping (SLAM) problem. A mobile robot "set at an unknown location in an unmapped environment" reflects the SLAM problem to which different solutions have already been proposed [38].

2.3 Navigation and Safety

As argued by Günter U. in [16], navigation cannot be addressed separately from safety when designing an AGVS. The safety system and the guidance system together constitute central functions of an AGVS. The AGV cannot solely rely on localization or guidance elements, as collision avoidance is an essential feature for the vehicle to navigate the environment as well as for ensuring personnel safety. This is a functionality which only a properly designed safety system can provide to an AGVS, making safety not a secondary component for emergencies and, instead, setting the safety system as an active element in the navigation of an AGV.

Given the focus of the project and the argued importance of the safety system of an AGVS, the concept will be introduced in further detail in the following chapter.

2.4 Conclusions

The objective of this chapter was to provide the context for a better comprehension of the developed work. Towards this purpose, this chapter presented the concept of AGVS and the driving reasons behind the prosperity of this technology in industrial manufacturing. Furthermore, different AGV designs and navigation technologies were introduced to showcase the current state of the AGVS in the Industry, as well as to introduce some of the underlying concepts of the developed AGV.

Chapter 3

AGV Navigation Safety

The current chapter clarifies the safety concepts that enable an AGVS for the industrial setting. Furthermore, the methodology for attaining safe machinery is presented as is standardized for the Industry.

3.1 Machine Safety

In the industrial manufacturing environment, the increasing need for flexible machines, capable of autonomously adapting to changes in production, prompts an increase in human-machine interaction where a permanent physical separation between them is no longer feasible. Both must now coexist in a shared environment, whether for maintenance tasks or, in the case of mobile machines, on shared pathways. Given the inherent characteristics of machines, this interaction presents hazardous risks to personnel. Therefore, the increased machine flexibility results in evermore stringent safety requirements, with the goal to minimize risks and severity of accidents [9].

3.1.1 Safety Regulation

Operators and personnel must be able to rely on the safety of a machine, and, in order to guarantee safety levels in industrial manufacturing, governments impose mandatory standards. The EU introduced the Machinery Directive in 2006, with the essential safety and health requirements, which manufacturers in member states

are obliged to comply with when designing their machines. The directive instructs the manufacturer to firstly perform a risk assessment on the machine, identifying all possible hazards and reviewing their severity, followed by addressing the respective risks. Based on the assessment, the machine manufacturer will eliminate hazards whenever possible and minimize the remaining risks with appropriate protection measures. As a last resort, for unavoidable and exposed hazards, machines must employ warning systems and guidelines for users [39].

Further Advantages of Safe Machinery

The added design and manufacturing efforts by the required safety systems do not, however, imply an added cost to the final product. A 2018 report by the EC evaluated the performance of the Machinery Directive, between 2008 and 2013, on the EU market. The study results, addressing the entirety of the EU market, point to estimated cost savings of €401 million per year, conclusively outweighing the €136 million per year of costs incurred as a result of the directive. These estimated savings are forecast direct costs alone, which results from accidents and injuries avoided. Further savings occur from indirect costs as the prevention of hazards reduces equipment loss and production downtime, thereby increasing process efficiency [10].

The EU machinery directive requirements are universal and nonspecific on achieving the targeted safety in order to support different approaches and solutions, nevertheless ensuring machine safety is met. Standards and norms, created in agreement between stakeholders (including manufacturers, governments and end-users), harmonize the machinery directive requirements. They specify in further detail the requirements for the different machine elements, functions and technologies in order to comply with the broader directive. In addition, using conventional requirements avoids redundant development efforts.

By following the set standards, a machine is considered to provide the required safety levels, as well as legal protection for both manufacturer and user [40].

3.1.2 Safety in Control Systems

For the design and integration of a safety compliant machine, a conventional risk assessment system is necessary. In the safety of control systems, the Performance Level (PL), defined by the International Organization for Standardization (ISO) in the EN ISO 13849-1 norm, is a standardized metric to measure and evaluate the effective reliability and performance of safety-related elements.[1]

[1]The Safety Integrity Level (SIL) convention, defined in norm EN 62061, is also commonly used for measuring the safety level. The PL and SIL standards produce analogous results, given both categorize safety levels based on the Probability of a dangerous Failure per Hour (PFH_d) achieved. Some safety elements, including several of the components used in the project of this thesis, are

The evaluation is applicable to describe a complete functionality, as well as individual components, and provides a letter rating classification. The rating ranges from PL a to PL e, with the latter representing the highest level of reliability based on the assessed Probability of a dangerous Failure per Hour (PFH_d), as presented in Table 3.1.

Table 3.1: Performance Level according to the PFH_d [42].

PL	Probability of dangerous failures per hour
a	$10^{-4} \geq PFH_d \geq 10^{-5}$
b	$1 \times 10^{-5} \geq PFH_d \geq 3 \times 10^{-6}$
c	$3 \times 10^{-6} \geq PFH_d \geq 1 \times 10^{-6}$
d	$10^{-6} \geq PFH_d \geq 10^{-7}$
e	$10^{-7} \geq PFH_d \geq 10^{-8}$

Safety System Development Process

Following the identification of the intrinsic hazards of an envisaged machine, each must be assessed so as to establish the protective measures that mitigate the associated risks [43].

In the context of safety systems, the protective measures are referred to as **safety functions**. Via the implemented safety functions, the machine will then achieve **functional safety**, meaning a safe machine operation compliant with the directive.

The risk assessment phase must then determine the necessary reliability, the PL requirement (PL_r) for the safety functions. To estimate the PL_r, the standard follows a risk assessment chart (Figure 3.1) that factors in: (1) the severity of the injury; (2) the frequency and duration of the hazard exposure; (3) and the possibility to avoid the accident or mitigate the damage [41, 42].

Each PL_r class then also translates to a PFH_d range of Table 3.1. For instance, to achieve a PL *d* classification, the system must guarantee a minimum PFH_d of 10^{-6} (one dangerous failure in one million hours). In other words, at most, the PL *d* average expectancy of a dangerous failure is once every 114 years.

The implemented safety functions must then achieve the PL_r demanded by the hazards they target. The reliability of the safety function is derived from the reliability of its elements. Each must be rated with a respective PL, which must be of equal or greater reliability level than the PL_r.

The underlying elements that drive the safety functions are the integrated components, such as controllers, sensors and actuators, and may even include other

redundantly rated with both metrics. Both are applicable to the same elements, with a preference between them depending only on the technology and experience of the user. Either can be followed to validate a safety system as they are harmonized under the EU Machinery Directive, and might be merged as the Industry matures to further standardization of safety in control systems [41, 40].

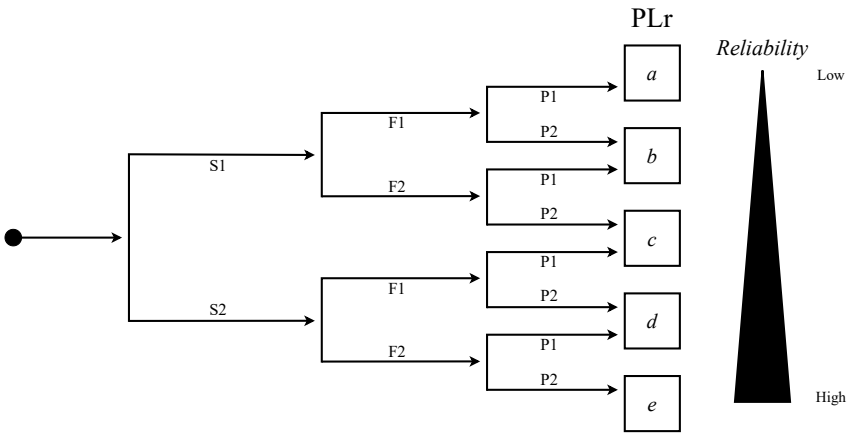

Risk parameters:

- S - Severity of the injury:
  - S1 - Minor, with reversible injury;
  - S2 - Serious with irreversible injury or death.
- F - Frequency and/or duration of exposure to the hazard:
  - F1 - Rare or only often with a short exposure period;
  - F2 - Frequent or continuous with a long exposure period.
- P - Possibility of avoiding the hazard or limiting the damage:
  - P1 - Possible under certain conditions;
  - P2 - Hardly possible.

Figure 3.1: Risc PLr assessment chart [44].

functions. A safety function is then fully dependant on the reliability of its elements, where a single element failure in the chain of the process will compromise the entirety safety function.

Furthermore, the architecture of the safety function affects the ensuing reliability. The safety functions may employ multiple channels (redundant elements) so that individual failures do not compromise the safety function. These architectures result in a lower PFH_d, allowing the safety function to achieve a higher PL rating.

Often, the safety function assessment process is simplified by using certified safety elements, which have identified PFH_d and respective PL ratings. Otherwise, the reliability of all elements of the safety function must be determined.

For the components of a safety function, the assessment of the PFH_d follows a standardized process that relies on the following performance metrics:

- The Mean Time To dangerous Failure ($MTTF_d$), measured in hours, represents failure rates of the safety function elements.[2]

[2]When not provided by the component supplier, the user must manually determine the $MTTF_d$. The metric is derived from the component's B_{10d} (average cycle number until 10 % of the component parts have a dangerous failure), and the expected number of cycles that the element is to perform in a year [42].

- The Diagnostic Coverage (DCO) is a metric representing the capability of the component to detect dangerous faults, measured in a percentage value. The DCO percentage measures how many of the component's potentially dangerous faults present a fault detection mechanism.
- The Common Cause Failure (CCF) is quantified by a point-scoring process, attributed by following a checklist of measures provided by the standard [45].[3] The checklist audits the component's measures for resisting external influencing factors common in machinery conditions, such as short-circuiting, extreme temperatures, or electromagnetic interference [39].

Subsequently, following the EN ISO 13849-1 norm, the presented metrics are combined to attain the PFH_d for the safety function components. Should the safety function depend on other underlying functions, each must be assessed beforehand via this same presented process.

Having established the reliability of all elements of the safety function, the sum of the respective PFH_d values provides the overall probability of a dangerous failure. Finally, the resulting PFH_d can be matched following Table 3.1 to attain the safety function's effective PL rating, as exemplified in Figure 3.2 [40, 42].

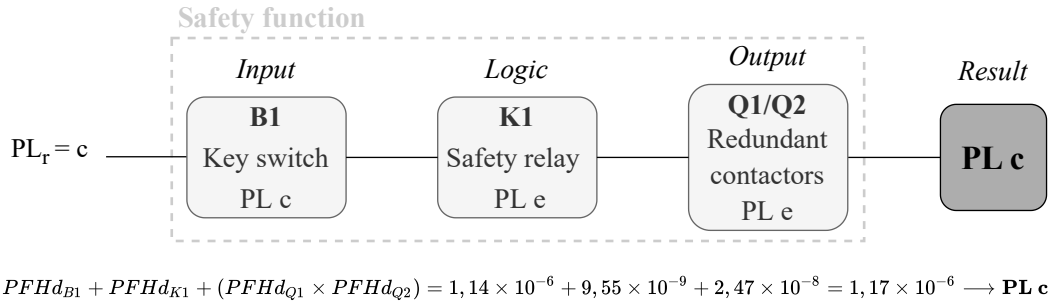

Figure 3.2: Assessment of a conventional safety function [42].

Machine Safe Stop

Whether undergoing an expected task, reacting to a manual emergency trigger, or following the detection of a hazard, the machine must provide safe stop mechanisms, which bring its actuators' motion safely to a halt.[4]

Three safe stop categories are standardized under EN/IEC 60204-1 [46], and, although all aim at bringing the actuating motors to a standstill, they differ in their procedure to achieve the safe stop:

[3] A CCF can simultaneously affect multiple channel systems and jeopardize the safety function.

[4] The "safe" or "safety" terminology, used throughout this document to describe elements such as interfaces, components or functions, indicates that they possess the required reliability and have an attributed safety rating such as a PL.

- In a category 0 stop, mandatory in all machines, the motor is stopped by instantly removing the power supplied to the drive elements. This action leaves the motor to move freely with the accumulated momentum, being therefore designated as an uncontrolled stop, and has the highest priority of the safe stops. When available, a mechanical brake can be deployed at power loss in order to reduce the braking time, and therefore, hazard exposure.

- The category 1 stop delegates the still powered machine to stop the actuating motion, such as in a regular motor control procedure, where, only after reaching a standstill, is the power from the motor removed. However, as it does not immediately remove power from the motor, a controlled stop presents a prolonged hazard, and its application must be considered by the risk assessment.

- A category 2 stop, similarly to a category 1, brings the actuator to a standstill in a controlled manner while retaining power. However, unlike the former, the power from the motor will not be removed, keeping the motor standstill while powered. Given the motor is still powered after coming to a halt, presenting a mechanical hazard risk even standstill, category 2 is not designated an emergency stop.

3.1.3 Drive-based Functional Safety

Machines often comprise moving elements with variable speeds, which are accompanied by mechanical hazards. Namely, the unintentional movement actions due to control failures pose a risk to both people and surrounding elements. Therefore, achieving functional safety in control systems often involves safely monitoring the motion aspects of its motors, including speed or position, rotation direction, stopping actions, and the standstill state. Here, a drive-based functional safety presents an opportunity to address the mechanical hazards, in an effort towards machine safety, via drive enabled safe monitoring and control [47].

The EN/IEC 61800-5-2 norm (for "Adjustable speed electrical power drive systems - Part 5-2: Safety requirements - Functional" [48]) was established to harmonize drive-based functional safety [40]. The standard proposes the safety functions for variable speed drives presented below, which include monitoring functions to detect hazardous conditions, and safe stop functions to enact safe stops in accordance with the previously introduced EN/IEC 60204-1. In machine systems consisting of multiple drives, a safety Programmable Logic Controller (PLC) is necessary to centralize the safety system control and simultaneous enact drive-based safety functions to the drives in the system. For example, a fault detected by a monitoring function must then trigger an emergency stop, not only on the responsible drive but on all drives in the machine system [49].

Safe Stop Functions

A fundamental element of drive-based functional safety is the Safe Torque Off (STO). This safety function is employed to bring the drive to a safe stop by inhibiting the motor from generating any torque and therefore eliminating the associated mechanical hazards. The function corresponds to a category 0 stop, and therefore, in the context of drive-based safety, it is referred to as Safe Stop 0 (SS0). As a result, the STO also functions as a prevention mechanism for an unexpected startup (i.e. restart after a power failure) by requiring a manual reset before restoring power to the motor. In addition to STO, safety rated drives might also support the Safe Brake Control (SBC) function so as to reliably set off a safe mechanical holding brake, available to provide further braking capacity. Notably, in scenarios where the STO function was triggered and the motor is subject to an active load, such as a suspended weight in a forklift, external mechanical brakes are required to hold the motor in place. Otherwise, the hazard would remain after enacting the SS0 function.

The Safe Stop 1 (SS1) function uses the drive to decelerate the motor in a controlled manner, and, after the motor reaches a standstill, the STO function will be triggered to remove power from the motor. SS1 targets applications where the motion can be brought to a stop in a controlled manner before switching to a no-torque state in order to prevent an automatic restart. The SS1 then fulfils the category 1 stop.

A Safe Stop 2 (SS2) function, similarly to the SS1 procedure, will decelerate the drive in a controlled stop, braking using the motor torque. However, contrary to the former, SS2 will not trigger the STO nor SBC functions, and therefore, not remove power from the motor. Instead, after the SS2 stop, the drive is kept at a standstill in torque. Consequently, conforming with a stop category 2, as the motor is still powered after coming to a halt, SS2 is not eligible as an emergency stop, contrary to SS0 and SS1. Therefore, the SS2 usage is reserved to provide a safe stop for the machine tasks, as part of the main application, due to providing certain advantages over the emergency stops. Given that SS2 does not employ either STO or SBC, the function allows for a faster restart procedure in comparison to SS0 and SS1, and, therefore, an earlier resume of the application, reducing operation downtime. In addition, by not applying the mechanical brake, deploying SS2 minimizes the abrasion of mechanical components, therefore prolonging the lifespan of the machine.

Moreover, depending on the application, by being able to utilize the power of the motor to bring it to a standstill, both SS1 and SS2 controlled stops may immobilize the drive quicker than a category 0 stop.

Nevertheless, for each designed machine, the entailing hazards and risks must be considered when selecting the drive stop procedures so as to best suit the system and fully achieve functional safety.

Safe Monitoring Functions

The Safely Limited Speed (SLS) function is provided to limit the operating speed of a drive, allowing the application to set different speed limits according to its needs. The function can then be used to reliably limit the operating speed, providing different limits according to the application. Therefore, SLS provides the means to increase productivity due to the added reliability of operation during hazardous conditions. For example, in the presence of an operator, the safety function enables the machine to remain in operation, even if at lower speeds, avoiding a full interruption of the process. The function monitors the active speed limit, which, if exceeded, shall trigger an emergency stop. Additionally, the Safe Maximum Speed (SMS) function provides an analogous functionality to SLS, although constantly limiting the maximum operating drive speed permitted in the application (not to be mistaken with the drive rated maximum speed). This limit is always active in the application, regardless of the current operating state and independent of an active SLS.

The Safe Speed Monitor (SSM) function provides the means to safely monitor the speed of the drives. The function differs from SLS or SMS, as it does not operate to trigger an emergency stop to a set speed limit. Instead, the purpose of SSM is to provide the monitored speed to the safety control system so as to enable other safety functions. By way of example, when operating at lower speeds, a personnel detection area can be reduced accordingly, as the hazardous region shrinks.[5] As the safety system supports a reduced protection area size for lower operating speeds, the system is able to avoid a false hazard detection caused by an exaggerated area design (to comprise higher speed conditions) that will needlessly trigger an emergency stop. With the SSM reliable speed measurements, an oversensitivity of the safety system can be mitigated, which would otherwise be required to address all possible hazardous conditions. Hence, the usage of the function leads to an increase in machine flexibility and productivity.

Safe Direction (SDI) enables the prevention of machine operation by unexpected drive rotation direction. The function monitors whether the motor rotates in a clockwise or counterclockwise manner. Should a “forbidden” drive direction be detected, SDI will trigger an emergency safe stop. The function may be useful in a variety of applications, similarly to SSM, so as to increase a safety system flexibility and further reduce safety hindered productivity.

As an example, a robot arm that should only be able to retract, as per application, by relying on SDI, the machine will not be required to consider the space of a possible arm extension as a hazard. In another instance, an autonomous vehicle backing out of an obstacle may only move in a specific direction. As the vehicle may

[5]The concept and importance of detection areas for the safety, driven by the SSM function, is further described later in the document, in the context of personnel detection systems for AGV.

still be allowed to move away from it, SDI ensures the drive backing movement, and the safety system no longer needs to ponder the hazard in the space of the obstacle. The machine then avoids the need for a manual intervention, otherwise damaging to productivity. By this same principle, the vehicle does not need to consider the areas opposite to its travel direction as hazards to monitor.

The characterized safety functions are represented in Figure 3.3, illustrating their procedure in regards to the drive velocity (V). Should the drive infringe the operating range restrictions (red striped areas), the monitoring function shall trigger an emergency stop.

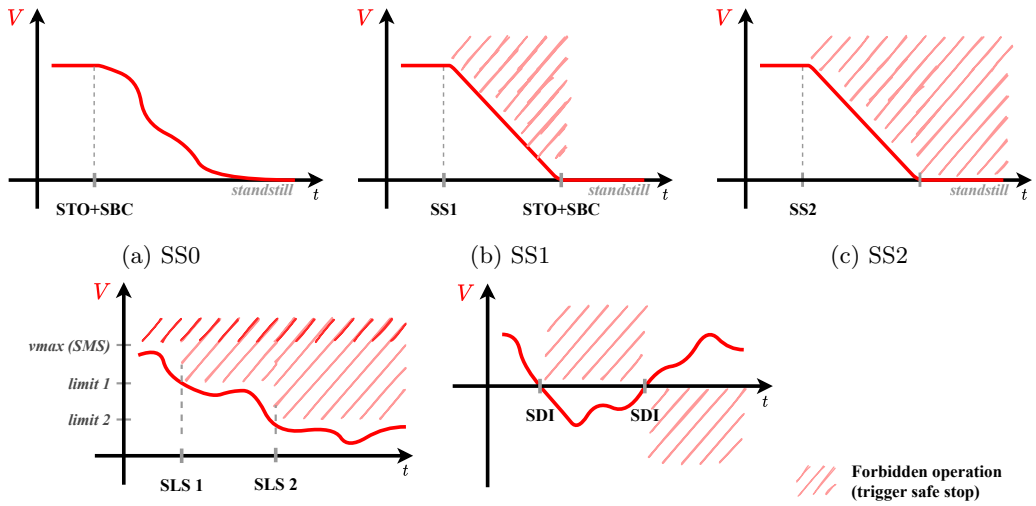

(a) SS0 (b) SS1 (c) SS2

(d) SLS and SMS (e) SDI

Figure 3.3: Drive safety functions.

3.2 AGV Safety

The intrinsic nature of an AGVS application makes it unfeasible to prevent access to the hazardous area with physical barriers, the common approach to industrial machinery. This is not only due to the hazardous area not being stationary but also due to the shared operating space with personnel, including the transit paths, as well as loading sites. In applications with either cooperative tasks (human-machine encounters but without direct interactions required by the process) or collaborative tasks (with active human-machine interaction in the process), an AGVS will often operate under a shared workspace [9]. Accordingly, AGVS are subject to stringent safety requirements so as to prevent the associated hazards that present risks to the physical integrity of a present bystander.

Unlike stationary machines, where unexpected events of their operating space being breached are uncommon, an AGVS application must foresee an high frequency of encounters with personnel breaching its hazardous region. Moreover, a mobile

machine is capable of invading the operator space. This is an added challenge when designing an AGVS safety system, given the frequent occurrence of unpredictable human-machine interactions. Handling these scenarios as emergencies and halting operation until manual intervention, the standard approach for industrial machines, is untenable. Production downtime will increase proportionally to the emergency halts, and, given the high encounter frequency in AGVS applications, this approach must be avoided. Additionally, AGVS must provide a safety system with the reliability to "justify" being able to autonomously resume operation after an encounter.

3.2.1 Protection Measures

In a typical AGV application, as described in Section 2.2, the ensuing mechanical dangers from machine mobility can be identified. These are the intrinsic hazards to which a person is exposed, such as impact, crushing, drawing in or trapping [40, 50]. Referring back to the PL_r assessment chart, these hazards hint at high-level safety requirements, given that they present risks of serious injury-causing hazards, which are of frequent exposure. However, the vehicle can be fitted with protective equipment in an effort towards avoiding and mitigating the danger, therefore lowering the risk and severity of hazards.

Personnel Detection System

Human protection is of high priority to AGVS, and therefore, a personnel detection system is essential in their application. This system must reliably detect the presence of a person or object on the course of the AGV in order to trigger a safe stop that avoids any injury or damage [6]. Commonly employed solutions in AGVS applications are Pressure-Sensitive Protective Equipment (PSPE) devices, such as sensitive bumpers, that on physical contact will trigger a machine stop, and Electro-Sensitive Protective Equipment (ESPE) sensors, which deploy the stop procedure whenever a monitored protection zone is breached, therefore avoiding any physical contact.

Collision is to be avoided whenever possible so as to minimize the risk of an injury. Nevertheless, the usage of PSPE, such as foam bumpers or plastic bars (Figure 3.4), is a last resort solution for a personnel detection system [28].

In particular, applications set in outdoor environments call for a PSPE implementation, given that a laser-based detection system is not viable due to lighting and weather conditions, which may tamper with laser sensors' reliability. As the detection occurs only after the collision, having the available braking distance shortened, the vehicle speed is highly limited in order to prevent any serious harm. Consequently, this approach yields a lower production efficiency when compared to the preventive ESPE approach.

(a) Foam bumper [51].

(b) Plastic bar bumper [52].

Figure 3.4: PSPE devices for AGVS applications.

In contrast, ESPE are "contact-free" sensors, which are able to monitor the AGV hazardous areas, including the space ahead of the vehicle travel direction, functioning as virtual bumpers [50]. A laser scanner based ESPE fits the LiDAR concept as it utilizes laser beams to detect an object within range and measures its distance relative to the sensor. The "ranging" function is based on the time-of-flight principle, using the measured time interval between a laser beam is emitted, reflected on an object and then detected by the sensor. The duration of the beam "flight", knowing it travels at the speed of light, can be used to derive the distance to the reflecting object [53]. The principle is demonstrated in Figure 3.5a.

The 2D laser scanner is then able to monitor horizontal hazardous planes (referred to as protection area) for any personnel presence, where it can be used to enable a mobile hazardous area protection system of an AGVS navigation, as seen in Figure 3.5b.

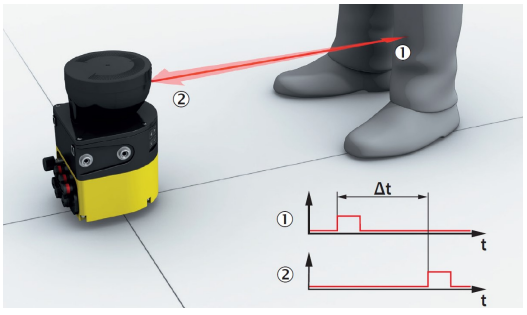

1. Transmitted light pulse
2. Reflected light pulse

(a) Laser ranging based on the time of flight principle [53].

(b) Mobile hazardous area protection via ESPE devices [40].

Figure 3.5: Laser scanner ESPE for safety in AGVS applications.

Drive Monitoring in AGVS Functional Safety

Rundong Yan, *et. al.*, in [54], in an effort to investigate the safety and reliability issues of AGV components, modelled and analyzed an AGVS composed of a "laser navigation system, safety system, manual interface, batteries, AGV software control system (ASCS), drive unit, brake system, steering system and attachments". From the study, the drive unit, control software, and battery system arose as the most vulnerable to fail. A drive-based functional safety in an AGVS addresses two of the major fail prone elements appointed in this study. Both the drive unit and control software have a direct influence on the AGV hazards presented above, as both elements are responsible for the navigation functions of the vehicle. A safety system employed in an AGVS will monitor both subsystems and intervene with safety measures in the event of a failure. Should the control system decree a collision bound route, or the drive unit control fail to follow the requested speed or position, a person in the AGV path might be submitted to danger. The drive monitoring safety functions, which continuously supervise these subsystems, are then able to detect the resulting hazardous conditions and trigger the fitting safe stop function to eliminate, or at least mitigate, the hazard risk.

Conjugated with an ESPE, the AGVS drive monitoring functions are extended, and the system is able to safely bring the vehicle to a stop, regardless of the hazard being originated by a system failure or disruption by personnel. Furthermore, as encounters with people and obstacles are expected to be frequent, the usage of an SS2 stop allows for personnel detection to be handled as a non-emergency and autonomously resume operation after the safe stop. Additionally, the safely monitored speed can be used to adapt the size of the scanners protection area. As the safety system becomes less restrictive and hindering to the application, with functions such as an adaptive protection area to better suit the vehicles manoeuvres and increased permissible speeds, the flexibility of the AGVS is improved, and consequently, also increases process productivity. Being performed based on safe information by safe elements, the protection area is adjusted in a reliable manner, therefore not compromising the safety of the AGVS.

3.2.2 Residual Risks Reduction

Furthermore, as noted in the Machinery Directive risk reduction strategy, upon inevitable exposed hazards, measures shall be taken in order to mitigate the possibility of an accident occurring. The mobile hazardous areas resulting from the AGVS operation are of continuous exposure, where a warning system can take on the role of risk reduction. Although the protective measures above can reduce risk, they do not completely eliminate the hazards present in the shared workspace. The frequent encounters with personnel make recurrent use of a warning system to inform them

of the impending hazards, as well as possible residual risks associated with the AGV application [40].

Visual and acoustic warning alerts can be used by the AGVS to signal any personnel and indicate the current vehicle assignment, making the machine predictable to bystanders [28]. During higher-risk conditions, such as detecting a person approaching the hazardous area, during machine startup, or under load transfer operations, a warning signal allows personnel to react accordingly and remain alert to the danger, actively reducing the hazardous risk. Furthermore, even during navigation, a persistent operation warning, such as a rotating light, can announce the presence of an AGV and actively prevent encounters with personnel, as well as interruptions to the machine tasks.

In order to achieve the desired effect, however, warning functions must be designed and arranged so that they are easily perceived and interpreted by a vulnerable individual. The system is then required to take into account the context of the environment, where "sensorial" saturation must be avoided. As other machines in the workspace have their own warning signals, similar cautions might result in misinterpreting or ignoring the warning signal. Personnel education, and training on how to interpret the warning signals and react in emergency situations, is also crucial to the effectiveness of the warning system.

The aftermath of these employed measures is a significant contribution to risk reduction, as well as, being of particular interest to AGVS applications, a significant improvement to production efficiency by preventing personnel detection.

3.2.3 Standardization in AGVS Safety

Marvel and Bostelma [8], in 2013, reviewed the available standards which outlined the safety systems for the use of mobile robots, including the AGV. The study revealed that the existing safety requirements, namely regarding human detection systems, was lacking and unfit for the industrial setting, pressing the need for new safety standards to enable a next-generation cooperative manufacturing environment.

Given the AGVS growing presence in the Industry, since the 2013 review, efforts have been made to standardize the technology, which aimed to include risk assessment and safety design proposals for a conventional AGVS. For the safety design of industrial trucks, encompassing the AGV concept, the ISO 3691-4 standard was recently established, in 2020, for "Driverless industrial trucks and their systems" [50]. Focusing on safety-related elements and aspects of the machine, the document differentiates the general AGVS into the following subsystems: the control system (either remote or embedded in the vehicle), the "guidance means" system and the

power system.[6]

The standard aims to specify the safety requirements with their respective validation procedures and criteria. In order to achieve this, the standard performs a risk assessment of the general AGVS, where the document identifies risks and foreseeable hazards associated with the different systems constituting the AGV. For each of the targeted systems and their respective safety functions, in consensus with the norm for the safety in control systems (EN ISO 13849-1), the standard defines the safety functions to address each identified risk, as well as the corresponding minimum PL_r.

Standardized Protective Measures

As protective measures, the standard firstly imposes the implementation of an emergency stop function, able to stop all movements of the AGV. The function must then be accessible to personnel via a dedicated device, such as emergency buttons, for a manual emergency trigger. In addition, the emergency stop must be actuated by default whenever the machine power supply is interrupted, as well as whenever a system fault is detected, a common requirement to all industrial machines.

Moreover, as a protective measure to address the inherent hazards of the autonomous driving machine under a shared environment, the standard defines the personnel detection system. This system shall then provide the AGVS with the means to stop the vehicle before contact between the vehicle rigid structure or load, and a stationary person, where either an ESPE or PSPE can service the function.

Upon a vehicle stop due to personnel detection, anticipating the autonomous design, the standard defines the automatic restart conditions. In summary, for an ESPE system, should the minimum surrounding clearances defined in the standard be respected, and if the detection system no longer indicates the presence of personnel in the hazardous area, following a 2 seconds delay and appropriate warning signals, the vehicle is permitted to automatically resume operations, dismissing a manual intervention.

The personnel system requirement does not, however, contemplate hazards caused by a person stepping into the truck path or moving towards the vehicle. These actions effectively incapacitate an early detection and therefore inhibit the AGVS from stopping the vehicle before a collision. This exemption showcases the necessity to instruct personnel on how to coexist with the AGVS. In this regard, the standard specifies the addition of a mandatory machine handbook, to be provided by the AGV manufacturer, with the required training and competency of personnel, as well as the identified risks to personnel.

[6]The power system design is nonspecific to AGVS, and therefore, the respective safety measures are not defined in this standard.

Risk Assessment of AGVS Subsystems

The standard risk assessment of the different control systems of the AGVS, notable to the implementation scope of this thesis, are compiled under Table 3.2, identifying the associated risks and resulting PL_r. Nevertheless, should the risks of an AGVS deviate from the foreseen in the table, a new assessment is required in order to address the hazards with the appropriate protective measures.

Table 3.2: AGVS safety functions as per ISO 3691-4 [50].

Control subsystem	Associated safety function	Corresponding risk to function failure	PLr
Braking system	Braking system control for stopping	Collision before braking to a standstill	d
	Parking braking system control	Collision due to unintended motion of a parked AGV	b
Speed control	Over speed detection system	Collision due to detection failure during over speed	c
	Adaptation of the sizes of safe detection fields	Collision due to inadequate area for AGV manoeuvre	d
Emergency stop	Stop hazardous movements and functions	Hazardous event not prevented	d
Personnel detection system	Stop the AGV following the detection of a person in the direction of travel	Collision with person upon detection failure	d
Warning systems	Optical, acoustical signals/systems	-	a

However, the standard does not define the equipment or control modules architecture and, instead, only specifies the necessary functionality to be achieved and the respective reliability. The approach to fulfil the presented requirements may then be defined by the manufacturer so as to best suit their AGVS application.

In regards to the braking system and emergency stop functions, as the standard does not delineate a mandatory approach, it allows for an implementation of the previously introduced drive safe stop functions to achieve these requirements. Additionally, the personnel detection system, as showcased in the risk assessment table, is defined to be dependant on the speed monitoring of the vehicle. Namely, the safe fields to be monitored are to be selected based on the vehicle speed. These specifications fit the capabilities of the drive-based functional safety. The safe monitoring functions, SMS and SLS drive the "Over speed detection system" function, and SSM enables the "Adaptation of the sizes of safe detection fields", for adjusting the safe protection fields fitting the mobile hazardous area according to the vehicle speed.

3.3 Conclusions

This chapter introduced the safety concepts and challenges prevalent in AGV safety systems. Furthermore, it detailed the methodology later employed in the envisaged AGVS to achieve functional safety.

The chapter began by submitting the driving reasons for improved and more complex safety systems. Then it presented the established requirements, concepts, as well as the design process pertaining to safe industrial machines. The chapter subsequently defined drive-based functional safety, the underlying principle followed by the implemented safety system, and showcased the common approaches to AGVS safety. Lastly, it reviewed the current state of standardization in AGV safety, by which the design proposal in this thesis complies.

From this review on AGVS safety, it can be concluded that the drive safety functions jointly with a personnel detection system enable an AGVS to fulfil the required protective measures. The drive-based functional safety fully adheres to the ISO 3691-4 standard for an AGVS design, sanctioned for the industrial setting.

Chapter 4

AGVS for Creel Applications

The following sections specify the approach to resolve the subject of this thesis. The chapter introduces the target application and details the architecture and systems that enable a safe AGVS for a creel spool supply system.

4.1 Creel Systems in the Tyre Industry

One of the major components required in the manufacturing of a modern vehicle tyre is the bead. The tyre beads are composed of a rubberized (coated with rubber) steel wire bundle, used as a reinforcement component that maintains the tyre structure and secures the tyre to the wheel rim [55]. In order to streamline the tyre bead manufacturing process, the handling, transport and storage of the steel cords are facilitated by using spools (also referred to as bobbins), a standardized holding frame for the cords. The steel wires are reeled into the spools to serve as carriers (depicted in Figure 4.1a) [56]. Subsequently, the spools are brought and loaded into racks (Figure 4.1b) so that a creel system, by unwinding the spools, is able to collect the steel wires to be used in the tyre bead manufacturing.

Providing a continuous supply of steel wire to the tyre beads manufacturing process involves different stages. The process begins with the transport of the spools to be loaded to the wall racks and the empty spools must then be unloaded from

(a) Steel wire spool [57]

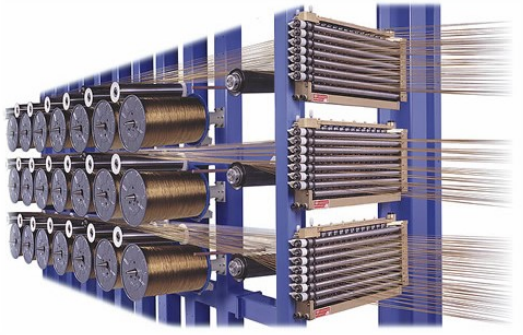

(b) Creel rack by RJS [58]

Figure 4.1: Creel system for tyre bead manufacturing.

the rack and transported back to be stored so that they are again whorled with steel cords [58]. The spool racks are able to hold multiple spools and, therefore, may present a prolonged layout in order to serve as a buffer to the creel system. The creel design must aim to avoid production downtime, and, in order to avoid interrupting the creel operation due to lack of supply, a consistent restock of the spools is required. Furthermore, another characteristic to consider for the creel design is the storage area of the spools, dedicated to pick up and drop empty spools, which may be distant to the racks to allow an extended rack layout.

The remaining stage, the loading and unloading of the spools in the creel rack, can conventionally be handled manually, such as the example in Figure 4.2. With this approach, the spools are loaded by an operator using a specialized handling tool. An operator then relies on pallets for transporting the spools between the different rack positions and storage areas.

(a) Spool grasper

(b) Rack loading

Figure 4.2: Manual creel loading process by RJS [58].

4.1.1 Automating the Creel System

The manual approach to the supply system of a creel system, presents, however, acute limitations to the process.

Requiring continuous operator involvement, for both handling and transport of spools, greatly hampers the scalability and flexibility of a creel system, despite the repetitiveness of these tasks. Moreover, a slower creel loading process, in order to avoid production downtime, will require a larger spool buffer. This results in additional rack space, and consequently, an increase in operating costs and complexity.

Given the presented process characteristics, as well as the, already standardized, format for material handling via the uniform spools and racks, the creel loading process proves an enticing target for automation.

The Conveyor Belt Solution

When analyzing a transport conveyor approach, the solution presents compromising challenges for automating the supply of a creel system.

The transporting role of the process presents the requirement for a vast and intricate conveyor network, given the distance to transport the spools between the racks and storage area. Additionally, the racks may be extensive and the creel system might employ multiple rows of racks. Furthermore, the loading position in the rack varies as spools are depleted.

The loading and unloading process further hinders the argument for a conveyor based solution, given the supply process requires to be performed along the entire racks. This characteristic implies the necessity of a spool handling solution per rack, as this function cannot be performed by the conveyor. An augmented conveyor solution with an automated crane system, dedicated to performing spool handling tasks between conveyor and rack, would need to cover the entirety of the rack area.

The extensive conveyor belt network, in addition to the required automated crane system for spool loading, would result in a costly and complex solution, as well as, become a cumbersome factor when scaling or adjusting the creel system layout.

AGVS as a Spool Supplier for the Creel System

The shortcomings of the conveyor based approach, in line with the issues raised in Section 2.1, have the AGVS emerge as a prominent solution for the supply of a creel system. The spool loading tasks fit the AGVS target applications, given their requirements for long distant hauling of supplies, flexibility and scalability.

The distance between the storage areas and the racks, as well as the rack length, do not present an added cost for an AGVS based creel system. The same applies should the rack layout change, either due to scaling the process or a shift in spool

demand between different racks. In such cases, a past AGVS implementation can be readily adapted to guarantee the creel supply according to the new specifications.

In addition, the AGVS approach overcomes the challenge of a dynamic spool loading position in the rack. The vehicle can navigate to any accessible location in the layout of the creel system, reacting as required by the application.

In regards to the spool handling service, unlike the conveyor solution, an AGVS provides the possibility for the handling equipment to be embedded in the vehicle. This approach eliminates the need for a crane, greatly reducing the cost for automating the creel system and further increasing its flexibility with a less intrusive approach, as the spool handling functionality requires only AGVS accessibility.

The AGVS by Gislotica

Given the presented comparison between the automation solutions, a creel system automation justifies the added engineering challenge of an AGVS resulting from the navigation system and stringent safety requirements for the autonomous machine coexisting in a human shared environment.

Seeking to further automate traditional creel system solutions, Gislotica aimed to introduce an AGVS for the spool transport and handling tasks in a creel system.

The envisaged AGVS employs a natural navigation system, based on 2D LiDAR technology, with the aim to reduce intrusiveness in the creel layout and enable inexpensive system adaptations to accommodate rack layout changes. Furthermore, given the numerous load positions in the racks, the solution provides the flexibility needed by the creel system, being able to address any rack position.

For the spool handling tasks, the proposed AGV integrates a spool loading tower, designed to interface with creel racks directly, and is capable of simultaneously transferring multiple spools (Figure 4.3). Having the equipment installed in the structure enables spool handling for the entire rack layout operated by the AGVS.

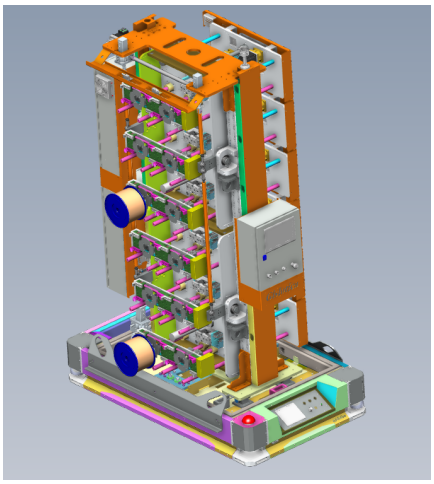

Figure 4.3: AGVS with Spool transferring tower.

4.2 AGVS Architecture

The envisaged system architecture, represented in Figure 4.4, encompasses the different roles which enable the AGVS for creel applications. These roles encompass the navigation for manoeuvring the creel layout, the safety for enabling an autonomous navigation and achieving functional safety for the creel application, as well as the powertrain support for vehicle mobility.

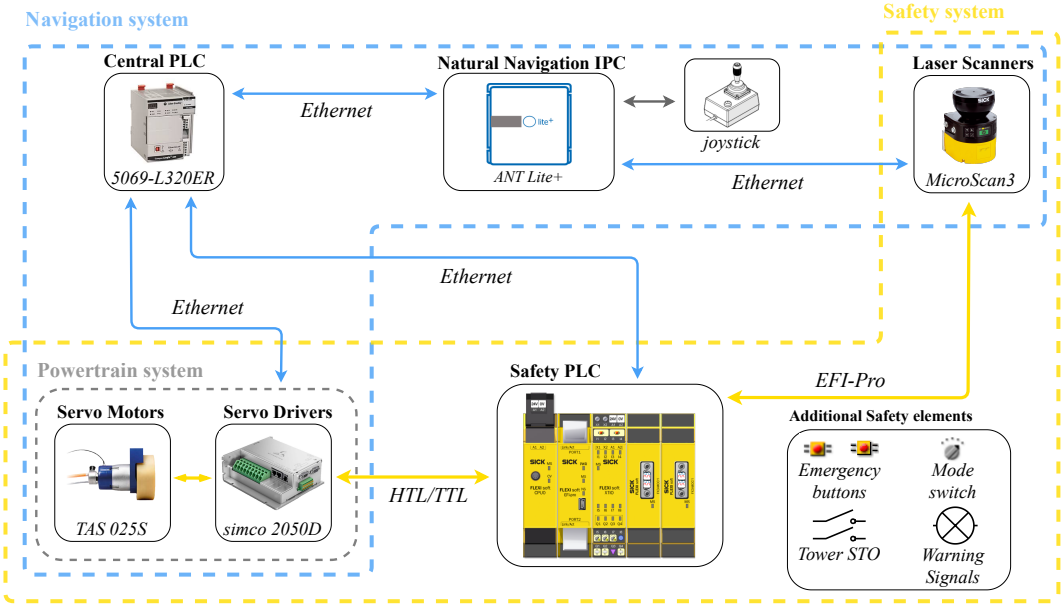

Figure 4.4: AGVS overall architecture [53, 59, 60, 61, 62].

4.2.1 Subsystems Interaction

The designed AGVS architecture, consistent with the presented roles, may be broken down into different subsystems, which are centralized by the entitled central PLC. The central system role, entrusted to the Rockwell 5069-L320ER PLC, undertakes several functions of the AGVS, which, along with coordinating the interaction between the different subsystems and their respective elements, is also responsible for running the creel application. This process includes managing the rack targets for the navigation system, as well as operating the spool transferring tower accordingly.

Navigation and Safety

As argued by G. Ullrich [16], the navigation and safety of an AGVS are not independent, "but rather interconnected functions". Accordingly, aiming to achieve autonomous navigation for the industrial setting, two subsystems conduct these key roles, the navigation (controlled by the navigation Industrial Personal Computer (IPC)) and safety systems (controlled by the safety PLC).

In turn, both subsystems operate the powertrain so as to perform their respective functions. In that endeavour, the central system provides the needed interface to the powertrain system, for both navigation and safety systems.

Furthermore, both navigation and safety subsystems are reliant on the LiDAR functionality, where the two MicroScan3 safety laser scanners, able to fulfil their respective functional requirements, are then shared to encompass the roles of the two subsystems.

AGVS Fieldbus Network

As manifested in the architecture (from Figure 4.4), the designed AGVS presents a highly interactive system, requiring the appropriate infrastructure to accommodate the interconnected subsystems.

The AGVS then relies on an EtherNet Industrial Protocol (Ethernet/IP) network to enable the communication for the necessary interaction between the different subsystems [59]. However, given its low reliability, the usage of Ethernet/IP is restricted to non-safe communication. In other words, the protocol can only enable communication for safety functions when involving lower PL_r. Employing a non-safe communication, the "weakest link" in a safe process, would compromise the reliability of the entire function. Consequently, the unreliable communication would hinder the achieved PL out of specification of the safety standard. Therefore, safety functions rely on safe communication (marked as yellow in Figure 4.4) to ensure the corresponding PL_r.

The high bandwidth exchange between the laser scanners and the Safety PLC, associated with the LiDAR data, requires a safe communication interface. As a solution for the interface, this interaction relies on Enhanced Function Interface Protocol (EFI-Pro), a proprietary protocol by SICK, which aims to enable safe device communication for industrial automation [63]. The protocol builds upon the standard Ethernet/IP stack to achieve safety functions PL_r, and is rated for applications up to SIL3 (equivalent to PL e [47]). In the current AGVS design, the EFI-Pro is responsible for enabling a safe personnel detection function, as the safety function requires a safe communication interface between the scanners and the safety PLC.

However, for the interaction between the safety PLC and the powertrain system, needed by the safety functions, the contact relies on safety rated High Threshold Logic (HTL) and Transistor-Transistor Logic (TTL) interfaces, having no need for data exchange.

Nevertheless, Ethernet/IP is able to drive non-safe high bandwidth communication in the AGVS. Such is the case of the navigation system, where the laser data required by the natural navigation control can rely on the protocol. Additionally, Ethernet/IP also plays a part in the safety system, where it bridges the interaction

between the safety and central PLC. This connection is used to provide the safety system's state and diagnostic data to the central system. Furthermore, the protocol fulfils safety functions in tasks without stringent PL_r (controlled stops).

4.2.2 Natural Navigation System

The Natural navigation system is driven by an off-the-shelf product, provided by Bluebotics, the "ANT lite$^+$". The product has been previously tested and validated by Gislotica, in [15], as a solution on a prototype AGV. For the creel application, the solution needed now to be ported to the industrial setting, with the AGVS achieving the required functional safety.

The ANT lite$^+$ system is designed to provide vehicle control and positioning for AGVS applications. Regarding the vehicle position in the navigation layout, the product advertises a localization accuracy of up to $\pm 10\,\text{mm}$ and $\pm 1°$. The navigation functionality is achieved by relying on 2D laser scanner data, in conjunction with the vehicle motion odometry, so as to localize the vehicle in a mapped environment [62].

As a natural navigation solution, the system relies on static features endemic to the navigating environment. Nevertheless, the solution supports the introduction of artificial landmarks to the layout, enabling applications set in environments that lack "good" natural features.[1] This is an essential function as the lack of features would hinder the precision performance of the localization, and consequently, the control functions of the navigation system.

Nevertheless, retro-reflectors can be added to these environments to be used as landmarks by the system. The layout may be easily adapted with reflecting tape and without further changes to the infrastructure. This approach preserves the benefits of a natural navigation approach, namely the inexpensive adaptability and scalability of the navigation system.

Furthermore, appended to the navigation function, ANT lite$^+$ provides collision avoidance functionality. When presented with an obstacle in its path, the vehicle will stop by command of the navigation system in order to prevent a collision with stationary objects.

However, it is worth noting that the solution does not support an obstacle avoidance function, as the vehicle cannot manoeuvre around the obstruction to resume the operation. This aspect once more raises the importance of personnel training

[1] The ANT lite$^+$ system requires that the natural features considered in the mapping process present a flat surface of at least 400 mm, deeming them "good" features for the navigation system [62]. The specification intends to improve the navigation system performance by relying solely on the distinct elements of the layout. This filters out ambiguous features, which would be perceived interchangeably or mistaken with new elements in the environment, and alleviates the stringency on the laser scanners. However, this approach leads to less feature-rich environments. In turn, this disadvantage is counteracted by the support of artificial landmarks.

in AGVS environments, as the layout must be kept unobstructed. Any objects or stationary elements in the environment may serve as obstacles in the navigating path, completely halting the AGV operation until manual intervention, hindering process autonomy and efficiency.

The system supports a list of selected laser scanners, which includes the MicroScan3, as well as several other safety laser scanners. By acknowledging the safety function requirement in AGVS, the navigation system may repurpose the LiDAR function, and hereby, avoid redundant costs.

The Bluebotics solution, founded on Ethernet/IP communication, is integrated into the AGVS via the dedicated ANT lite$^+$ IPC (presented in Figure 4.5).

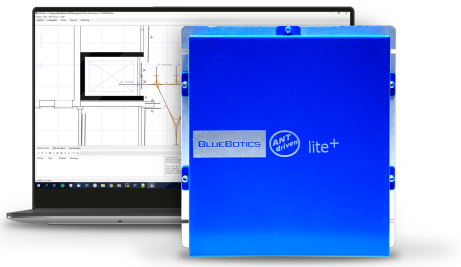

Figure 4.5: ANT lite$^+$ navigation system by Bluebotics [62].

Subsequently, the user is able to interface with the navigation computer via ANT lab. This software enables the offline configuration of the navigation system, which includes designing routes and stopping points to be used by upper application control. Additionally, the interface enables online monitoring for tracking and debugging the running navigation system.

Furthermore, the navigation system includes a joystick which allows to manually control the vehicle direction and speed.[2] The functionality is rather convenient for AGVS since permitting operators to handle the vehicle manually facilitates specific tasks. These include performing maintenance work on the system, managing the AGV fleet, or even enabling manual operation of the AGVS application.

4.2.3 Powertrain System

The powertrain system is responsible for controlling and delivering the mechanical motion to the AGV structure, including enabling the directional control for the navigation system. The “cyber iTAS system” by Wittenstein, presented in Figure 4.6, is an integrated drive solution conceived specifically for AGVS drive systems [64].

[2]The ISO 3691-4 standard for AGV safety foresees the support for manual control of the vehicle by an operator, to be included alongside the autonomous navigation system.

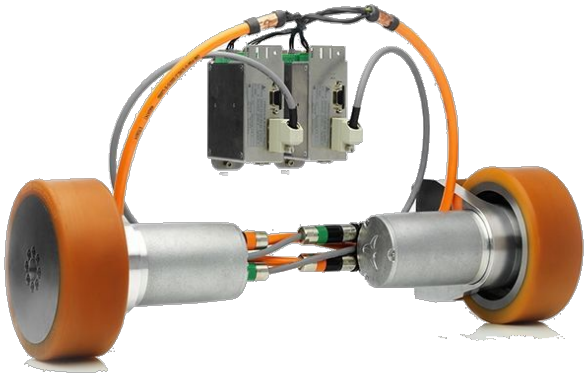

Figure 4.6: iTAS drive system for AGV [64].

The iTAS Drive System

The system is based on a pair of three-phase AC servo motors, classified as Permanent Magnet Synchronous Motor (PMSM).[3] The motors then drive the two traction wheels of the vehicle, following a 31:1 reduction gearbox.

Servo motors are characterized by comprising a rotor position feedback sensor, which enables the closed-loop control of the motor, particularly advantageous for precision control application [65]. Such is the case in AGVS, where the increased precision of the wheel control directly improves the navigation precision.

Along with the servo motors, the solution includes both accompanying 2050D servo drive amplifiers, which are responsible for the control and powering of the motors [60]. Furthermore, the drive provides an Ethernet/IP interface to interact with the AGVS application.

Powertrain Specifications

The requirements for the AGV powertrain, set by the creel application, must be fulfiled by the iTAS drive system specifications. The solution is rated for vehicle speeds up to $1.2\,\mathrm{m\,s^{-1}}$, with an acceleration of $0.4\,\mathrm{m\,s^{-2}}$, considering a powertrain load of 2200 kg (including vehicle structure and payload) [61].

The powertrain structure is then integrated into the AGV following a differential drive system for directional control, with two drive wheels and four additional castor wheels on each corner to address vehicle stability.

[3]The AGV is to be powered by batteries, and subsequently, the servo drive is supplied with Direct Current (DC) power. However, given the motor characteristics, the drive includes a DC to AC converter.

Differential Drive

The differential drive architecture is commonly employed in terrestrial, wheeled, mobile robots, allowing a two dimensional (2D) plane mobility with three degrees of freedom x, y and θ (referred to as the pose of the vehicle). This design consists of two fixed drive wheels mounted in parallel along the horizontal axis of the driven structure. This approach provides a high motion and positioning flexibility, enabling the vehicle to turn on its axis (*pivot*) [66, 67].

Only requiring two drive wheels (excluding additional weight support wheels), this architecture offers a solution with reduced complexity and cost. Two wheels are driven independently, with both speed and rotational direction controlled individually on each wheel motor. The resulting motion of the structure is then the combination of the wheels individual speed and follows the kinematics of a differential drive mechanism.

G. Duke and M. Jenkins, in *Computational Principles of Mobile Robotics* [68], describe the principles of the differential drive kinematics as follows: the velocity relation (both peak and difference) between the two wheels will determine the trajectory of the vehicle. As a result, from a differential speed configuration, at a given instant, the vehicle will travel along a circular path centred on a fixed Instantaneous Center of Curvature (ICC) point in the 2D plane (depicted in Figure 4.7).

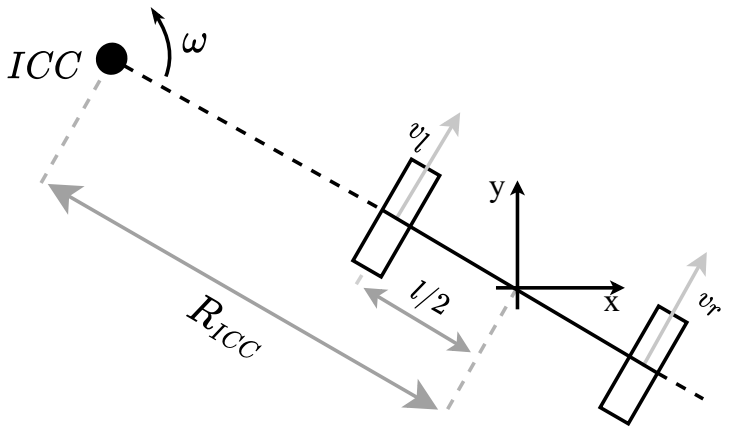

Figure 4.7: Differential drive kinematics (Amended from [68]).

When travelling at constant differential wheels speed, therefore maintaining a circular trajectory, the ICC point is stationary, aligned perpendicularly and at a constant distance to the drive wheels. The distance from the ICC to the middle point between the wheels is the radius of the circular path (R_{ICC}). Additionally, although the wheels move at different linear speeds, as they both revolve around the ICC, parallel to the circular path, it can be concluded that they travel in the plane at the same rotational speed (ω) along with the vehicle. Where l represents the axle

length separating the two wheels, Equation 4.1 presents the conversion from linear to angular velocity, based on each wheel turning radius ("$R_{ICC}+\frac{l}{2}$" and "$R_{ICC}-\frac{l}{2}$", the furthest and closed to ICC respectively).

$$\begin{cases} \omega = \frac{v_r}{R_{ICC}+\frac{l}{2}} \\ \omega = \frac{v_l}{R_{ICC}-\frac{l}{2}} \end{cases} \tag{4.1}$$

From the equation defining the angular speed of each wheel, the formulas for determining the trajectory turning radius and turning speed, for a given wheel speed configuration, can be derived from Equation 4.2 (demonstration available in Annex A).

$$R_{ICC} = \frac{l}{2} \cdot \frac{v_r + v_l}{v_r - v_l} \ , \ \omega = \frac{v_r - v_l}{l} \tag{4.2}$$

Three particular configurations, which are characteristic of a differential drive setup, can be predicted on the R_{ICC} formula. With the same rotational direction, as both wheels speed approximate ($v_r = v_l$), the turning radius converges to infinity, representing a straight moving vehicle. However, when the speeds are the same but rotating in opposite directions ($v_l = -v_r$), the R_{ICC} is null and the vehicle performs a *pivot* motion. Lastly, when a single wheel is stopped ($v_r = 0 \veebar v_l = 0$), the ICC point converges with the stopped wheel ($R_{ICC} = \frac{l}{2}$), and the vehicle turns on its wheel.

4.3 AGV Safety System

As stated in Subsection 3.2.3, in order to ensure personnel safety and commercialize the designed AGVS in the EU market, the vehicles must comply with the EU Machinery Directive. This may be achieved by developing and certifying the AGV safety system following the ISO 3691-4 standard. The safety system must then provide the required safety functions for the AGVS, namely the ones presented in Table 3.2, in order to enable the creel application to achieve functional safety.

As was concluded in the safety systems review from Chapter 3, a drive-based safety presents a befitting approach for safety systems in AGVS applications. Following this premise, the resulting drive-based safety system design, as represented in Figure 4.8, is centred in the safety PLC as the controller to carry out the safety functions. The safety PLC then comprises different functions and modules to coordinate the sensors and actuators associated with the safety functions. Furthermore, all the modules and respective functions are rated up to PL e safety applications. Nevertheless, the safety system control is not restricted to the safety PLC and presents a somewhat distributed architecture.

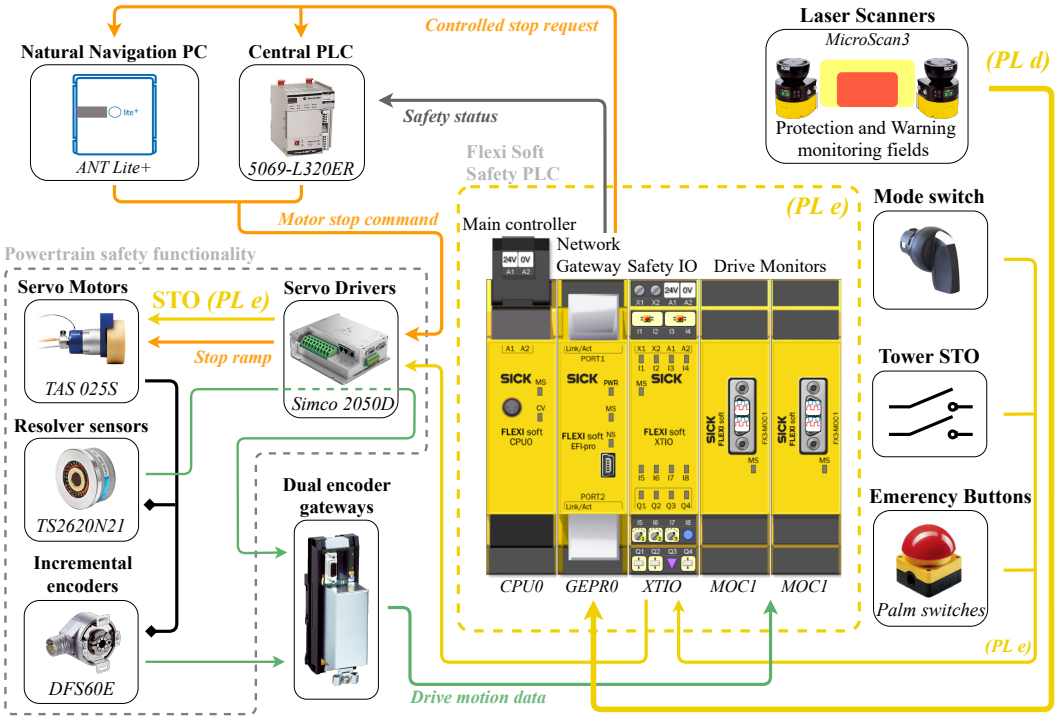

Figure 4.8: Safety system architecture [69, 70, 71, 72, 73, 74, 75].

In the context of drive-based safety systems, functional safety heavily relies on powertrain safety functionality. Both safe control and monitoring of the drives are requirements met, in this architecture, by relying on the servo drive functions. Likewise, the personnel detection function is primarily administered by the safety laser scanners, exchanging only the bare necessary information with the safety PLC needed to perform the respective safety function.

4.3.1 Safety System Controller

The safety PLC solution is based on the Flexi Soft system by SICK, a modular hardware platform for safety control in industrial applications. The system is configured with the addition of the necessary modules for the creel AGVS application, as presented in Figure 4.9. The Safety Designer, a software interface for users developing a safety system based on Flexi Soft, provides the means to configure and monitor each of the PLC modules to devise the safety program for the target application. The program is designed via function blocks, which are certified for use in safety-related applications and therefore suited for implementing the safety functions of the AGVS [76].

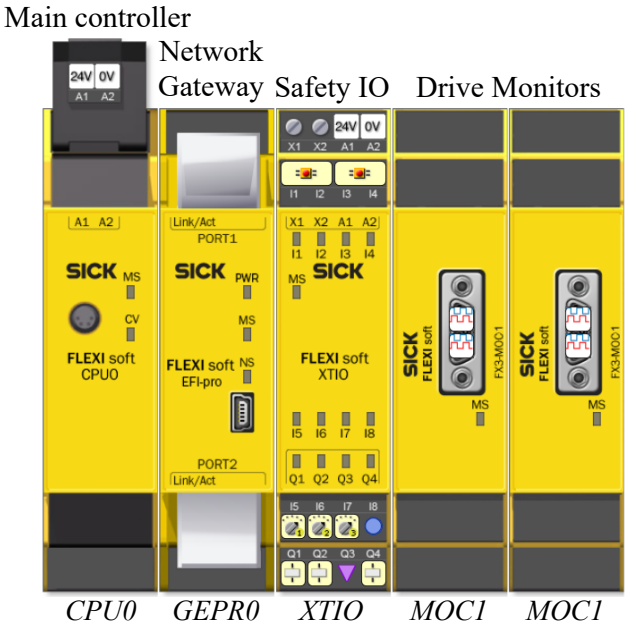

Figure 4.9: Flexi soft PLC configuration [76].

CPU0 - Main controller

The main controller module, CPU0, is the centrepiece of the safety PLC, directly interacting with the other modules. This module is responsible for processing the logic of the safety program, as designed by the user [71].[4]

GEPR0 - Network Gateway

The network gateway, GEPR0, drives the fieldbus communication for the safety PLC, enabling both the safe communication via EFI-Pro, as well as the standard non-safe Ethernet/IP protocol [77, 70].

In the context of the AGVS application, the gateway enables the personnel detection safety function by providing the required safe communication between the laser scanners and the safety PLC.[5]

Furthermore, Ethernet/IP provides a non-safe interface between the safety PLC and central PLC to exchange data for control and diagnostic purposes [78]. The interface is used to coordinate the main application and safety system ("safety status" in Figure 4.8). Notably, the emergency status indicates to the application controller whether or not it may resume operations. Similarly, the status data of the safety

[4]With the exception of drive-based safety functions, which are in part operated by the drive monitor modules.

[5]The laser scanner's LiDAR data, used for navigation purposes, is transmitted via the GEPR0 gateway, as there is no direct physical connection between the lasers and the navigation system. Nevertheless, the gateway serves only as a routing device, given the non-safe data is directly addressed to the navigation IPC. In practice, this configuration results in a direct communication between the laser scanners and the navigation system.

program, drives, and scanners allow the identification of safety-related issues that might be affecting the AGVS application.

In addition, although the Ethernet/IP protocol is not safety rated, safety functions rely on this interface for the non-safe controlled stop requests (further explained in Subsection 4.3.3).

Lastly, the gateway provides the user with an interface to the Flexi Soft system for configuration and diagnostics of the safety system.

XTIO - Safety IO

The XTIO module supplements the Flexi Soft system with eight safe inputs and four safe outputs, which are made available for the safety program running in the CPU0 module [72]. Similarly to the safe communication role, these interfaces are required to sustain the reliability of the safety functions that interact with safe external elements and the safety PLC.

In the context of the creel AGVS application, safe inputs are employed for reliably "reading" the state of the emergency buttons, used for a manual trigger of the emergency stop safety function. The emergency buttons are two latching push buttons with a Dual-Channel Normally-Closed (2NC) interface for redundancy to reach the set PL_r [73], therefore each requiring two safe inputs.

Additionally, a safe mode switch position is connected through the module so as to ensure a safe transition to autonomous navigation from manual mode.

The safe outputs are required for a safe control of the SS0 functions. These include both SS0 interfaces per servo drive, as well as the AGV tower STO function required to safely stop the drives corresponding to the spool transferring tools.

MOC1 - Drive Monitors

The MOC1 elements of the PLC are motion control modules, which enable drive-based functional safety via safe drive monitoring, embracing AGVS among the targeted applications [79]. The modules present the functionality for monitoring drive speed or position, as well as stop and braking actions.

For monitoring the drive, the modules rely on shaft encoders to measure the motion of the motor and support different encoder models, such as the incremental and sine-cosine variants. Each MOC1 contains an interface for up to two encoders, which can be cross-compared when attached to the same drive. This allows an increase in monitoring reliability, and consequently, enables the application to achieve a higher safety PL rating [69].

The motion module then provides several of the safety functions as defined by the standard EN/IEC 61800-5-2 for safety speed control of electrical drives. These encompass the safety functions introduced under Subsection 3.1.3, including the safe

drive stop (SS0, SS1, SS2) and safe drive monitoring functions (SSM, SLS, SMS and SDI).[6]

4.3.2 Powertrain Safety Functionality

As was previously defined, under a drive-based safety system, the safety functions rely on drive monitoring and control to achieve functional safety for the application. In particular, all AGVS safety functions presented in Table 3.2 are directly dependant on the powertrain capability to provide the drive functions they rely on. Being tailored for AGV applications, the iTAS drive system is set to fulfil these requirements.

The servo drives integrate the STO safety functions, rated for PL_r e applications [60], which enable the SS0 function for the drives. In addition, the SIMCO drive operates a mechanical service brake in conjunction with the STO function, which effectively provides the SBC function.

The powertrain emergency braking system enables the safety function presented in Figure 4.10.

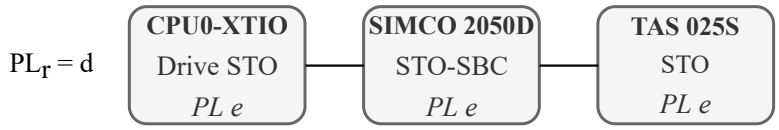

Figure 4.10: Safety function - Braking system.

Both aforementioned functions, constituting SS0, are active for the AGVS application by default. The safety system via the safety PLC will then disable the functions, should the applications safety requirements be met, in order to begin operations. Should the power be cut or the communication with the safety system be interrupted, both STO and SBC will be triggered. This design is a preemptive measure for unsecured operation and an unwanted start of the autonomous machine.

In addition, the system supports SS1 and SS2 functions by providing controlled stop ramps profiles in the SIMCO drive to be deployed by the application [64].

4.3.3 AGVS Drive-based Functional Safety

Being an essential role on a drive-based safety system, the drive monitoring function must provide a reliability so that the safety functions which depend on this feature achieve their respective PL_r rating. The safety functions in Table 3.2 rely on safe drive speed monitoring (via SSM) in either direct or indirect manner, where the

[6]The STO and SBC procedures are, however, operated by the servo drives. Instead, the powertrain system provides a dedicated safe interface for triggering these functions according to the safety program.

most stringent of them has a reliability requirement of PL_r d. Accordingly, following the concepts introduced in Subsection 3.1.2, the reliability of the drive monitoring function must reach a minimum PL d rating.[7]

Drive Encoders

As previously stated, the MOC1 motion module of the safety PLC performs the Safe Speed Monitor (SSM) function suited for up to PL e applications. The module, however, requires the drive motion data to be provided with the appropriate reliability. Therefore, the encoders providing the data from the drives must achieve the PL rating of the associated safety functions.

A safe encoder, capable of achieving PL d as set by the safety functions, was not compatible with the servo motors. Instead, the powertrain system supports a dual encoder solution, used in cross-compare mode by MOC1, in order to achieve the set PL_r ("Drive motion data" process denoted in green in Figure 4.8).

In cross-compare encoder mode, the module will continuously compare the motion data of both encoders, which, by monitoring the same drive, both ought to be matched [76]. Should one of the encoders fail by providing incorrect motion values, the data mismatch will report the failure to the drive monitor. Subsequently, the event will trigger a safe machine stop, and therefore, the dangerous failure will be avoided.

Furthermore, under the cross-compare mode, a dangerous failure of the monitoring function, meaning an undetected speed monitoring failure to which the safety system cannot react, will only occur in the event both encoders fail and still report matching data. This approach then results in a lower PFH_d, given the lower probability of the undetected match failure. Accordingly, the setup increases the reliability rating of the monitoring function up to PL e [60], despite relying on lower PL grade encoders.

As one of the encoders, the iTAS powertrain solution includes an incremental encoder, the DFS60E by Sick rated for PL c applications [74]. However, the motor shaft does not support a second encoder. As a workaround, the 2050D servo drives provide a function to emulate an additional encoder, relying on the motion information provided by the resolver [75], in use by the servo control loop. Furthermore, given the dual encoder approach, two MOC1 modules are then required by the safety system, one per servo drive.

[7] So as to reiterate the development process of safe machinery, after finalizing the design of the machine safety system, the effective reliability PL of each safety function must again be evaluated and judged against the appointed PL_r during risk assessment. Therefore, the assigned PL_r for the drive monitoring function must be reviewed regarding the resultant reliability of the AGVS safety functions.

Safe Speed Monitoring

The safe drive monitoring functions complete the set of function requirements for achieving functional safety.

By relying on the Safe Maximum Speed (SMS), the speed of the drives is safely limited following the servo motors rated speed of $1.2\,\mathrm{m\,s^{-1}}$, during the entire operation of the AGVS.

Similarly, the Safely Limited Speed (SLS) function is relevant for speed-limiting the vehicle in particular modes of operation, as deemed by the application. During manual control, it may be required to disable the personnel detection system. A constant detection of a fixed object results in a "stuck" vehicle, requiring disabling the protection system to move the AGV manually. Also when manoeuvring the vehicle through congested environments for maintenance work, the personnel detection system might needlessly be active as the vehicle is not autonomous. For disabling the safety function, the vehicle speed must then be safely limited to $0.3\,\mathrm{m\,s^{-1}}$, as defined by the safety standard [50].

The Safe Direction (SDI) function further secures the operating scope of the vehicle, as the differential drive system may require the wheels to rotate in the same direction. In particular, when travelling at higher speeds, the vehicle may become unstable if it inadvertently performs *pivot* or sharp turning manoeuvres, driving the wheels in opposite directions. When the application does not intend such behaviours, the system can rely on SDI to safely restrict the vehicle motion as specified by the application.

The drive monitor safety function encompassing the three presented functions is outlined in Figure 4.11. A failure detected by the drive monitoring function represents a failure of the control system and an AGVS operation out of specification. Given this, the function was set to initiate an SS1 to handle the control failure as an emergency and prioritize a controlled stop, requiring manual intervention before resuming the operation. The safety function also fulfils the "Over speed detection" function set by the safety standard (Table 3.2). However, as was previously asserted for this AGVS application, a $\mathrm{PL_r}$ d has been set for the safety function to meet the $\mathrm{PL_r}$ of functions that rely on drive monitoring.

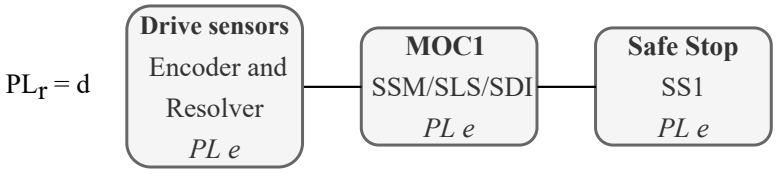

Figure 4.11: Safety function - Drive monitoring.

AGV Safe Stops

A notable aspect of this safety system design is that the controlled stops (SS1 and SS2) are not actuated with the required safety rating. Depending on the active operating mode of the AGVS, the controlled stops will be performed by different system elements (outlined in orange in Figure 4.8).

During autonomous navigation, designed with consideration to the personnel detection system, the ANT lite$^+$ collision avoidance function will control the vehicle velocity to follow the controlled stop ramp. For a personnel detection while in manual mode (SS2) or if a failure is detected in autonomous mode (SS1 emergency), the safety system will instead directly signal the central PLC of the hazard, which in turn will trigger the servo drive to perform the controlled stop.

In both procedures, the controlled stops are triggered and enacted by non-safe elements and functions, and therefore, the control of SS1 and SS2 is not safe. Instead, the reliability required to achieve the PL_r of both the emergency stop and braking systems (PL_r d), is ensured by the monitoring functions. This approach is sustained by the Flexi Soft solution and the drive-based functional safety. Upon triggering a controlled stop on the drive, the safety PLC motion control modules, via SSM, continuously monitor the speed of the drives and checks that the stop ramp is being correctly enforced. In the event the non-safe control fails, the safety controller will then enact the safety-rated SS0 function on the servo drives and accordingly trigger STO and SBC. In effect, with this approach, the reliability and, therefore, the PL ratings of SS1 and SS2 are assured by the SS0 safe control.

The AGVS safe stop functions, showcased in Figure 4.12, in conjunction with the safety function from Figure 4.10 fulfill the "Braking system control for stopping" requirement from Table 3.2.

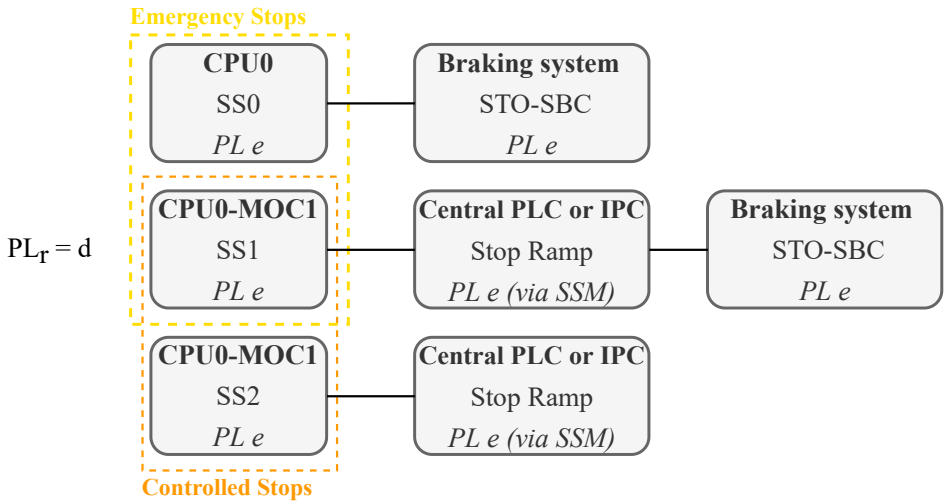

Figure 4.12: Safety function - Safe Stops.

Manual Emergency Stop

In addition to enacting a safe stop upon the detection of hazards by the machine, an emergency stop may be triggered by a person. As required by the AGV safety standard the AGV structure will then be suited with emergency buttons accessible to personnel.

As depicted in Figure 4.13, the manual emergency stop function shall rely on palm switches (represented in the diagram of Figure 4.8) to reliably trigger the SS0 function.

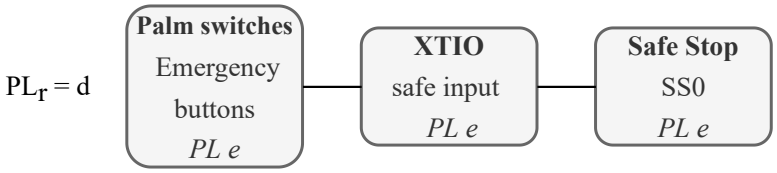

Figure 4.13: Safety function - Manual emergency stop.

Although an uncontrolled stop, this safe stop allows the instant removal of power from the machine. A passerby may be facing hazards other that the ones associated to the AGV navigation, such as electrical malfunctions. Therefore, given a controlled stop would prolong such hazards, the design choice was to deploy the SS0 function instead.

4.3.4 Personnel Detection System

As the protection measure to mitigate the intrinsic hazards of the vehicle, resultant of sharing the workspace with people, the personnel detection system is a fundamental safety function to enable AGVS for industrial applications, such as the creel supply system. The role of the safety function, in accordance with the ISO 3691-4 standard, is to detect a person present in the direction of travel of the AGVS and stop the vehicle to prevent mechanical hazards.

Being set in an indoor environment, the creel AGVS application is able to benefit of the ESPE approach, which, in contrast to a PSPE solution, enables the vehicle to navigate at higher velocities and entirely avoid colliding with a stationary person. Furthermore, given that the AGVS also requires LiDAR equipment for navigation, an appropriate safety laser scanner would merge ESPE and mapping functions. Thus, equipment costs may be reduced as the devices fulfil both safety and navigation subsystems.

Adaptation of the Detection Fields

In order to fulfil its role, the designed safety function must monitor the entire mobile hazardous area. As the vehicle speed and travel direction vary, so does the region presenting the risk of collision to any present personnel. Accordingly, the safety function must dynamically adapt to the vehicle navigation. Therefore, the designed personnel detection system relies on drive-based functional safety.[8] The SSM function is necessary to safely monitor the hazardous area, as well as the safe stop functions for stopping the vehicle with the required reliability.

The SSM function, provided in the safety PLC, is then utilized to safely monitor the AGV manoeuvre and speed to identify the corresponding monitoring case. While relying on the safe communication channel by EFI-Pro, the safety controller then activates the monitoring case in the safety laser scanners, with the fields that comprise the ensuing hazardous area. This functionality is showcased in Figure 4.14.

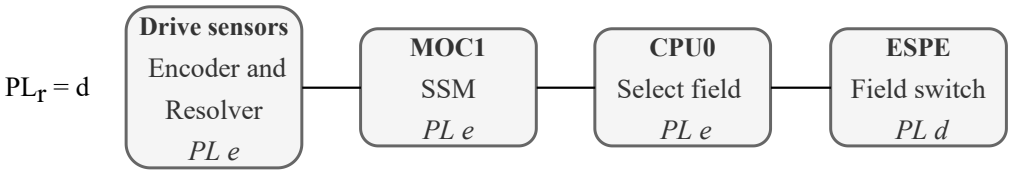

Figure 4.14: Safety function - Detection fields size adaptation.

Safe Stop for Personnel Detection

The personnel detection system in a ESPE approach, as per the requirement in Table 3.2, shall enable the AGVS to stop before colliding with a person in the direction of travel of the vehicle. The subsequent safety function is portrayed in Figure 4.15.

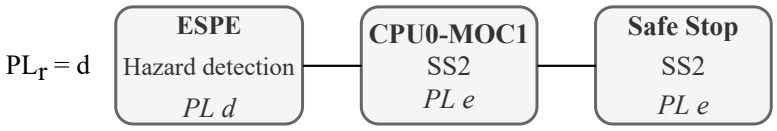

Figure 4.15: Safety function - Personnel detection.

The detection of personnel is not a failure in the control system but rather an impending hazard to be addressed with a reliable stop procedure. As asserted in Subsection 3.2.1, handling a personnel detection as a non-emergency will avoid a

[8] Both supporting safety functions, SSM and effectively SS0, fulfil the PL d required by the standard for the personnel detection system.

manual intervention to restart the machine following the encounter with personnel. Hence, SS2 provides the reliable means to stop the vehicle before colliding with a person, and, by permitting an autonomous restart, improves the AGVS productivity. In case the controlled stop fails as dictated by the SSM function, the event escalates to an SS0 emergency stop.

Safety Laser Scanners

The MicroScan3 equipment, presented in Figure 4.16a, is sanctioned as an ESPE device, rated for up to PL d safety systems, and is designed for applications requiring hazardous area protection [53].

(a) MicroScan3 safety laser scanner [53]

(b) MicroScan3 protection (red) and warning (yellow) fields [80]

Figure 4.16: Safe personnel detection with MicroScan3.

The safety laser sensor is a 2D scanner capable of monitoring a plane. The device is able to detect a person entering a defined area to safely stop a machine operation, providing mobile hazardous area protection suited for AGVS [80].

The device supports two different field types, each providing different functions (represented in Figure 4.16b). The protection fields monitor the hazardous areas with a reliability of up to PL d for a safe personnel detection function. The warning fields are reserved for non-safe warning functions.

The selected scanner model provides a sensor capable of detecting an object in a 64 m range. Furthermore, the sensor is able to scan an area of 275°, surrounding the sensor, by emitting radial beams at an angular resolution of 0.1° (Figure 4.17).

However, the safety functionality regarding the protection fields is restricted to a maximum 9 m range. The decrease in reliability can be attributed to the diverging laser beams radial with the increasing distance, compromising the effectiveness of the sensor to detect an object. This indicates that the scanner will ensure the PL d rating for the smaller protection fields, as required by the ISO 3691-4, to enable the personnel detection system, while supporting a 64 m less reliable range, suited to both warning fields (requiring PL a) and navigation system.

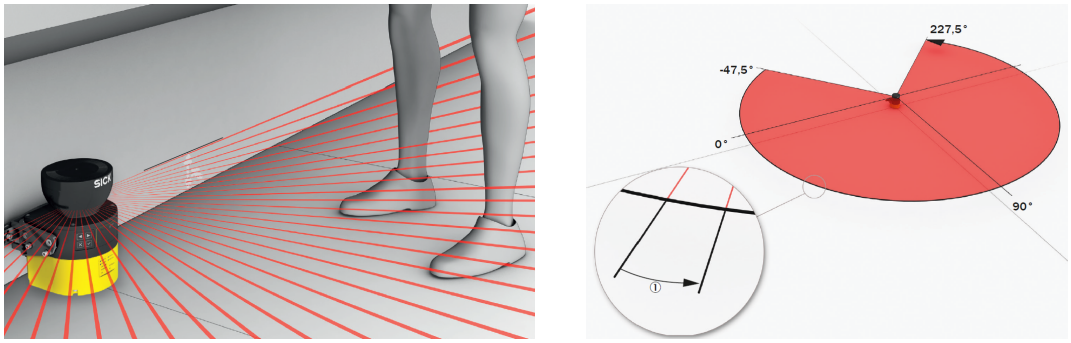

1. Angular resolution (divergence angle between beams)

Figure 4.17: Microscan 3 radial LiDAR functionality [80].

As previously stated, when a vehicle is moving at different speeds, turning or inverting the direction of travel, the mobile hazardous area will vary in shape and size. To address this, the MicroScan3 provides up to 128 "monitoring cases", of which multiple can be configured so as to enable the safety system to switch between fields and accompany different AGV manoeuvres.

Furthermore, the Microscan3 complements the navigation system, with LiDAR functionality, via the data output mode. This mode, which can be enabled to function in parallel to the safety functions, then provides navigation with the scanners measurement data, a cloud of points mapping the surroundings of the sensors.

Moreover, the scanners report additional info of the active monitoring case and field intrusion status to the navigation system. The non-safe additional data then enables the ANT lite$^+$ collision avoidance function, where, based on the active monitoring cases, the AGV routes, speed and manoeuvres can be planned so as to not trigger a safe stop by the protection fields. Therefore, the navigation system requires, a priori, the specification of the protection fields, namely their size and shape, corresponding to each monitoring case of the application.[9] In addition, upon personnel detection, the field intrusion status will signal the navigation system to carry out a controlled stop ramp so as to avoid an unnecessary SS0 trigger during autonomous navigation.

4.4 Conclusions

The current chapter presented the proposed methodology for tackling the problems set for this thesis.

[9]This functionality is available via the "hull shapes" of ANT lite$^+$, later detailed in Subsection 5.3.2.

This chapter firstly described the spool handling and transport required by creel systems for tyre manufacturing and subsequently identified the AGVS as a prominent solution for the process. The chapter then examined the targeted industrial application so as to define an AGVS architecture capable of carrying out the spool supply role. Furthermore, it reviewed the AGVS subsystems, describing their functionality and hardware, to establish the safety system for the creel AGVS application. The envisaged safety system is then described in further detail, showcasing the elements and architecture constituting the safety functions that will ensure the functional safety of the AGVS.

Chapter 5

Implementation

The following chapter outlines the carried out AGVS implementation, in accordance with the envisaged approach in Chapter 4. The first section details the design and configuration of the safety control logic. Subsequently, the chapter presents the approach to enable an effective personnel detection system. The third section delineates the implementation of the remaining AGVS modules required for validating the safety system, namely the drive controller and the natural navigation system, as well as a test environment modelled after the creel application.

5.1 Safety Control System

The defined approach to achieve functional safety for the AGVS application is centered on the Flexi Soft safety PLC. The control logic of the safety system was devised to perform the defined safety functions and tailored in particular for the creel AGV application.

The implementation of the safety system oversaw the design of the control logic for the Flexi Soft system (available in Annex B). The CPU0 controller module directs the safety program, interacting with the MOC1 module to access the drive-based safety functions and controlling the external elements connected via the XTIO module.

5.1.1 Drive Monitoring with MOC1

Drive-based functional safety, a crucial element of the established approach to AGVS safety, relies on the safe monitoring and control of the AGV drives. Accordingly, the MOC1 module was configured to provide the required drive-based safety functions.

Motion Data Acquisition

The foundation for the safe monitoring function of the AGV drives lies in measuring the drive motion with the encoder sensors. As was previously indicated, the resolver used in the close-loop control by the servo drives can be used as a second encoder to increase the reliability of the drive monitoring and achieve the set PL_r. For this purpose, the SIMCO servo drives were configured to emulate their respective resolver as an incremental encoder, encoding the sin-cos signal carrying the angular position of the motor shaft. The two encoder signals are subsequently sourced to the respective MOC1 module via an encoder gateway (depicted in Figure 4.8).

For monitoring the velocity (speed and direction) of the AGV, the safety system control requires the motion data of each wheel of the vehicle. Encoders are position sensors, and therefore, to attain the drive's operating speed, the MOC1 modules need to derive the wheel velocity from the position variation in time. The safety module then obtains the drive motion data as a rotational velocity, measuring the drive speed in Revolutions per Minute (RPM).

However, for AGVS applications, the safety functions depending on drive monitoring rely on the linear speed of the vehicle motion. The MOC1 module was then configured to convert the drive motion data to the linear velocity of the wheel based on the powertrain characteristics. The radius of the monitored wheels (r_w), measuring 0.1 m, is required for determining its linear speed. One revolution of the wheel implies different linear speeds for different wheel perimeters [81]. Moreover, the encoder sensors measure the motion of the drive directly on the motor shafts. Hence, the ratio of the reduction gearbox (1:31) between the wheels and motors must be considered.

Based on the presented principles, the conversion of the motor rotational speed (w_m RPM) to the wheel linear speed (v_w $\mathrm{m\,s^{-1}}$) is presented in Equation 5.1:

$$v_w = \frac{2\pi \cdot r_w \times w_m \times 31}{60} \tag{5.1}$$

After the speed conversion in MOC1, the encoders were set in the cross-compare mode for detecting motion acquisition failures and accordingly raised the PL of the function ("Speed Cross Check" function in Figure B.1).

Safe Discrete Speed Monitoring

The high reliability of the MOC1 drive monitor entails a trade-off in terms of logic flexibility and monitoring granularity. The safety system is not able to monitor the continuous speed of the drives. Instead, the system provides a discrete metric which encodes the drive's operating speed into successive Speed ID ranges.

The speed IDs also serve the SLS function for enacting a different speed limit based on the selected Speed ID. The drives are not allowed to exceed the upper limit of the active SLS Speed ID, in addition to the set SMS value of $1.2\,\mathrm{m\,s^{-1}}$ (according to the application's rated speed).

Furthermore, the modules provide the standstill status of the drive, required by particular operations of the creel AGVS. A safe validation of the vehicle standstill conditions is necessary when switching the AGV mode between manual and autonomous operation, as well as during the spool transferring operations.

The drive speed monitoring function provided by the MOC1 module is portrayed in the example diagram in Figure 5.1. The diagram showcases the monitoring function, namely the drive speed information provided to the safety program, in response to the varying linear speed of a drive. The SSM is represented in the "Speed status IDs", the SLS as the "Speed limits" and the SMS function as "Max speed limit".[1]

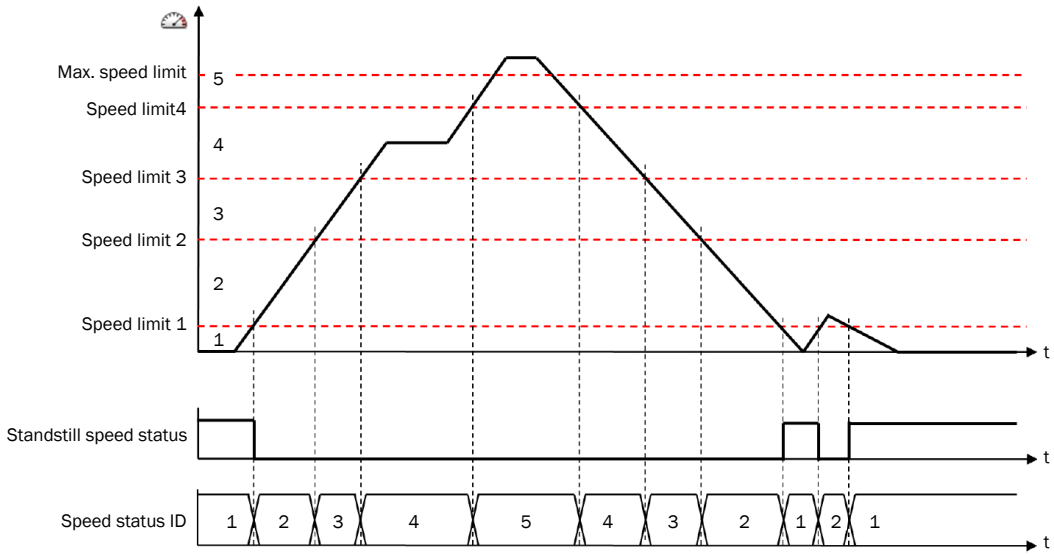

Figure 5.1: SMS sequence with five Speed ID (Amended from [76]).

[1]The speed ID 1 is reserved for the standstill range, a configured range where MOC1 reports a standstill status to the safety control program. This tolerance is necessary for filtering noise from the measured drive speed, which would invalidate the standstill position.

Safe Stop Monitoring

The safe stops of the AGVS, in particular the controlled stops of vehicle wheels, are implemented via the MOC1 modules. As previously described, the controlled stops reliability is not intrinsic given the unreliable speed control by the SIMCO drives. Instead, the safe monitoring of their stop ramp and a "fallback" safe stop achieve their set PL_r.[2] Therefore, the MOC1 module was configured to perform the SS1 and SS2 procedures and monitor the stop ramp to trigger an SS0 function should the non-safe control fail.

Upon receiving an SS1 or SS2 command from the safety program, the MOC1 module will process the respective function following the sequences presented in Figure 5.2, in accordance with the EN/IEC 61800-5-2 norm.

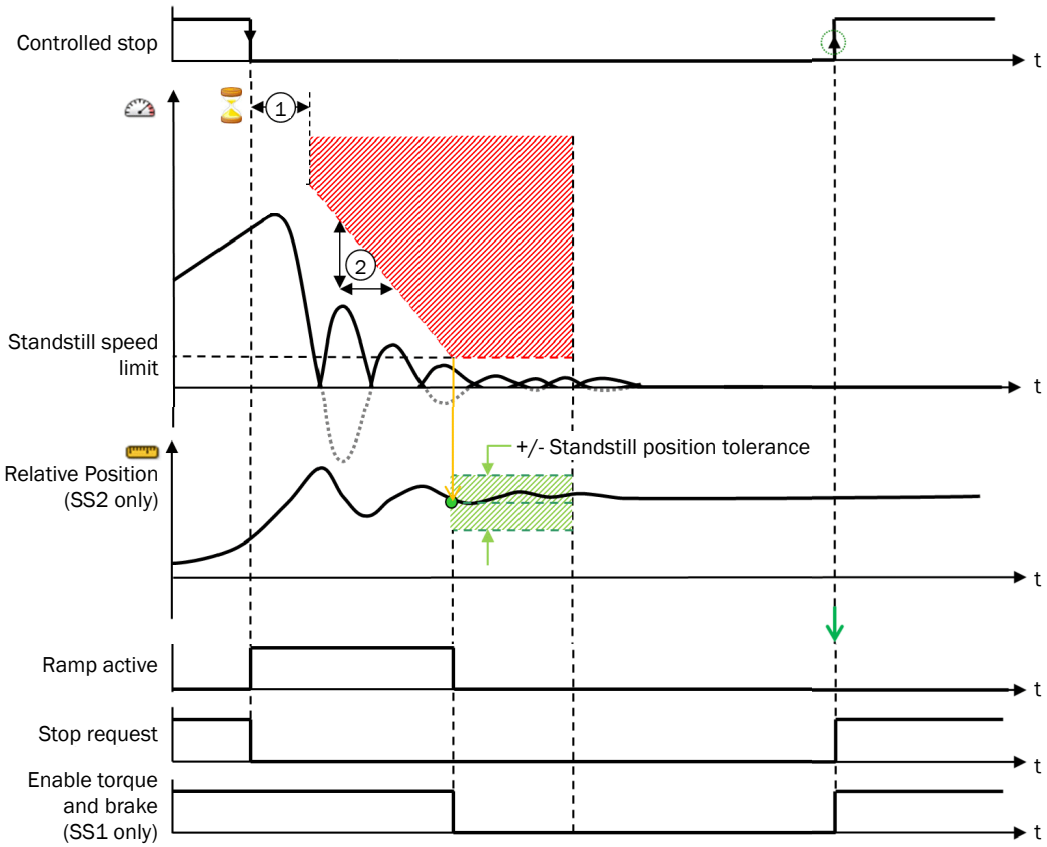

1. Delay time until start of ramp
2. Steepness of stop ramp

Figure 5.2: Safe controlled stops sequence (Amended from [76]).

The safe stop function will immediately emit a "Stop request" so that the drive controller initiates a controlled stop. Once the wheel has reached a standstill, with

[2]Unlike the SSM function, the safe stop monitoring relies on continuous drive speed rather than the Speed ID approach.

the drive operating below the delimited “Standstill speed”, the procedures are taken according to the respective stop function.[3]

In an SS2, during the remainder of the controlled stop, the MOC1 module continuously oversees that the standstill speed is not exceeded.

For an SS1 type stop, after reaching the standstill speed, the module enacts STO and SBC via the "Enable brake" and "Enable Stop" signals. Unless an SS0 stop was triggered during the controlled stops, the functions are concluded when the safety program lifts the respective “Controlled stop” request to the MOC1.

The steepness of the ramp (② from Figure 5.2) must be configured according to the deceleration capacity of the drive during a controlled stop. Furthermore, a ramp start delay (① from Figure 5.2) is necessary to account for the reaction time of the drive system in responding to the stop request of the safety system. An incorrect configuration of these parameters might result in unnecessarily triggering an SS0, even when the motor is decelerating as intended.

The steepness of the stop ramp directly impacts the personnel detection system, given that a slower deceleration results in a larger hazardous area from the moving vehicle. Accordingly, the increased braking space requires larger protection fields, reducing the AGV flexibility for navigating through narrow environments. Therefore, a faster deceleration is advantageous for the AGV application.

The AGV controlled deceleration (a) is determined by the servo motors torque (τ) [82], the mass of the structure that the two motors must decelerate ($M/2$), and the radius of the vehicle wheels (r_w). Equation 5.2 demonstrates how to calculate the resulting deceleration of the AGV structure with two traction wheels [81].

$$\begin{cases} \tau = r_w \cdot F_a \\ F_a = \frac{M}{2} \times a \end{cases} \quad (=) \quad a = \frac{\tau}{\frac{M}{2} \times r_w} \tag{5.2}$$

The minimum guaranteed torque provided by the motor, the continuous stall torque, is of $62.5\,\mathrm{N\,m}$, resulting on a deceleration (a_{stall}) of $0.569\,\mathrm{m\,s^{-2}}$, as shown in Equation 5.3:

$$a_{stall} = \frac{62.6\,\mathrm{N}}{\frac{2200\,\mathrm{kg}}{2} \times 0.1\,\mathrm{m}} = 0.569\,\mathrm{m\,s^{-2}} \tag{5.3}$$

Although the acceleration requirement for the AGVS ($0.4\,\mathrm{m\,s^{-2}}$) is fulfilled by a_{stall}, this deceleration proved too slow for the differential drive braking kinematics, resulting in large protection fields that would compromise the creel application.

[3]The standstill tolerance potentiates a hazard caused by a low-speed motion. To counteract this exemption, the module monitors the travelled distance with the drive during the SS2 standstill, which, when surpassing a configured threshold (“Standstill Position tolerance”), escalates to an emergency SS0 and inhibits further movement.

Nevertheless, the servo motor provides a peak torque (τ_{peak}) profile, capable of providing a torque up to 223 N m for short periods.[4] With τ_{peak} the AGV is able to reach a deceleration (a_{peak}) of 2.027 m s^{-2}, as shown in Equation 5.4:

$$a_{peak} = \frac{223\,\mathrm{N}}{\frac{2200\,\mathrm{kg}}{2} \times 0.1\,\mathrm{m}} = 2.207\,\mathrm{m\,s^{-2}} \tag{5.4}$$

The service brake included in the powertrain system provides a braking power torque of 5 N m [84], which, following the 1:31 gearbox ratio, provides a braking torque at the output of 155 N m. The ensuing deceleration (a_{br}) of the AGV with the service brake is of 1.409 m s^{-2} (as shown in Equation 5.5), which is the effective deceleration (a_{ss0}) during an SS0 emergency stop.

$$a_{br} = a_{ss0} = \frac{155\,\mathrm{N}}{\frac{2200\,\mathrm{kg}}{2} \times 0.1\,\mathrm{m}} = 1.409\,\mathrm{m\,s^{-2}} \tag{5.5}$$

Defining the controlled stop ramp with a steeper deceleration than that of the fallback SS0 brake deceleration would prolong the hazard in case of a ramp failure. Therefore, the lower deceleration of the two was considered for the stop ramp. Accordingly, the controlled stop deceleration was configured as 1.3 m s^{-2} (slightly lower than a_{ss0} for a tolerance margin).

The delay for the start of the stop ramp considered the cycle time of the MOC1 and CPU0 modules (respectively 4 ms and 8 ms) and the controller reaction time to actuate the motors (70 ms), totalling an 82 ms delay.[5]

Drive Monitor Integration in the Safety Program.

The MOC1 module provides the configured drive-based safety functions to the CPU0 controller module, and the safety program will subsequently enable functional safety for the AGVS application. Therefore, the CPU0 is required to interact with the MOC1 modules of each drive and exchange the necessary data for the functions.

The data exchange between the safety program in CPU0 and the MOC1 drive-based safety functions is summarized in Figure 5.3.

For the drive monitoring functions related to the wheel velocity, the MOC1 modules provide the detected Speed ID and wheel direction of each respective drive so that the safety program is then able to identify the motion of the AGV.

[4]The τ_{peak} is typically provided for accelerating and decelerating the load against the inertia in the system. The motor operation under τ_{peak} conditions for longer periods would overheat the motor, which could result in permanent damage [83]. Nonetheless, the AGVS application will operate the drives in the "Profile Velocity" mode, where the SIMCO drive system controls the servo torque and prevents the motor from overheating.

[5]The performance requirements by the Ant lite^{+} were used as the cycle time of the drive control system, setting a maximum 20 ms delay signal propagation and 50 ms control reaction time [62].

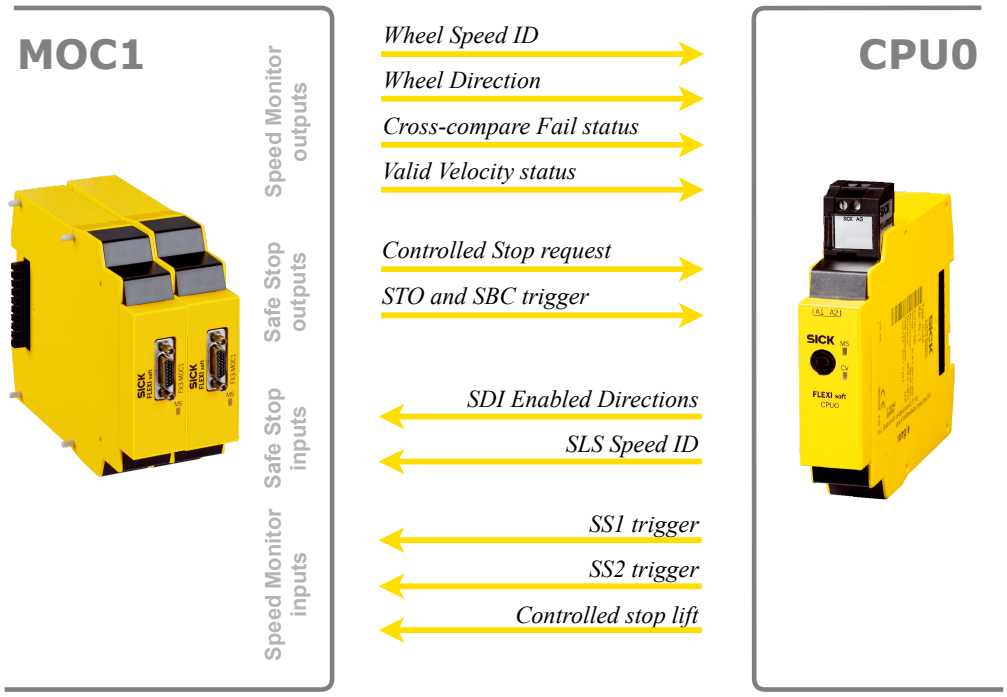

Figure 5.3: Drive-based function information flow for the safety control logic [69, 71].

Furthermore, the "cross-compare status" indicates a failure during the motion data acquisition and a "velocity validity status" reports any violations of speed or direction limits by the drive motion, such as the SMS and active SLS and SDI.

From the safety program, the MOC1 modules receive the active Speed ID limit (SLS) and permissible wheel directions (SDI) to enforce on the respective drive, according to the operation requirements of the AGV application.

For enacting a safe stop, the safety program will trigger either an SS1 or SS2 on the MOC1 modules. Upon fulfilling the safe stop conditions, a reset signal is sent to the modules for lifting the active stops.

For processing the safe stop procedures, the MOC1 modules signal CPU0 to request a controlled stop to the drive controllers. Furthermore, the modules issue a command signalling the safety program to enact STO and SBC at the end of the SS1 procedure or SS0 in the event the controlled stop fails.

The resulting logic configuration of the MOC1 drive monitor modules in the Flexisoft system is available in Annex B.1.

5.1.2 Safety Control Program with CPU0

The safety program has the role of monitoring the AGVS application and coordinate the safety system to react accordingly to any emerging hazards. The CPU0 module

was then configured to execute the safety program logic that provides functional safety for the creel application, with the emphasis on ensuring personnel safety during the AGV navigation.

Discrete Motion Detection

Identifying the motion of the vehicle is of particular importance for the personnel detection system, as the protection fields must be adapted to attend to the hazards presented by the AGVS manoeuvres.

From the motion data provided by the MOC1 modules, namely the speed and direction of each drive, the safety program is then able to detect the motion that the AGV is performing. Given that the drive motion data is provided via Speed ID ranges, the approach was to categorize the different motions of the AGV in line with the "differential IDs". These motion categories result from the combination of the Speed ID of each wheel and their respective direction. As a result, the safety system cannot identify the precise motion of the vehicle.

If both drives report the same Speed ID, possibly travelling with the same velocity set at both wheels, the safety system cannot reliably assess that the AGV is moving in a straight motion. Instead, the safe speed monitored value, with the reliability of the defined PL_r, is the infinite set of vehicle manoeuvres within the motion category.

The increasing AGV speeds require larger braking spaces. As a result, broader Speed ID ranges and motion categories lead to larger protection field areas which compromise the AGV navigation flexibility. The presented issue is intrinsic to discrete drive monitoring and can be addressed by increasing the monitoring granularity. This was achieved by utilising all nine available Speed IDs in MOC1 and, subsequently, segmenting the introduced motion patterns into different motion categories. Consequently, the granular monitoring reduced the protection fields required by the safety system, particularly important for the higher speeds straight categories.

AGV Motion Categorization

For defining the motion categories that the safety system will enforce on the AGV, it is necessary to understand the motion requirements of the creel application.

The assessment of the application routes and manoeuvres identified that the AGV is not required to turn at the drive's rated speed. In effect, turning manoeuvres are limited to slower operations. The manoeuvres for navigating around the spool rack aisles, positioning the AGV for spool transfer operations, stationing in the battery charging docks, or other position adjustments are all operations performed under lower speeds. In addition, the manoeuvres requiring tight space clearances do not permit the larger protection fields imposed by higher speeds.

Therefore, the safety system will "forbid" movements outside the scope of the application, namely turning and *pivot* manoeuvres at higher velocities (configured logic available in Annex B.2). The application, in particular the navigation system, must in turn be designed to not operate at these conditions to avoid triggering the safety system.

The application's permissible arrangements of differential Speed IDs, each representing a reliable set of AGV motions, were then grouped into motion categories in Table 5.1.[6] Given the considered AGV motion requirements, except for the *pivot* motion, all other categories require the same direction on both wheels. Additionally, each category is subdivided between forward or backward motions, according to the simultaneous direction of the wheels.

Table 5.1: AGV motion categories.

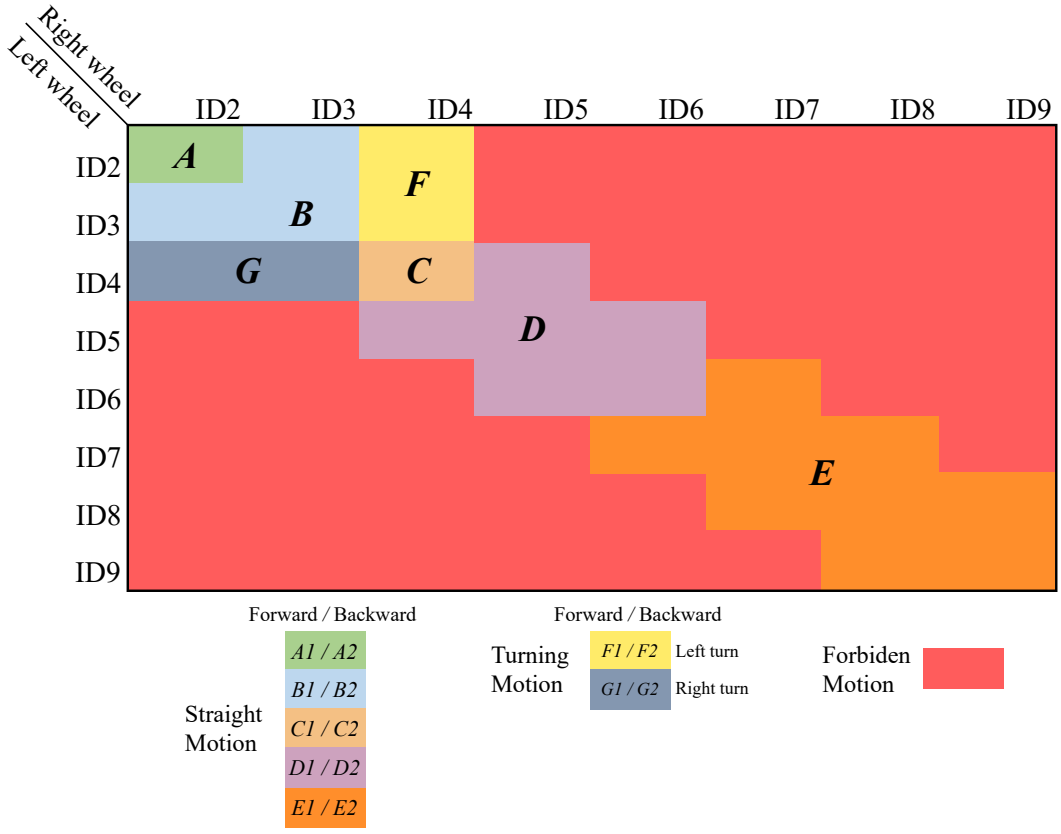

The presented categorization resulted from the following distinct motion patterns:

- Straight motion (**A** to **E**) - When the wheels report the same Speed ID, the AGV movement was categorized as a "straight" motion (the safety system still accommodates turning manoeuvres within the ID Speed ranges). These are

[6]The implemented logic for the detection and categorization of the AGV motion is available in Annexes B.3 and B.4

the only motion categories allowed for higher speed operation of the vehicle. In a notable characteristic, the drive monitors may report different Speed IDs as the wheels rotate near the limit between two Speed ID ranges, despite the vehicle travelling in a relative straight motion. Therefore, to accommodate these "transitory speeds", the straight motion categories needed to include consecutive Speed IDs. The AGVS can then rely on the safety system to guarantee a straight motion category at higher speeds.

- Turning motion (**F** and **G**) - When the monitored wheels report different Speed IDs (excluding the transitory speeds), the safety system is able to reliably detect a turning motion and its direction (the lower ID wheel side will be the turning direction). By segmenting the turning categories for single side turning (such as categories F and G), the protection fields are no longer required to consider the opposite side of the manoeuvre, increasing the navigation flexibility. Furthermore, for effectively exempting the sharper turns out of the operation, turning differential Speed IDs more than two ranges apart are to be considered forbidden turning.

- *Pivot* motion (**H2**)- The assessment of the straight and turning motion categories ensures that the wheels operate in the same direction. However, for *pivot* manoeuvres, the safety system permits the AGV wheels to function in opposite directions. The *pivot* category was then restricted to lower speeds (ID2) via the SDI function of the drive monitor.

Speed ID Ranges

The assignment of the Speed ID ranges in the MOC1 module was configured according to the needs of the creel application, as presented below:[7]

- ID2- The more intricate manoeuvres requiring a *pivot* motion, such as navigating tight spaces, require the smaller protection fields. These maneuvers operate within lower speeds ranging between $0.0\,\mathrm{m\,s^{-1}}$ (ID1) and $0.2\,\mathrm{m\,s^{-1}}$.

- ID3- The Speed ID3 range was set between $0.2\,\mathrm{m\,s^{-1}}$ and $0.3\,\mathrm{m\,s^{-1}}$, following the safe limits set by the standard for the maintenance mode [50]. The safety program can then enforce SLS with the Speed ID3 limit when the maintenance mode is selected.

- ID4- Subsequently, the Speed ID4 defines the higher permissible turning speeds limited to $0.6\,\mathrm{m\,s^{-1}}$. Up to ID4, the safety system permits all AGV differential speeds. The speed limit was determined according to the available clearance

[7] The values of the Speed ID ranges were determined in an iterative tuning process relying on the protection field simulation results presented in Table 6.4. Based on the resulting field sizes, it was possible to specify the speed ranges that fulfil the roles assigned by the creel application.

for turning, namely the space between spool racks for circumnavigating the rack isles.

- ID5 to ID9- The remainder of the Speed IDs are strictly used for straight motion category manoeuvres. As previously stated, segmenting the straight motion category reduces the mobile hazardous region, thus allowing for smaller protection fields. Otherwise, due to the uncertainty of the AGV motion detection with discrete monitoring, the high-speed protection areas would become too large for the application. The Speed ID9 then sets the limit to the AGV rated speed ($1.2\,\mathrm{m\,s^{-1}}$) with SMS.

Table 5.2 presents the configured ranges for each Speed ID, defining the maximum wheel speed preceding the next Speed ID reported by the MOC1 module.

Table 5.2: Speed ID ranges.

Speed ID	ID1	ID2	ID3	ID4	ID5	ID6	ID7	ID8	ID9
Max range speed ($\mathrm{m\,s^{-1}}$)	0.0	0.2	0.3	0.6	0.75	0.9	1.0	1.1	1.2

Safe Stop Control

For a safe operation of the AGVS application, the safety system must ensure that emerging hazards are addressed accordingly. The system then relies on the implementation of the safety program logic to deploy the safe stop best suited to the encountered danger and interrupt the machine's operation.

The implemented control logic was designed to react to hazard indicators such as a manual emergency, a personnel detection, or a detected control failure of the application to operate within specification.[8]

Emergency Stop Control

As per the design presented in Subsection 4.3.3, a manual emergency enacts an SS0 procedure for immediately removing the power of the drives. The vehicle was suited with two emergency buttons, ensuring their accessibility to personnel, which are monitored by the safety program to trigger an SS0 when pressed.

Furthermore, the safety program was designed to handle a powertrain control failure as an emergency stop. However, unlike manual emergencies, these incidents provide the leeway for performing an SS1 controlled stop without the need for an abrupt interruption and, as a result, avoid any abrasion to the machine. Therefore,

[8]The program logic for enacting the safe stops, including the respective stop conditions and reset procedures, is available in Annex B.5.

the safety program monitors drive control failures reported by the MOC1 modules, namely the "cross-compare status" and "velocity validity status" (Figure 5.3), to trigger an SS1. In addition, the detection of a forbidden motion, as per its definition in the previous section, represents an AGVS operation out of the application's specification and thus is also handled as an emergency stop. These presented monitored elements are the SS1 conditions, which, should either one indicate a drive control failure, trigger the emergency controlled stop.

Following an emergency stop, the program then requires manual intervention for restarting the operation so that an operator may assess and address the encountered hazard. The vehicle is embedded with a dedicated button for a manual reset, which, after the conditions triggering the emergency are rectified, can be operated to request the safety program to resume the application.

The flowchart in Figure 5.4 showcases the implemented program logic for the SS0 and SS1 emergency stops, including the controlled stop procedures by the MOC1 module.

Personnel Detection Control

The safety program manages the personnel detection system according to the AGVS application.

The adaptation of the protection field requires the AGV motion details to fully encompass the mobile hazardous area according to the vehicle manoeuvres. In turn, the personnel detection system alerts the safety program to any imminent hazard perceived so as to safely stop the vehicle before a collision.

Based on the motion detection function, the safety system is able to reliably attribute the appropriate protection field to each motion category matching the AGV manoeuvres. The program interacts with the safety laser scanners to select the protection fields throughout the AGVS operation.[9]

For the active motion category, the personnel detection system safely monitors the corresponding mobile hazardous region. The system detects any breach in the protection field, which will then signal the safety program to trigger a non-emergency controlled stop via the SS2 function.

Following the safe stop, the AGV operation is automatically restarted after the protection fields are cleared and a mandatory two seconds delay with the appropriate warning signals.

The presented functionality was implemented following the logic flowchart in Figure 5.5.

[9]The field switch logic implementation is available in Annexes B.6 and B.7.

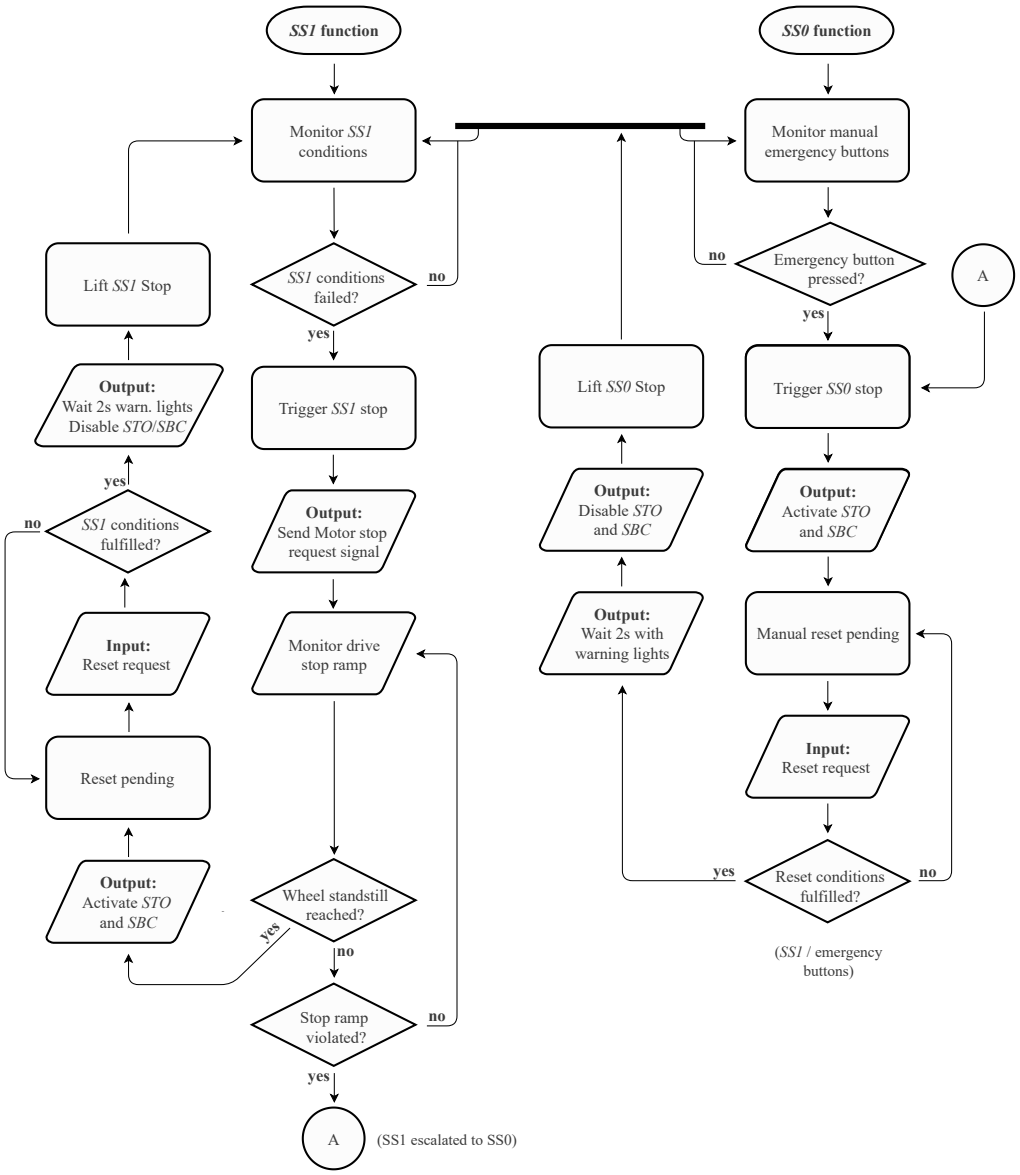

Figure 5.4: Flowchart of the safe control logic for emergency stops.

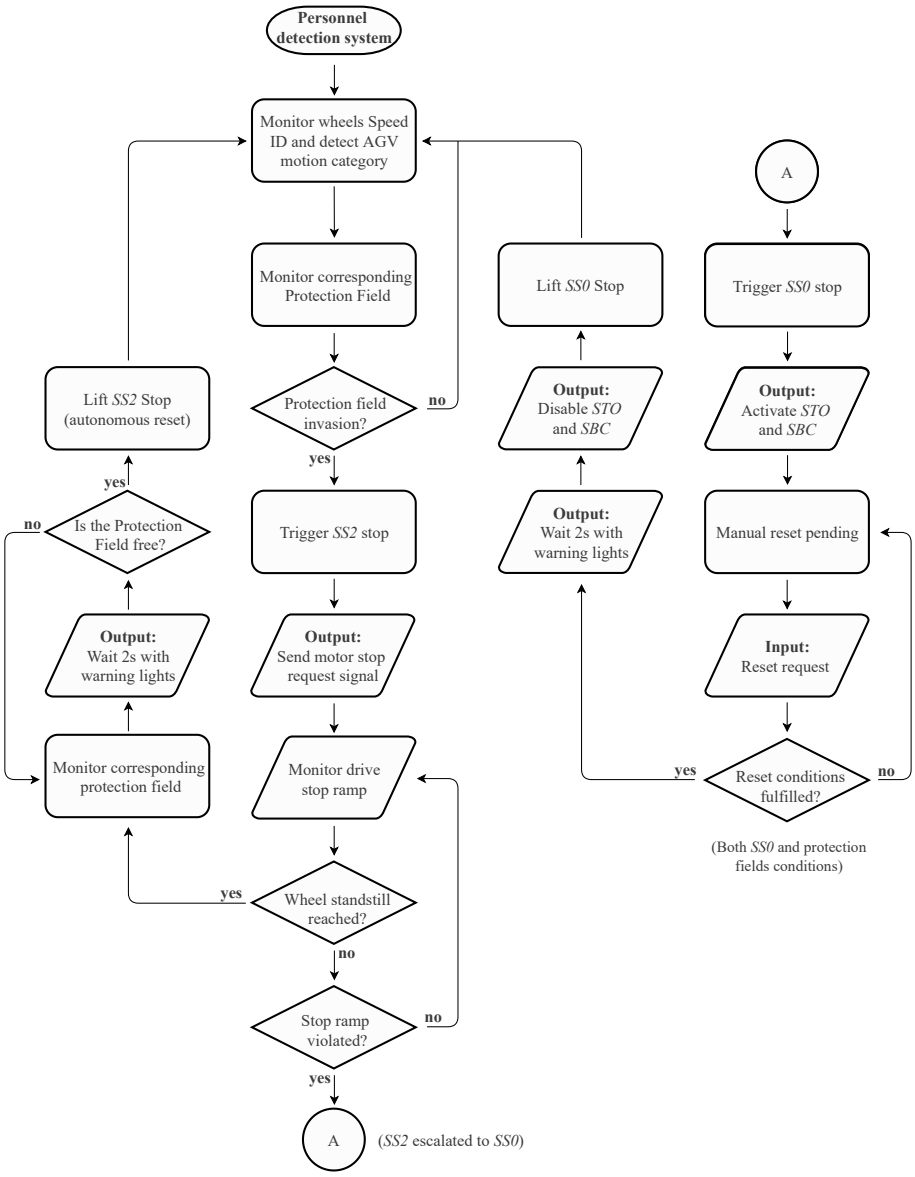

Figure 5.5: Flowchart of the personnel detection system control.

5.2 Personnel Detection System

The implementation of the personnel detection system must ensure the protection of people from the intrinsic hazards of the AGV navigation in an unconstrained environment. In order to preserve the functional safety of the application, the protection fields must comprehend the entire mobile hazardous region. To achieve this, it was first necessary to determine the ensuing hazardous area from the AGV manoeuvres and then configure the ESPE devices, the MicroScan3 scanners, to monitor their respective protection fields.

5.2.1 Determining the Hazardous Area of an AGVS

The vehicle must be safely stopped before impact with a stationary person. The personnel detection system must then continuously monitor the protection field so that the safety system can react in case the area is breached. The necessary space to react and brake the vehicle to a standstill, considering the reach of the AGV structure, in effect, represents the hazardous area, as the safety system cannot prevent an imminent collision.

Thereby, determining the necessary stopping distance requires predicting the movement of the AGV during braking. Subsequently, it is possible to identify the reach of the vehicle structure in the traversed space and accordingly design the protection fields that cover the hazardous area.

Envisaged Implementation Approach

To effectively provide personnel protection, the safety system must consider the full range of manoeuvres intended by the application and address the danger posed by the AGV structure under the operating conditions.

Therefore, the approach to determine the mobile hazardous area from the AGV application was to model the vehicle structure kinematics. Furthermore, given the discrete speed monitoring, with each motion category comprising a range of possible wheel speed arrangements, all permissible manoeuvres were considered to attain the limits of the hazardous region.

Modelling the Vehicle Braking Kinematics

For defining the kinematics of a differential drive vehicle, the drive wheels, which determine the velocity of the AGV, must be modelled. Aiming to analyse the hazardous region of the vehicle, the origin of the braking kinematics is set to the instantaneous position when the braking space is breached. Therefore, the model must take into account the reaction time (t_r) between the occurring hazard until the AGVS initiates the controlled stop.

Following the equations of linear motion mechanics [85], each wheel's speed until the vehicle brakes to a halt ($V = 0$) can be described in function of time following Equation 5.6. The AGV initially travels with constant wheel speed (v_i). After reaching t_r, the vehicle begins braking with a continuous deceleration (a_b) specified by the drives.[10]

$$v(t) = \begin{cases} v_i \ , & t \leq t_r \\ v_i + a_b \cdot (t - t_r) \ , & t > t_r \end{cases} \tag{5.6}$$

The vehicle motion can be modelled by the differential drive kinematics introduced in Subsection 4.2.3. However, as both the turning radius (R_{icc}) and rotational speed (ω) are contingent on the instantaneous speed of the wheels (in function of v_l and v_r), these differential drive principles will change dynamically during the braking motion, as represented in Equation 5.7.[11]

$$R_{ICC}(t) = \frac{l}{2} \frac{v_l(t) + v_r(t)}{v_l(t) - v_r(t)} \ , \quad \omega(t) = \frac{v_r(t) - v_l(t)}{l} \tag{5.7}$$

The space referential, necessary to determine the reach of the AGV during braking, was set to the initial conditions of the braking event (upon breach of the protection field) and was defined as presented in Figure 5.6. The origin of the Cartesian coordinate system was set at the midpoint between the wheels (AGV centre), the x axis aligned with the axle of the wheels and the y axis accordingly perpendicular.

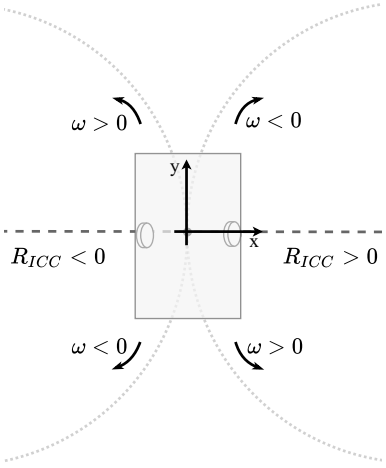

Figure 5.6: Frame of reference for the differential AGV.

[10] Assuming a constant v_i and a_b is a simplification of the model that may be improved in the future. These shortcomings are reviewed in Subsection 6.2.1.

[11] The differential drive referential was defined differently than in [68], previously presented in Equation 4.2. The turning radius R_{icc} referential remained the same. Turning right $\left(|v_l| > |v_r|\right)$ results in $R_{icc} > 0$, and $R_{icc} < 0$ when turning left ($|v_l| < |v_r|$), fitting the x axis reference. However, the vehicle rotation velocity ω was set to follow counterclockwise direction ($\omega > 0$ for $v_r > v_l$) so as to follow the trigonometry unit circle and directly translate to the Cartesian coordinate system.

Furthermore, the model showcased in Figure 5.6 foresees four distinct turning movements available to the AGV. Based on the movement direction on each axis, the vehicle is travelling forwards ($y > 0$) or backwards ($y < 0$), in combination with turning either left ($x < 0$) or right ($x > 0$).

The linear speed ($V(t)$) of the AGV centre is defined in Figure 5.7.

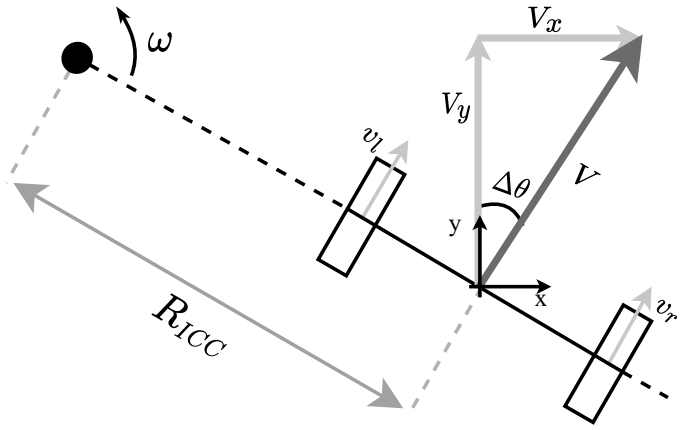

Figure 5.7: Differential velocities diagram.

Following the principle of rotational to linear motion conversion of instantaneous velocity [81], $V(t)$ can be derived from the rotational speed ($\omega(t)$) given the turning radius (R_{ICC}), as showcased in Equation 5.8.[12]

$$V(t) = -\omega(t) \cdot R_{ICC}(t) = \frac{-(v_r(t) - v_l(t))}{\cancel{l}} \cdot \frac{\cancel{l}}{2} \cdot \frac{v_l(t) + v_r(t)}{v_l(t) - v_r(t)} (=)$$

$$V(t) = \frac{v_l(t) + v_r(t)}{2} \tag{5.8}$$

As previously established, the AGV can be described in the space by the vehicle pose (x, y and θ). The vehicle orientation shift, since the beginning of the braking event, is represented by $\Delta\theta$. Given the defined frame of reference, the vehicle is initially aligned with the vertical y axis, and, therefore, $\Delta\theta$ differs from the vehicle's actual orientation θ by $\frac{\pi}{2}$.

From the pose velocity $(V_x(t), V_y(t), \omega(t))$, the vehicle's position in the plane can be outlined, since the start of the braking event. By calculating the integral of the function describing the velocity, one is able to determine the travelled distance and

[12] As the rotation reference for ω was inverted to the counterclockwise direction, the sign inversion affects the calculation of $V(t)$, which is inverted. The linear speed sign, although a scalar metric, results in a shift of $-\pi$ when calculating the vector $\mathbf{V(t)}$ for determining the AGV velocity on each axis. A negative $V(t)$ would represent a starting backwards movement of the AGV. Therefore, to restore the correct value with a total 2π shift, $-\omega$ is used to determine $V(t)$.

orientation within the said time interval [85]. Following this principle, the vehicle's pose throughout the braking motion can be attained from the pose velocity.

As seen in Equation 5.9, the vehicle orientation shift, $\Delta\theta(t)$, can be determined from the rotational speed.

$$\Delta\theta(t) = \int_0^t \omega(t)dt \tag{5.9}$$

Furthermore, following the motion diagram in Figure 5.7, the linear velocity on each axis can be derived from the vehicle velocity and its orientation during the braking motion θ, as presented in Equation 5.10. Subsequently, the position of the AGV centre on each axis is outlined by Equation 5.11.

$$\begin{cases} V_x(t) = V(t) \cdot \cos\left(\Delta\theta(t) + \frac{\pi}{2}\right) \\ V_y(t) = V(t) \cdot \sin\left(\Delta\theta(t) + \frac{\pi}{2}\right) \end{cases} \tag{5.10}$$

$$\Delta x(t) = \int_0^t V_x(t)dt\ , \quad \Delta y(t) = \int_0^t V_y(t)dt\ . \tag{5.11}$$

Kinematics of Hazardous Area

As the collision prone area comprises the reach of the entire AGV structure, its own kinematics must be assessed so as to effectively monitor the hazardous area.

The corner edges of the structure trace the reach of the vehicle in the horizontal plane.[13] Based on the outlined pose of the AGV throughout the braking action, it is possible to trace the motion of the vehicle corners, as they are fixed to the structure, and determine the full reach of the hazardous area.

The structure edges, represented in Figure 5.8, are all equidistant to the AGV centre (D_{edge}) and slanted from the vehicle's vertical axis by θ_{edge}. Following this premise, and based on the structure dimensions, length (l) and width (w), the edge defining parameters can be determined according to the Equations in 5.12.

$$\theta_{edge} = \tan^{-1}\left(\frac{w/2}{l/2}\right), \quad D_{edge} = \sqrt{\left(\frac{l}{2}\right)^2 + \left(\frac{w}{2}\right)^2} \tag{5.12}$$

As the edge corners parameters describe the constant offset of each corner relative to the AGV centre, the kinematics which outline the edges can be derived from the pose kinematics of Equations 5.9 and 5.10.

[13] For this approach to be valid, all vehicle elements must be enclosed inside the rectangular-shaped vehicle and shall not "leak" out during navigation. If required, the rectangular area must be increased to encompass the extent of all elements.

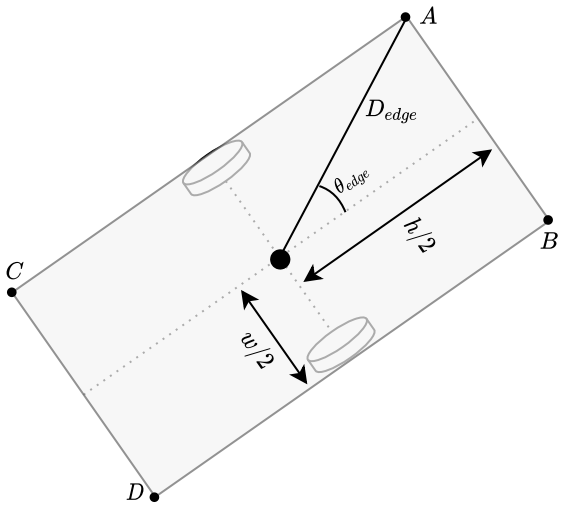

Figure 5.8: Edge geometry of the AGV structure.

Following the diagram in Figure 5.8, the orientation of the corner edges relative to the defined frame of reference in Figure 5.7 was profiled in Equation 5.13.

$$\begin{cases} \theta_a = \Delta\theta + \frac{\pi}{2} + \theta_{edge} \\ \theta_b = \Delta\theta + \frac{\pi}{2} - \theta_{edge} \\ \theta_c = \Delta\theta + \frac{3\pi}{2} - \theta_{edge} \\ \theta_d = \Delta\theta + \frac{3\pi}{2} + \theta_{edge} \end{cases} \tag{5.13}$$

Subsequently, based on each corner's orientation and their distance to the centre of the structure, the corners' kinematics is outlined in Equation 5.14. The reach of the structure, throughout the braking motion of the AGV, can now be outlined in order to identify the hazardous region.

$$\begin{cases} a_x(t) = \Delta x(t) + D_{edge} \cdot \cos(\theta_a) \\ b_x(t) = \Delta x(t) + D_{edge} \cdot \cos(\theta_b) \\ c_x(t) = \Delta x(t) + D_{edge} \cdot \cos(\theta_c) \\ d_x(t) = \Delta x(t) + D_{edge} \cdot \cos(\theta_d) \end{cases}, \begin{cases} a_y(t) = \Delta y(t) + D_{edge} \cdot \sin(\theta_a) \\ b_y(t) = \Delta y(t) + D_{edge} \cdot \sin(\theta_b) \\ c_y(t) = \Delta y(t) + D_{edge} \cdot \sin(\theta_c) \\ d_y(t) = \Delta y(t) + D_{edge} \cdot \sin(\theta_d) \end{cases} \tag{5.14}$$

The modelled braking AGV corners kinematics for a left-turning motion is portrayed in Figure 5.9.[14]

[14]The plots were obtained with the numerical simulation of the modelled braking kinematics of Subsection 5.2.2.

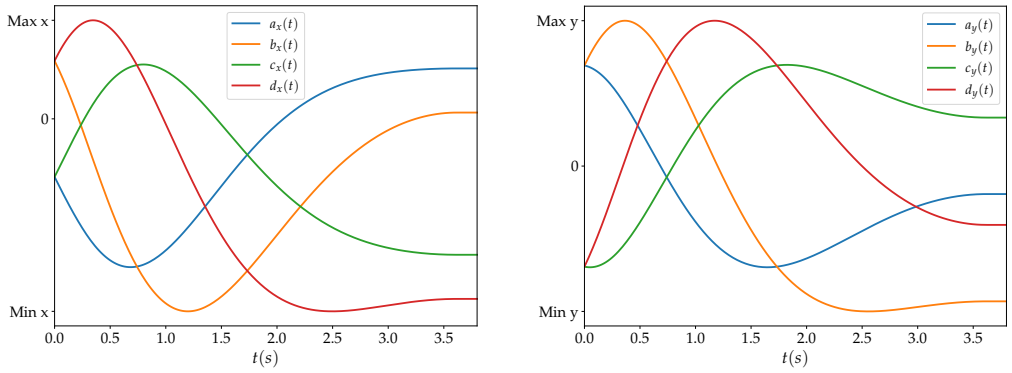

(a) Corners reach in x

(b) Corners reach in y

Figure 5.9: AGV corners braking kinematics following a hazard detection, for a given initial vehicle speed.

5.2.2 Protection Field Sizes

Determining the protection field areas for the personnel detection system relies on the developed mathematical model of the AGV structure kinematics.

However, calculating the mobile hazardous region associated with an AGV manoeuvre requires a complex evaluation of the reach of each corner throughout the entire braking motion. Furthermore, performing such an analysis for all possible differential arrangements within each motion category results in an arduous task. Therefore, the solution was to perform a numerical simulation of the conceived kinematic model to calculate the hazardous areas.

Discrete Simulation of the Braking Kinematics

For a given differential velocity, a simulation model is able to outline the AGV pose throughout the braking motion and determine the global maximums and minimums reached by the vehicle structure on each axis. The simulation was devised via the Python script available in Annex C.1, which reflects the defined kinematic model of the AGV and its structure.[15]

Furthermore, determining the resulting hazardous area for the creel application requires the AGVS-specific kinematic parameters.

The parameters defining the AGV structure follow the vehicle mechanical design for the creel application, which were set as follows:

- Width=1116 mm;
- Length=1936 mm;
- Axle length=903 mm.

[15]For determining the pose of the vehicle, the integrals were calculated using the midpoint Riemann sums, a numerical integration method. This method, as well as other approaches to numerical integration, are presented and compared in [86].

The reaction time (t_r) of the AGVS, since the breach of the protection field until the vehicle begins to decelerate, also needs to be evaluated. For the designed AGVS architecture, t_r comprehends the response time of the ESPE devices, the safety program logic processing time, and lastly, the delay of the drive control system to actuate the safe stop. The brake reaction stages are sequenced as follows:

1. MicroScan3 provides a scan cycle time of 40 ms, requiring four scan samples per measurement. Adding to the EFI-Pro communication link maximum delay of 35 ms, the total response time from the ESPE device results in 195 ms.

2. Subsequently, alerted to the hazard by the ESPE device, the safety program requires a CPU0 cycle of 8 ms to trigger the SS2 function on the MOC1 module (cycle of 4 ms). In turn, the MOC1 module signals the safety program to request a controlled stop to the drive controllers (additional CPU0 cycle). Thus, the safety program process requires a total of 20 ms.

3. Lastly, the drive control system (already evaluated in Subsection 5.1.1) follows a specified maximum delay of 70 ms to enact the controlled stop.

4. An additional delay is required when there is a change in the detected motion category and respective protection field. During the switching of the motion categories, the corresponding field may be invaded by a person, compromising the reaction of the safety system. Accordingly, the field commutation time of 52 ms must then be considered.[16]

Hence, the reaction time to be considered by the simulation model, totalling the presented stages, results in $t_r = 337\,\text{ms}$.

Following the reaction time, during which the vehicle is considered to travel at a constant differential velocity, the model simulates the deceleration of the drives. The braking follows a stop ramp at an a_b rate defined according to the AGVS powertrain specification. Considering that the personnel detection system is to deploy a controlled stop as the braking procedure upon detecting a hazard, the configured a_b needs to match the safe stop monitoring ramp of SS2. Therefore, the stop deceleration of the simulation was defined as $a_b = -1.3\,\text{m}\,\text{s}^{-2}$.

Hazardous Region Simulation for Discrete Drive Monitoring

Given the AGVS follows a discrete drive monitoring, all possible arrangements for the wheels' initial velocities (v_i) for each Speed ID must be simulated. Using the previous implementation of the kinematic model, it is then possible to determine the maximum reach of the AGV structure for each motion category of the application.

[16] This delay consists of a MOC1 cycle for detecting the new motion category, a CPU0 cycle for selecting the new field with a 28 ms network delay [80], and an additional 12 ms minimum delay for switching between fields in the MicroScan3 device.

To outline the limits of the hazardous area, the script in Annex C.2 will simulate all v_i arrangements and compare the registered global maximums and minimums on the x and y axes. For each motion category, the script will identify the furthest reaches of the structure in reference to the AGV's initial position.

For the motion categories with the same direction in both wheels, the script simulates the hazardous area for the different Speed ID ranges defined in Table 5.2, which can then be grouped to outline the hazardous area for each motion category. Likewise, the *pivot* category is simulated with both wheels' direction and limited to Speed ID 2, as defined by the application for permitting *pivot* manoeuvres.

Protection Supplements

In addition to the hazardous region caused by the AGV structure's reach, the protection fields are extended with supplements related to hardware specifications and the nature of the application. Supplements augment the protection areas in all four directions along the x and y axes to ensure their respective hazards are monitored.

The safety laser scanner requires a protection field supplement for a measurement error tolerance (T_Z). Within this tolerance, the reliability of the MicroScan3 complies with the set $\mathrm{PL_r}$. The value of T_Z is catalogued by the manufacturer, based on the range of the protection field, and in the case of the AGV creel application, results in a 65 mm extension.

Furthermore, given the ground clearance of the vehicle structure, the system might detect a person above the foot, as illustrated in Figure 5.10. When unaccounted for, due to the late detection of personnel, this could result in trapping or crushing the foot of a person. To address this hazard, the scanner manufacturer defines the ground clearance supplement based on the length of a foot in front of the point of detection, extending the protection field by 150 mm.

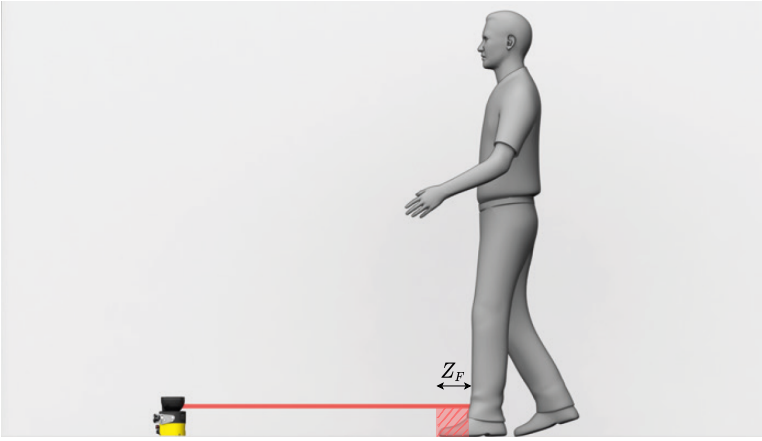

Figure 5.10: Ground clearance Z_F supplement (Amended from [80]).

Protection Field Area

The simulation of the hazardous region for discrete drive monitoring provides the area limits for each motion category. The presented supplements further augment the hazardous areas to determine the effective protection field dimensions, as represented in Figure 5.11.

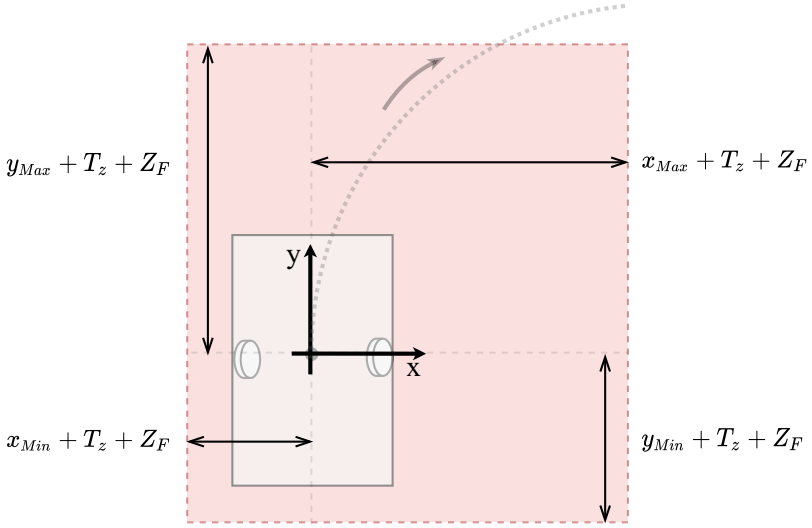

Figure 5.11: Calculation of a protection field size.

5.2.3 Integration of the Safety Laser Scanners

Following the definition of the protection field sizes, the ESPE devices must be configured in consensus with the safety program to ensure the effectiveness of the personnel detection system.

Hardware Mounting

To fully provide the necessary personnel protection, the detection system must then safeguard the entirety of the hazardous region that surrounds the vehicle. To carry out the assignment, two laser scanners were employed to monitor the mobile hazardous areas of the AGV. The devices were installed in the opposite corners of the vehicle for a full coverage of the hazardous area, as depicted in Figure 5.12.

Moreover, so as to not extend the hazard region any further, the sensors were fitted inside the vehicle. The structure includes an indentation along its sides with the necessary clearance for an unobstructed scanner sight. In addition, the MicroScan3 devices were mounted close to the floor, enabling the detection of an operator's leg.

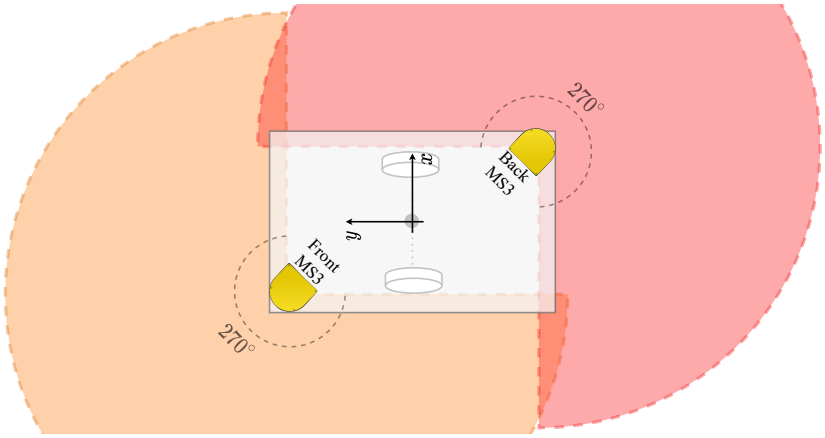

Figure 5.12: Safety laser scanners hazardous coverage (not to scale).

Scanner configuration

For the creel application, the MicroScan3 safety scanners were configured to monitor a horizontal mobile hazardous area, suited for AGVS, in the interface presented in Figure 5.13. The scanners were set to target an operator's leg and acquire four scanner samples per measure for increased reliability (recommended by the manufacturer for mobile applications).[17]

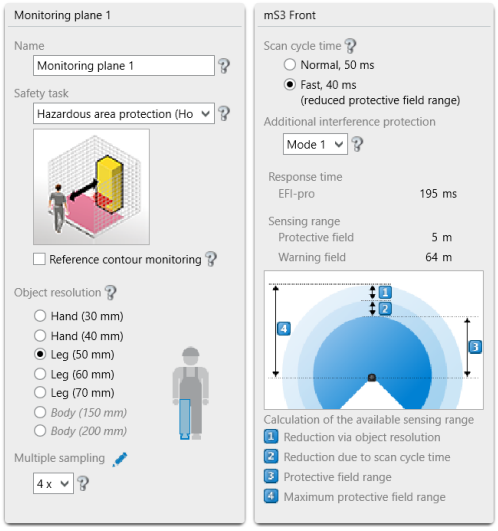

Figure 5.13: ESPE application settings.

[17]The configured object resolution is not a filter for the detection system and shapes of smaller dimensions will still be detected. Instead, this setting defines the minimum object resolution for which the scanner will achieve the set PL_r. Both the object resolution and the scanner cycle time configurations entail a trade-off with the available range for the detection system, reducing for smaller objects and shorter scan cycles [80]. Given the 5 m range sufficed for the resulting protection fields (validated by the results of the protection areas in Subsection 6.1.3), the minimum leg resolution and the fastest scan cycle were preferred.

Based on the protection field size calculation, the field dimensions were then added to the ESPE devices (Figure 5.14a).[18] Subsequently, the configured protection fields were attributed to different monitoring cases (Figure 5.14b), matching the defined motion categories in Table 5.1.[19] The safety program is then able to interact with the personnel detection system by selecting the monitoring case fitting the AGVS navigation.

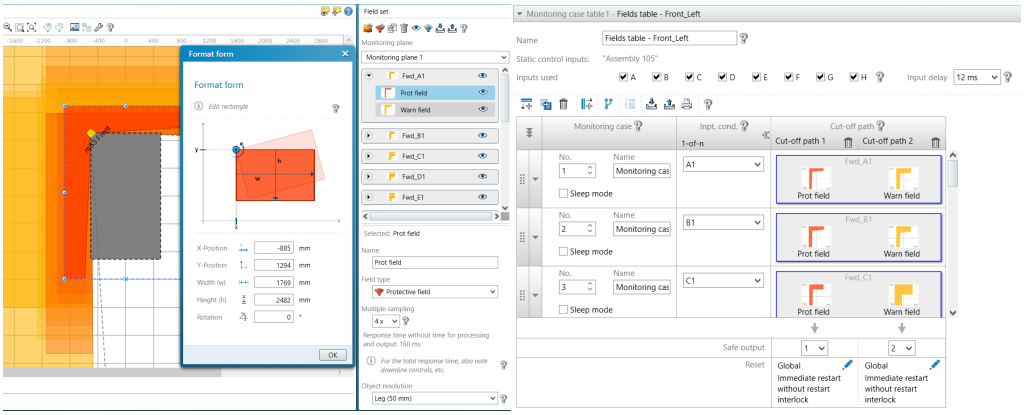

(a) Fields dimensioning (b) Monitoring cases

Figure 5.14: MicroScan3 monitoring fields configuration.

5.3 Integration of the Natural Navigation System

As emphasized throughout this thesis, navigation and safety are interconnected systems that enable an AGVS. Thus, the validation of the safety system is to be performed alongside the navigation solution for which it was developed. Accordingly, the natural navigation and powertrain solutions considered in the AGVS architecture were implemented and tested in the context of a creel application.

5.3.1 Drive System Control

For providing the vehicle motion control to the natural navigation system, the AGVS was configured to enable the ANT lite$^+$ module to operate the powertrain system properly.

[18] The difference in configuration between the scanners is limited to their positioning, sharing the frame of reference defined in Figure 5.6. With this approach, the hazardous area is agnostic to the scanners' placement.

[19] The monitoring cases directly translate to a motion category. In addition to the respective protection field, the monitoring case also defines a warning field to be active in parallel for signalling personnel of the possible hazard (not yet implemented in the AGVS for the scope of this thesis).

Differential Drive Configuration

The Bluebotics solution supports both a direct communication with the servo drives or an intermediary PLC architecture, as long as the control latency is inferior to 70 ms, as previously mentioned.

In the case of the creel application, the Central PLC requires access to the drive's control. Particularly during fine positioning manoeuvres, such as docking with the spool racks or at the charging bays, the controller will shortly take the role of the vehicle navigation. Moreover, during the manual control by an operator, an emergency controlled stop triggered by the safety system (SS1 conditions) requires the Central PLC to directly enact the stop ramp on the drives, bypassing the navigation IPC.

Therefore, the drive system control requires the central PLC to interface the two modules, as depicted in Figure 5.15.

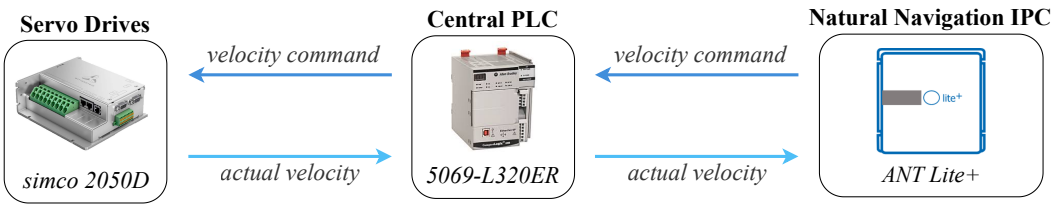

Figure 5.15: Natural navigation speed control.

The natural navigation algorithm relies on a closed-loop control system for driving the AGV, fitted specifically for the differential drive architecture.

For navigating the vehicle according to the application, the navigation system calculates the target velocity on each wheel to follow the correct path, which the PLC conveys on the servo drives ("velocity command").

The odometry algorithm used by the natural navigation system to estimate the vehicle position is based on the measured "actual velocity" of each wheel of the differential drive system. Each servo motion is monitored by the resolver sensors embedded in the motors, which the drive converts into a velocity measurement to provide as feedback to the central PLC. Subsequently, the controller provides the feedback data to the Navigation IPC.

Servo Drive Integration with Central PLC

The servo drives intermediate the control of the AGV wheels, regulating the servo via a proportional-integral controller to follow a commanded velocity [60]. The iTAS system was commissioned specifically for the creel application, and consequently, the drive controllers were accurately tuned beforehand by the manufacturer for the AGVS.

The central PLC interacts with the servo drive via a dedicated SIMCO module for Rockwell controllers (Figure 5.16a). The PLC is then able to access the wheel control functions provided by the drive, abstracting the servo control from the application.

The SIMCO module library provides an interface to the drives (Figure 5.16b), enabling the application to define the target velocity and acceleration, as well as retrieve the feedback data for the navigation system. Additionally, the drive modules provide other quick access functions, such as an interface to trigger a controlled stop following a set deceleration, used by the safety system to fulfil the SS1 and SS2 safety functions.

(a) SIMCO modules in Rockwell PLC (b) SIMCO drive control function

Figure 5.16: Central PLC configuration.

5.3.2 Bluebotics ANT lite$^+$ Setup

To achieve its bestowed role, the natural navigation controller was configured according to the creel AGVS.[20]

Foremost, ANT lite$^+$ required the pre-configuration of the AGVS drive system parameters and the vehicle dimensions. Accordingly, the motion architecture was specified for a differential drive, defining the pertinent drive parameters, namely, the radius of both wheels and the axle length between the wheels. Furthermore, the LiDAR function relies on the scanners' position and orientation, which were set according to their disposition in the vehicle structure. The navigation restrictions were then set to the rated vehicle maximum speed and acceleration, as well as the maximum turning *pivot* speeds, enabling a crude manual control of the vehicle.

After the pre-configuration following the vehicle specification, a manual calibration routine was performed using the joystick controller. Mechanical tolerances are

[20]The integration process of the ANT lite$^+$ solution involved the on-site support of a Bluebotics representative engineer.

inevitable in the assembly of a projected AGVS, and minor deviations from specification can escalate to substantial errors in the odometry process of the navigation system [62]. With the calibration process, the ANT lite$^+$ system estimates with better accuracy the "real" mechanical parameters of the vehicle, namely, the scanners' pose and wheels position and radius. After tuning the vehicle parameters, the creel AGVS is fit for autonomous navigation.

Integration of the Navigation Controller with the Creel Application

In addition to enabling the wheels' velocity control and feedback, the central PLC manages the Navigation IPC according to the creel process. The application interacts with the ANT lite$^+$ by selecting the destination target for the navigation system, a defined node in the mapped environment. In the case multiple defined routes are available to the destination node, the PLC may select the specific path to navigate, providing the application with thorough control of AGV manoeuvres. Upon reaching the node, the navigation system will then signal the application.

The AGVS employs this functional principle to navigate between the creel rack locations, according to the need for spool transferring operations. Via the ANT lab interface, the rack transferring locations can be configured as nodes and the navigation routes defined to best suit the creel application.

Moreover, the laser scanner doubling as safety ESPE devices, in addition to the LiDAR data, indicate the active protection field ID to the navigation controller.[21] In turn, the ANT lite$^+$ relies on the navigation hulls for the collision avoidance function. The hulls are detection areas that match the protection fields dimensions and ID defined in the safety system. Upon invasion of the active hull during navigation, following the same procedure of the personnel detection system, the ANT lite$^+$ IPC enacts a vehicle stop following a stop ramp (configured as $1.3\,\mathrm{m\,s^{-1}}$ to match a_b), to obey the SS2 function being concurrently monitored by the safety system.

Figure 5.17 summarizes the navigation system interactions with the AGVS.

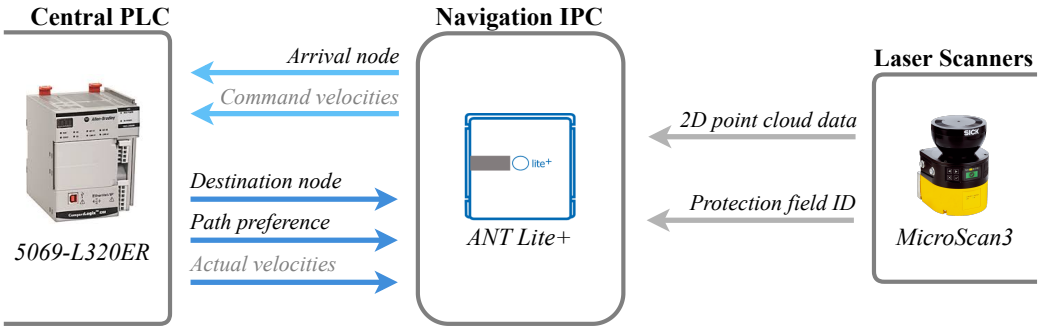

Figure 5.17: Navigation system data exchange for mission control and scanner data.

[21] The protection field ID is numbered according to the monitoring cases of Subsection 5.2.3.

5.3.3 Creel Test Environment

So as to assess and validate the AGVS application, namely for reviewing the interaction between the safety and navigation systems, the environment in Figure 5.18 was set up in an effort to recreate a creel layout. The environment format aimed to specifically test the personnel detection system during the AGV navigation through the layout. Furthermore, the configuration rendered the normal creel operation conditions for validating the AGVS implementation according to its safety standard [50].

(a) Configuration of rack aisles (b) Beam reflectors in the layout

Figure 5.18: Creel layout test environment.

The layout consisted of two connected corridors (Figure 5.18a), emulating the format of rack aisles, so as to submit the AGVS to rack docking operations and narrow turns between aisles. These recurrent manoeuvres of the creel application force the AGVS to operate close to the limits of the personnel protection system, testing its ability to navigate the environment without unnecessarily triggering the protection fields.

In another particular characteristic of the creel layout, the rack aisles are uniform and lengthy, leading to a poor longitudinal localization performance of the AGVS. To counteract this effect, given the feature-poor environment, reflecting markers are planned for the final creel environment. Therefore, the beam reflectors in Figure 5.18b were included in the test layout.

Following the installation of the natural navigation solution, the test creel layout was mapped with ANT lite$^+$ (Figure 5.19).[22] The mapping process required a manual traversal through the environment so that the system extracts the environment features to be used as landmarks during the autonomous navigation. Subsequently, the resulting map was "cleaned" by removing non-stationary and temporary mapped features to attain a high-quality map that enables an accurate and consistent AGVS navigation [62].

[22]The presented map already includes the creel routes and connecting nodes.

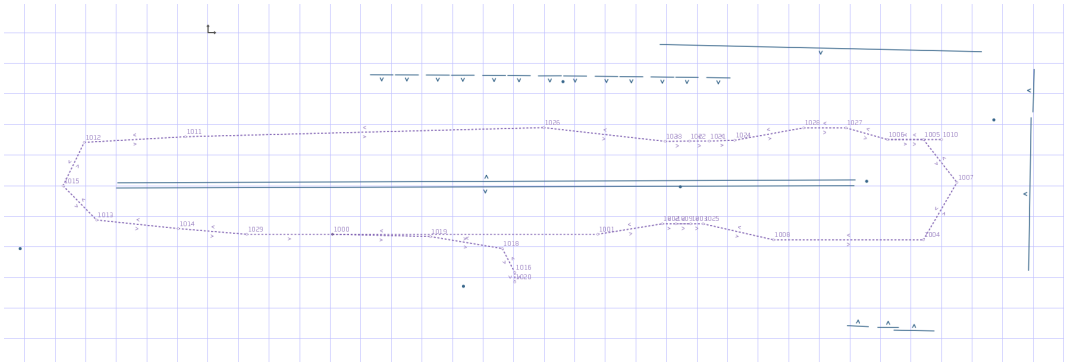

Figure 5.19: Mapped test creel layout in ANT lab.

5.3.4 Conciliating Safety and Navigation

The primary directive of the safety system is to safeguard the physical integrity of people. Nevertheless, a safety system that inhibits the operation of the machine, by compromising the efficiency or even fully inhibiting its application, sacrifices its own purpose.

Given the mutuality between safety and navigation, the challenge lies in designing a safety system that simultaneously preserves personnel safety while enabling the AGVS application. The navigation system must operate within the restrictions imposed by safety, and, in turn, the safety functions must be designed in such a manner that the navigation roles are not compromised.

As previously indicated, intricate manoeuvres, such as docking at the racks for spool transferring operations or turning around aisles, require the AGVS to operate within a confined space. For enabling the creel application, these operations demand reduced protection fields to fit the available clearance so as not to trigger a safe stop, apart from intrusive elements in the creel environment.

Thus, both subsystems were designed in a cooperative manner, considering the specifications each present, in order to harmonize the AGVS. Regarding the navigation system, the vehicle routes and manoeuvres, particularly their respective speed limits, were planned according to the envisaged operating range within the motion categories (defined in Subsection 5.1.2 following AGVS application needs). From the safety system's perspective, the Speed ID Table 5.2 was tuned to optimize the speed monitoring granularity so that the protection fields would achieve functional safety while enabling the application's required manoeuvres.

To further improve productivity, the collision avoidance function of the field hulls enables the ANT lite$^+$ solution to avoid triggering the protection fields and unnecessary downtime. The ANT lab platform provides a simulation tool, depicted in Figure 5.20, that projects the field hulls throughout a planned route in the navigation map. The tool allows the navigation routes to be planned so that the protection field of each manoeuvre does not overlap with the mapped environment features.

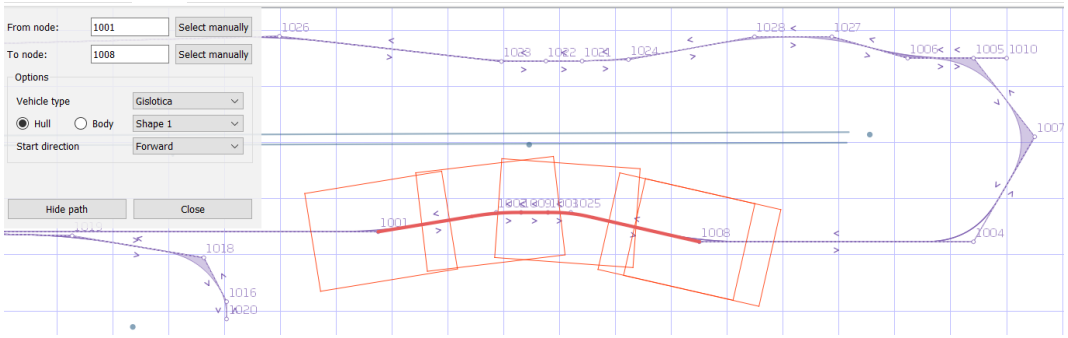

Figure 5.20: Field hulls projection for planning routes.

From the assessed leeway available to the protection fields in Figure 5.20, the ANT lite$^+$ can be configured to add a margin to the size of the hulls for anticipating the controlled stop. This margin reduces the likelihood of an SS0 being triggered due to a failure to follow the stop ramp. Although not inhibiting to the application, the failures may hinder the efficiency of the operation with interruptions requiring manual intervention.

5.4 Conclusions

The presented chapter detailed the implementation efforts undergone for realizing the subject of this thesis, following the outlined strategy in the previous chapter.

The chapter provided an in-depth review of the Flexi Soft system modules configuration and implemented logic design for the safety system's control which enable the drive-based safety functions.

The following section oversaw the implementation of the personnel detection system, emphasising the assessment of the protection fields for navigation. The implementation addressed the challenges with discrete drive monitoring and the ensuing hazardous regions via a simulation model of the AGV braking kinematics. Furthermore, the section details the configuration of the ESPE devices for performing the personnel detection function.

Lastly, the chapter described the implementation process of the navigation system, detailing the integration of the natural navigation IPC and servo drives with the application controller. Furthermore, the creel layout was configured with support for the natural navigation solution for validating the safety system in the context of the application. In addition, the section reviewed the necessary measures and design considerations for conciliating the navigation and safety systems to enable the AGVS application.

Chapter 6

Results and Discussion

The following chapter details the assessment of the resulting AGVS, with particular emphasis on validating the personnel detection system. The chapter reviews the devised safety system and respective methodology with the aim to validate the functional safety of the creel application. Subsequently, the chapter examines alternative approaches for determining the hazardous regions and evaluates the standardized personnel detection system.

6.1 Validation of the Safety System

Following the implementation of the AGVS with a focus on the safety system for the creel application, the resulting safety functions were tested and reviewed to validate the functional safety of the creel application.

The control logic of the safety functions and safe elements were individually tested via the Flexisoft system to match their implementation in Annex B. Namely, the drive-based safety functions (SMS, SLS, SDI), motion detection, field commutation and safe stop conditions (emergency buttons, drive faults and forbidden motion detection) were validated to fulfil their purpose as described in Chapter 5.

However, the personnel detection system required a more in-depth review for sanctioning it appropriate for the AGVS application.

6.1.1 Challenges in Validating the Personnel Detection System

In addition to the complexity of determining protection fields' size, the personnel detection system also proves difficult to validate. A safe stop test with object detection is able to verify the control logic of the safety function. A navigation test reviews whether the resulting protection field sizes are suited the creel layout. However, the problem is raised when validating that the protection fields fully encompass the hazardous region.

An empirical validation of the system would require repeating the procedure of the simulation and testing the reach of the AGV for every possible speed arrangement. Such an approach is unfeasible due to time constraints and presents challenging test control conditions. Instead, the compromise was to validate the simulation methodology by reviewing the kinematic model and testing the safe stop ramp that defines the braking kinematics.

6.1.2 Simulation Model for Differential Braking Kinematics

The vehicle's pose defined by the simulation model shall match the analytical model of differential kinematics. The kinematics complexity makes it difficult to determine the exact pose throughout the braking motion analytically.

However, two particular cases of the differential drive require simple analytical analysis. When the AGV brakes while moving in a straight line or travels in a constant circle, the analytical AGV pose can be derived without differential kinematics.

Thus, the following comparison trials were designed to validate the simulation model (set with a sample size (n) of 181).

Braking Distance of a Straight Moving Vehicle

Considering the AGV travels with both wheels rotating at the rated speed, it is possible to calculate the covered distance by the straight moving vehicle since the hazard was detected until the vehicle stopped.

The distance travelled (Δy) during the reaction (t_r) and braking time (t_b) can be determined according to Equations 6.1 and 6.2.

$$\Delta y = v_i \cdot t_r + v_i \cdot t_b + \frac{-(v_i)}{2 \cdot a_b} \cdot (t_b)^2 \tag{6.1}$$

$$t_b = \frac{-(v_i)}{a_b} \tag{6.2}$$

The simulation of the braking kinematics for the straight moving vehicle is traced in Figure 6.1. The simulation results were then compared with the analytical pose, as presented in Table 6.1.

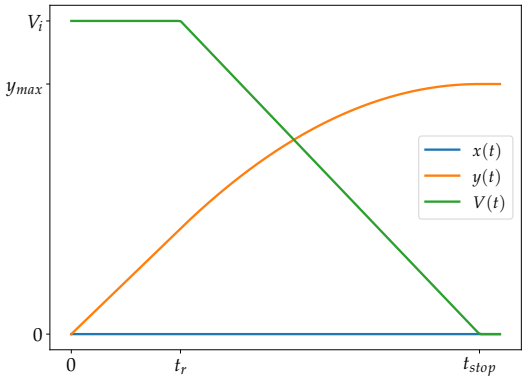

Figure 6.1: Simulated AGV pose throughout the controlled stop.

Table 6.1: Stop distance validation.

Parameters:				
a_{break}	vl_i	vr_i	n	(ω)
$-1.30\,\mathrm{m\,s^{-2}}$	$1.2\,\mathrm{m\,s^{-1}}$	$1.2\,\mathrm{m\,s^{-1}}$	181	$0\,\mathrm{rad\,s^{-1}}$
AGV stop	**Simulation** (m)	**Analytical** (m)		**Error** (m)
$x(t_{stop})$	0	0		$\leq 5 \times 10^{-11}$
$y(t_{stop})$	0.958	0.958		$\leq 5 \times 10^{-6}$

The results show that the simulation closely matches the braking distance (y_{max}) determined analytically and presents little deviation at the x axis.

Circular Trajectory of a Differential Vehicle

Considering that no braking occurs, with different speeds set at each wheel, the AGV's trajectory is bound to the differential circle. This manoeuvre is depicted in Figure 6.2a, and the vehicle's pose is outlined in Figure 6.2b.

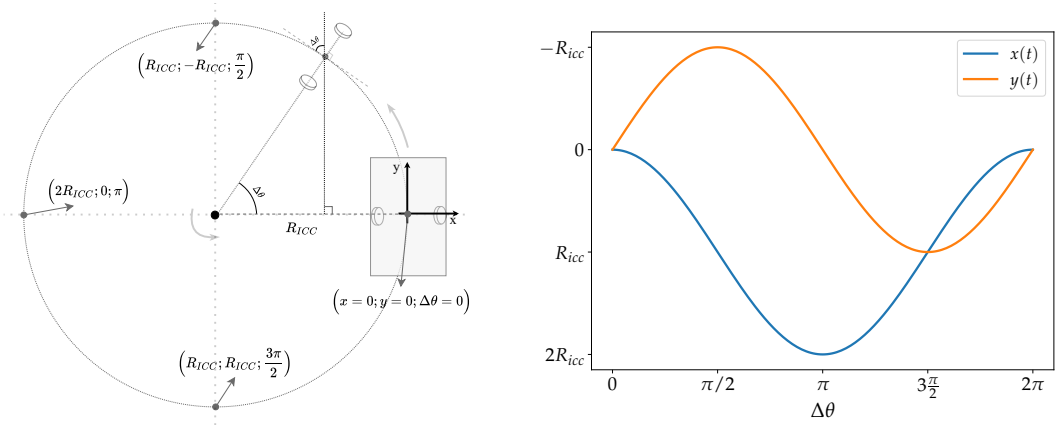

(a) Differential circle path.

(b) Simulated AGV pose.

Figure 6.2: Differential circle validation test.

The analytical values of the AGV pose in a differential circle of radius R_{ICC} can be directly derived at $\frac{\pi}{2}$ intervals. The values are compared to the simulation model in Table 6.2.

Table 6.2: Circular path validation.

Parameters:				
a_{break}	vl_i	vr_i	n	(R_{ICC})
$0\,\mathrm{m\,s^{-2}}$	$0.5\,\mathrm{m\,s^{-1}}$	$1.2\,\mathrm{m\,s^{-1}}$	181	$-1.097\,\mathrm{m}$
AGV centre	**Simulation** (m)	**Analytical** (m)		**Error** (m)
$x(\pi/2)$	-1.097	R_{ICC}		$\leq 2 \times 10^{-4}$
$y(\pi/2)$	1.097	$-R_{ICC}$		$\leq 2 \times 10^{-4}$
$x(\pi)$	2.193	$2R_{ICC}$		$\leq 3 \times 10^{-4}$
$y(\pi)$	0	0		$\leq 3 \times 10^{-16}$
$x(3\pi/2)$	-1.097	R_{ICC}		$\leq 2 \times 10^{-4}$
$y(3\pi/2)$	-1.097	R_{ICC}		$\leq 2 \times 10^{-4}$
$x(2\pi)$	0	0		$\leq 7 \times 10^{-16}$
$y(2\pi)$	0	0		$\leq 7 \times 10^{-16}$

The simulation model was able to determine the AGV pose according to the analytical results noted in Figure 6.2a, as showcased by the deviation error column of Table 6.2.

Review of the Kinematic Model Simulation

The errors between the exact analytical values and simulation results were presented in Tables 6.1 and 6.2. The observed deviations are attributed to the estimation errors of the numerical integration. This calculation relies on a finite number of velocity samples (n) to determine the vehicle's pose, which may be increased to reduce the error at the cost of simulation time.

The attained results showcase the vehicle navigating according to the analytical differential kinematics, indicating an error of the simulated AGV pose inferior to 1 mm. Furthermore, the different AGV turning movements defined in Subsection 5.2.1 were simulated to validate the structure kinematics. The described analysis is available in Annex D and outlines the vehicle pose, velocities, and corner kinematics of the four turning movements.

Ultimately, the tests validate the simulation model, corroborating the produced hazardous areas.

6.1.3 Mobile Hazardous Areas

Following the validation of the braking kinematics model, it was possible to assess the resulting hazardous areas of the different motion categories from Subsection 5.1.2.

Simulation Results

The forward manoeuvres of the AGV were simulated considering the different initial wheel speed (v_i) arrangements. The resulting reaches of the structure are presented in Figure 6.3.

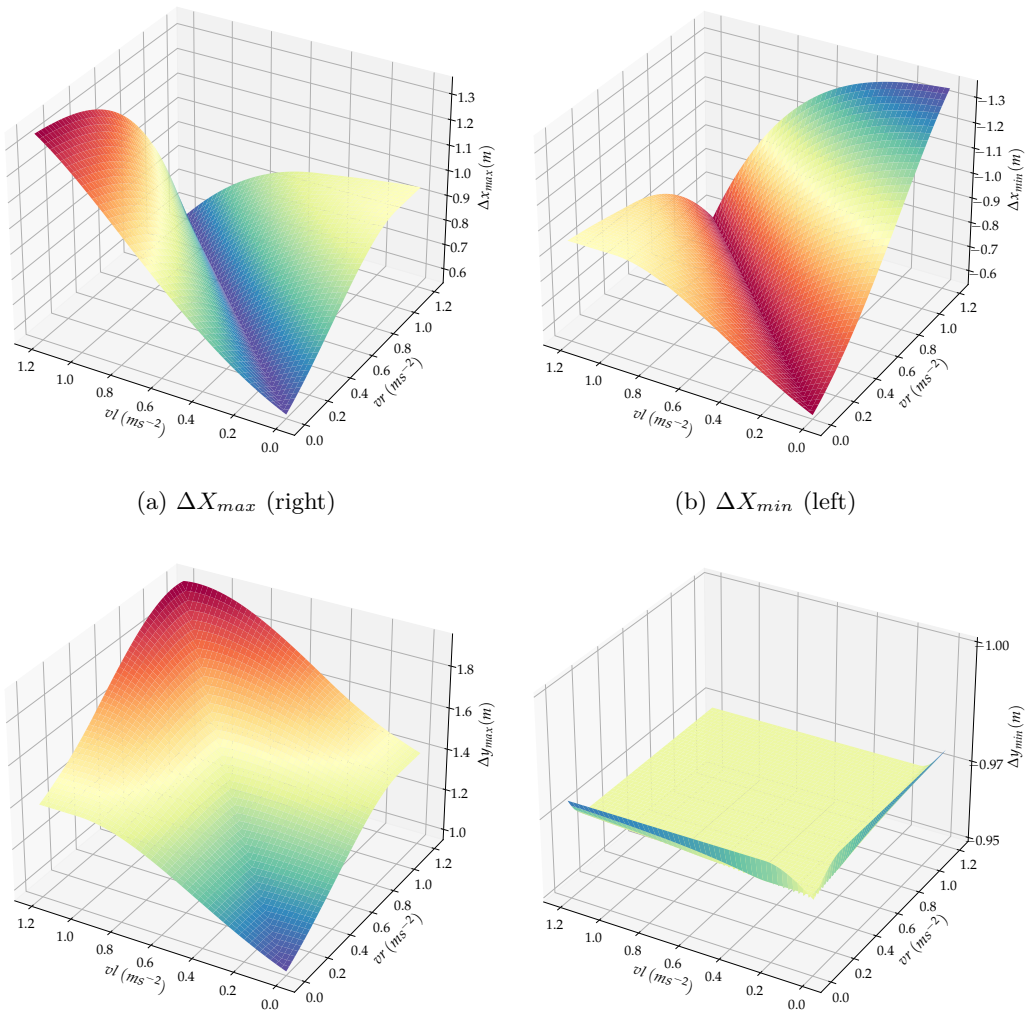

(a) ΔX_{max} (right)

(b) ΔX_{min} (left)

(c) ΔY_{max} (front)

(d) ΔY_{min} (back)

Figure 6.3: AGV structure reach for the different v_i arrangements.

From the plotted simulation results, the following observations were raised:

- The right and left halves of the plots respectively represent left and right turning motions, separated by the straight movements ($v_l = v_r$). The straight motions present the minimum deviations in the x axis (± 0.558 m corresponding to half of the structure's width).
- The reach in the x axis presents mirrored results for left and right turning motions. Additionally, the reach increases with higher differential speeds.

- The reach in the direction of travel of the vehicle (ΔY_{max}) increases with vehicle speed, particularly for straight motions.
- The hazardous region behind the vehicle (ΔY_{min}) is mostly uniform at $-0.968\,\mathrm{m}$ (corresponding to half the structure's length), however, it increases as the vehicle begins to turn on its wheel (one wheel stopped).

Subsequently, the speed ranges were grouped according to Speed ID. The relevant Speed ID arrangements for the creel application are presented in Table 6.3.[1] In addition, the table identifies the initial speed configuration of the wheels ($vi_l; vi_r$) that register the maximum reaches of the structure within the arrangement.

Table 6.3: Simulation results for forward, forward-right and pivot Speed ID arrangements.

Wheel ID		X_{min}(m)	X_{max}(m)	Y_{min}(m)	Y_{max}(m)	Speed configuration of:	
Left	Right	(left)	(right)	(back)	(front)	$X_{max}(\mathrm{m\,s^{-1}})$	$Y_{max}(\mathrm{m\,s^{-1}})$
ID2	ID2	-0.646	0.646	-0.974	1.056	(0.20; 0.00)	(0.00; 0.20)
ID3	ID2	-0.692	0.702	-0.974	1.109	(0.30; 0.00)	(0.30; 0.11)
ID4	ID2	-0.844	0.907	-0.974	1.296	(0.60; 0.00)	(0.60; 0.20)
ID3	ID3	-0.616	0.616	-0.968	1.108	(0.30; 0.20)	(0.20; 0.30)
ID4	ID3	-0.782	0.834	-0.968	1.306	(0.60; 0.20)	(0.60; 0.30)
ID4	ID4	-0.784	0.784	-0.968	1.314	(0.60; 0.30)	(0.48; 0.60)
ID5	ID4	-0.824	0.916	-0.968	1.441	(0.75; 0.30)	(0.75; 0.60)
ID5	ID5	-0.711	0.711	-0.968	1.442	(0.75; 0.60)	(0.65; 0.75)
ID6	ID5	-0.768	0.876	-0.968	1.586	(0.90; 0.60)	(0.90; 0.75)
ID6	ID6	-0.738	0.738	-0.968	1.588	(0.90; 0.75)	(0.81; 0.90)
ID7	ID6	-0.743	0.864	-0.968	1.694	(1.00; 0.75)	(1.00; 0.90)
ID7	ID7	-0.697	0.697	-0.968	1.695	(1.00; 0.90)	(0.92; 1.00)
ID8	ID7	-0.712	0.840	-0.968	1.809	(1.10; 0.90)	(1.10; 1.00)
ID8	ID8	-0.711	0.711	-0.968	1.809	(1.10; 1.00)	(1.03; 1.10)
ID9	ID8	-0.711	0.868	-0.968	1.930	(1.20; 1.00)	(1.20; 1.10)
ID9	ID9	-0.726	0.726	-0.968	1.931	(1.20; 1.10)	(1.13; 1.20)
±ID2	±ID2	-0.725	0.725	-1.057	1.057	(0.20; -0.20)	(-0.04; 0.20)

From the results presented in Table 6.3, it is possible to assess the following remarks:

- The reach in the x axis was symmetrical for the same Speed ID ranges in both wheels and is larger for right-turning arrangements (left ID> right ID).
- Consistently with Figure 6.3, the reach at $Ymin$ increased for Speed ID arrangements that support turn on wheel manoeuvres (ID2).
- Furthermore, the reach of the pivot category is symmetrical across both axes.

[1] Only the forward, forward-right motion arrangements and pivot speeds (±ID2) are presented in Table 6.3. The omitted results can be derived from the provided values by inverting the maximums and minimums of the respective axis.

- The maximum reach at the right of the vehicle (X_{max}) occurs for the highest wheel speed difference within each Speed ID arrangement.
- However, the speed configuration that registers the furthest reach in front of the vehicle (Y_{max}) is not a straight motion with the maximum speeds of the range.

Resulting Protection Fields

The simulation results of Table 6.3 were grouped according to the defined motion categories of Table 5.1, respectively identifying the maximum reach. Subsequently, the four parameters were extended with the protection supplements (0.215 m) for defining the protection fields dimensions presented in Table 6.4.[2]

Table 6.4: Simulation results for motion categories

Motion category	ΔX_{min}(m) (left)	ΔX_{max}(m) (right)	ΔY_{min}(m) (back)	ΔY_{max}(m) (front)
A1	-0.861	0.861	-1.189	1.271
B1	-0.917	0.917	-1.189	1.324
C1	-0.999	0.999	-1.183	1.529
D1	-1.131	1.131	-1.183	1.803
E1	-1.083	1.083	-1.183	2.146
F1	-1.122	1.059	-1.189	1.521
G1	-1.059	1.122	-1.189	1.521
H2	-0.940	0.940	-1.272	1.272

The calculated fields showcase the y axis reach scaling as the speed increases for straight motion categories (A-E). By contrast, the reach in the x axis scaling is less significant, even reducing for the top rated-speed given the lower differential speed of the range. A more granular monitoring system would reduce the reach in the x axis for straight motion categories and improve the AGVS flexibility. Nevertheless, the lower speed category A was successfully tuned to meet the side clearance requirement for approaching and docking at the creel racks of the spool transferring operations.[3]

Moreover, there was a minor difference (6 cm) between left and right turning categories. Due to the squared design of the protection fields, there were lesser benefits from segmenting F and G categories.

[2]The symmetrical hazardous areas are once again omitted from Table 6.4. The backward motion categories (A2 to G2) are symmetrical to their forward counterpart in the y axis, resulting in inverted ΔY_{max} and ΔY_{min} dimensions.

[3]The loading tower is restricted to a maximum 500 mm distance to the rack so as to be able to exchange spools. Therefore, the protection field size must not overlap with the rack and trigger a safe stop. After tunning the Speed ID from Table 5.2, the simulated protection field requires only a 0.303 m side clearance (in addition to the structure's 0.558 m). The targeted clearance for the field size was further reduced to accommodate the manoeuvring space when approaching the rack.

Regarding the H2 category for pivot manoeuvres, the resulting compact field area was suited for enabling AGV manoeuvres in tight spaces.

6.1.4 Safety Stops Tests

According to the safety standard, the "Braking system" safety function defined in Table 3.2 must be validated with the full load of the AGV. However, at the time of the project, the implemented AGV did not yet include the spool tower structure. Nevertheless, the following tests were performed to validate the control logic of the safe stops. During the tests, the speed and motor current of one of the servos was monitored via the SIMCO drive.[4]

For testing the SS0 function, the vehicle was manually controlled to collide with an object (Figure 6.4), bypassing the controlled stop request. The monitored wheel data is provided in Figure 6.5.

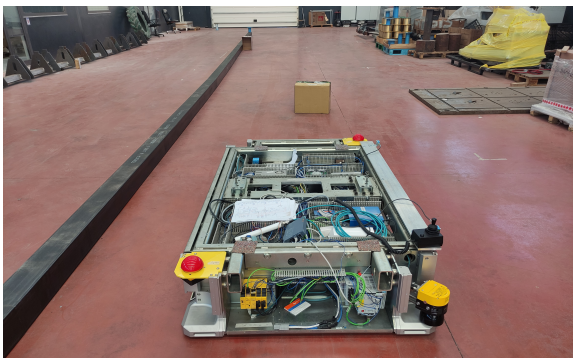

Figure 6.4: Safe stop testing with object detection.

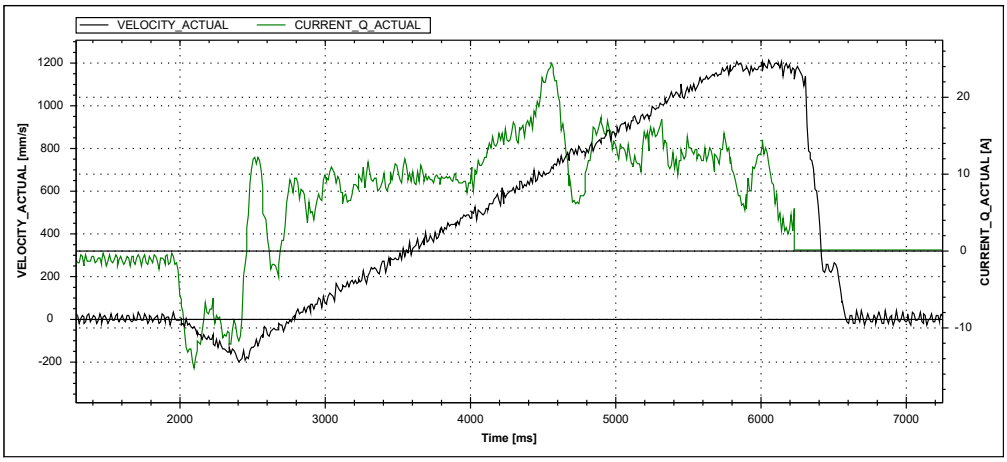

Figure 6.5: Wheel data during the SS0 function test.

[4]The wheel speed data presented in Figures 6.5 and 6.6 is based on the resolver signal, which presented inadequate noise for both wheels. This was identified as a malfunction to be addressed before the final release of the AGVS.

Subsequent to the failure of the controlled stop ramp, the safety system triggered the SS0 function. The results showcase the immediate power removal with STO (t=6.23 s), following the object detection. In addition, the procedure validated the personnel detection function to detect the object and initiate the safe stop.

For evaluating the controlled stop ramp, the test was carried out via the SS1 function. The stop was triggered after controlling the vehicle to perform a forbidden motion (sharp turn at high speeds). The results are displayed in Figure 6.6.

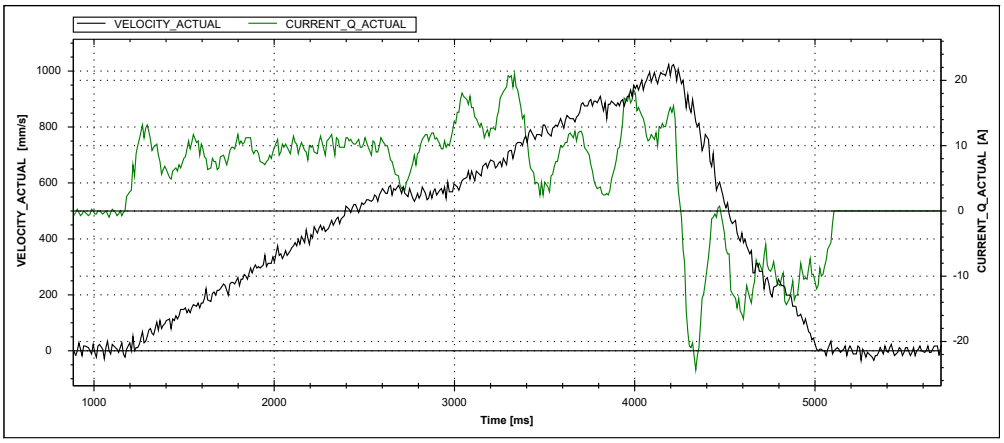

Figure 6.6: Wheel data during the SS1 function test.

The SS1 test results show the vehicle braking the wheel according to the controlled stop ramp. Only after reaching a standstill does the safety system enact STO (t=5.13 s), complying with the SS1 procedure.

Based on the measured speed (v_i) when the vehicle starts braking (t_i) and braking duration until standstill is reached, it was possible to determine the braking deceleration following Equation 6.3.[5]

$$a_b = -\frac{v_i}{t_b} \tag{6.3}$$

The safety stops test results are summarized in Table 6.5.

Table 6.5: Safe stop functions test.

Function	v_i ($\mathrm{m\,s^{-1}}$)	t_i (s)	t_f (s)	a_b ($\mathrm{m\,s^{-2}}$)
SS0	1.169	6.23	6.75	-2.23
SS1	1.021	4.23	5.01	-1.31

The SS0 braking deceleration was higher than designed ($1.4\,\mathrm{m\,s^{-2}}$) due to the service brakes operating a lower load (missing the spool tower). Nevertheless, the $1.3\,\mathrm{m\,s^{-2}}$ controlled stop deceleration followed the defined stop ramp.

[5]The timestamp reference for the braking start was set to the sharp decrease in the servo current.

Ultimately, the safe stop test results affirmed the control logic of the safe stops and the defined braking ramp for the controlled stops. The assessment allowed to proceed with the validation of the safety system along the application's autonomous navigation.[6]

6.1.5 Testing the Navigation System

Relying on the defined application route (Figure 5.19), it was possible to examine the performance of the natural navigation system and recreate the AGVS condition in the creel system.

The purpose of the navigation system test is not to thoroughly trial the autonomous navigation but instead to validate the personnel detection system for the creel AGVS application. Namely, it will be possible to verify that the ensuing protection fields do not "collide" with the natural features of the creel layout during normal operations.

The test consists of the AGV performing three runs of the defined path. For test control and guaranteeing the vehicle is following the application route, the precision of the navigation system will be assessed at three nodes. Node A was set at the start position of the path to track any cumulative errors between runs. Nodes B and C were defined for two rack positions, requiring the AGV to approach and stop in parallel to the rack to verify the protection field clearance.

The posed deviation error was assessed via two fixed lasers on the AGV (Figure 6.7). Each node was then marked with the referenced positions for measuring their distance to the lasers.

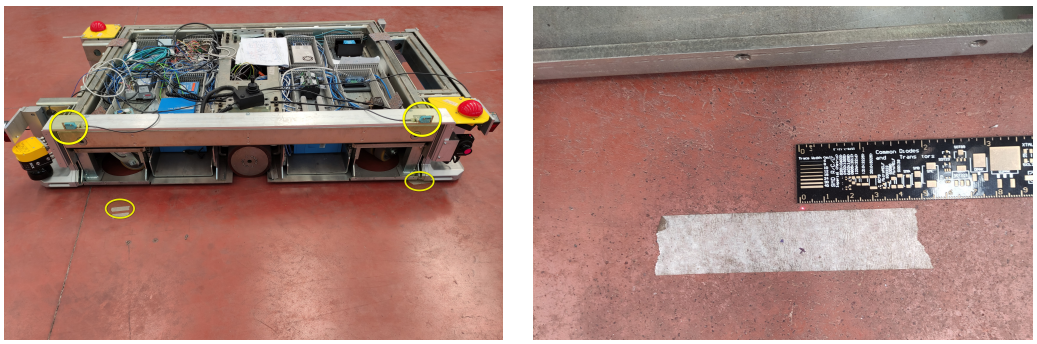

(a) AGV pose marker lasers. (b) Measuring deviation from node marker.

Figure 6.7: AGV navigation precision test.

[6]Given that the tests were carried out with a reduced AGV load and defective speed monitoring, validating the safety system for the final product will require a new braking evaluation with the spool tower.

Table 6.6 presents the pose error results from the creel navigation test.[7]

Table 6.6: Navigation system test in the creel layout.

Node	Test	Pose Error		
		Δx (mm)	Δy (mm)	$\Delta\theta$ (°)
A	1^{st}	−1	9.5	−0.30
	2^{nd}	2	5	−0.09
	3^{rd}	−2	−4	−0.51
B	1^{st}	1.5	−7.5	−0.13
	2^{nd}	−5	11	0.26
	3^{rd}	−4	1	0.09
C	1^{st}	−3	6.5	0.21
	2^{nd}	0	5	0.09
	3^{rd}	−1.5	2	0.17

From the measured pose error, it was possible to verify that the navigation path was followed with minor deviations. Hence, the test allowed to evaluate the safety system in the context of the creel application.

The three path runs were performed without triggering the personnel detection system. From this result, it was possible to conclude that the personnel detection system was correctly designed to accommodate the creel AGVS application. The safety system is therefore expected not to hinder the operation except for inadvertent obstacles, hereby preserving the efficiency of the application.

6.2 Review of the Safety System

The presented validation results sanctioned the implemented AGVS as suited to enable a creel application. The safety system achieves functional safety in compliance with the regulatory standard for AGVS safety [50] while accommodating the natural navigation solution and minimizing the impact on the flexibility of the AGV.

The reliability of the implemented safety functions cannot be assessed via validation tests, and instead is exclusively dependant on the safety architecture of Chapter 4 to ensure that the functions fulfil the respective PL_r set in Table 3.2.

Regarding the personnel detection system, the implemented solution was able to cooperate with the natural navigation system in addition to its primary role of providing reliable personnel protection. The conciliation of navigation and safety allows the AGVS to achieve functional safety and enable the creel application.

[7] The pose error defines the indirect measurement of the deviation in the AGV centre. The error was derived from the difference between of the equidistant markings of the lasers to the defined node reference.

Prominent Findings from the Simulation Results

As showcased in Figure 6.8, the maximum reach of the AGV structure may occur amid the braking manoeuvre. This premise is also perceptible in the plotted braking examples of Annex D, in which the global maximums and minimums for the x and y axes are reached at different instants. Therefore, for any given speed configuration, the vehicle's entire motion must be reviewed to attain the effective reach of the structure and not consider only the final pose of the vehicle.

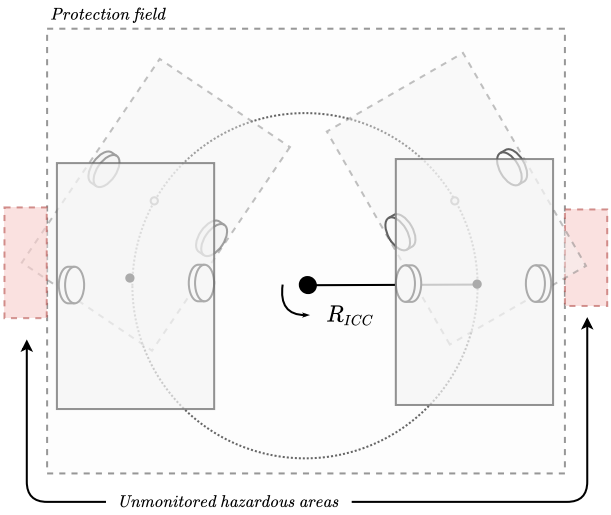

Figure 6.8: Undetected hazards while turning.

Furthermore, the furthest reaches of the structure within the set of speed arrangements of a motion category is registered at different speed configurations, as showcased in Table 6.3. Although the reach in the x axis occurs at the highest speed differential, the same is not true for every differential vehicle. As showcased in Figure 6.9, simulating a vehicle with a lower braking deceleration ($0.7\,\mathrm{m\,s^{-2}}$) results in unpredictable $Xmax$ speed configurations. The same behaviour was already denoted in the $Ymax$ of the creel AGV and results from the rotation of the structure extending its reach.[8]

The simulation results reveal that there are no shortcuts for determining the reach of the structure within a motion category. Namely, presuming that the maximum reach in the y axis occurs at the maximum speed of the range for both wheels or assuming the maximum reach in the x at the highest differential speeds.[9] Such erroneous heuristics might result in exposed hazards and an unsafe machine operation which would not comply with the Machinery Directive.

[8]The "faster" deceleration of the creel AGV results on the vehicle braking before the structure rotation extends the hazardous area as in Figure 6.9.

[9]This approach is later defined as the "Extremes" heuristic and assessed in Subsection 6.3.1.

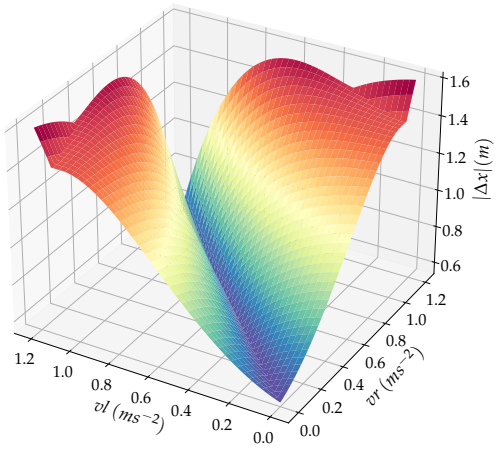

Figure 6.9: Simulated reach in x axis for a lower stop deceleration.

In conclusion, devising the personnel detection system of an AGV or any mobile robot requires a complete analysis predicting the kinematics of the structure throughout its braking motion, such as the approach taken in this thesis.

6.2.1 Shortcomings of the Personnel Detection System

The chosen approach to the personnel detection system nonetheless presents drawbacks in terms of flexibility and effectiveness that may be improved upon.

Protection Field Format

The purpose of the protection field is to exclusively monitor the hazardous area. However, the taken approach extends the field areas beyond the necessary for hazardous coverage.

As depicted in Figure 6.10a, the adopted rectangular format, based on the furthest reaches of the AGV, may detect an object outside the hazardous region and needlessly trigger a safe stop. In addition to the potential unnecessary downtime, the field format requires additional clearance for turning manoeuvres which hinders the flexibility of the AGVS.

Monitoring the optimal protection field, such as in Figure 6.10b, would reduce the protection field areas, enabling higher speeds for tight space manoeuvres such as turning around the creel racks. However, outlining the entire contour of hazardous region would require a more complex analysis.

Moreover, an increased monitoring granularity (increased number of available Speed ID) would further reduce the field sizes, as noted for the resulting protection fields (Subsection 6.1.3).

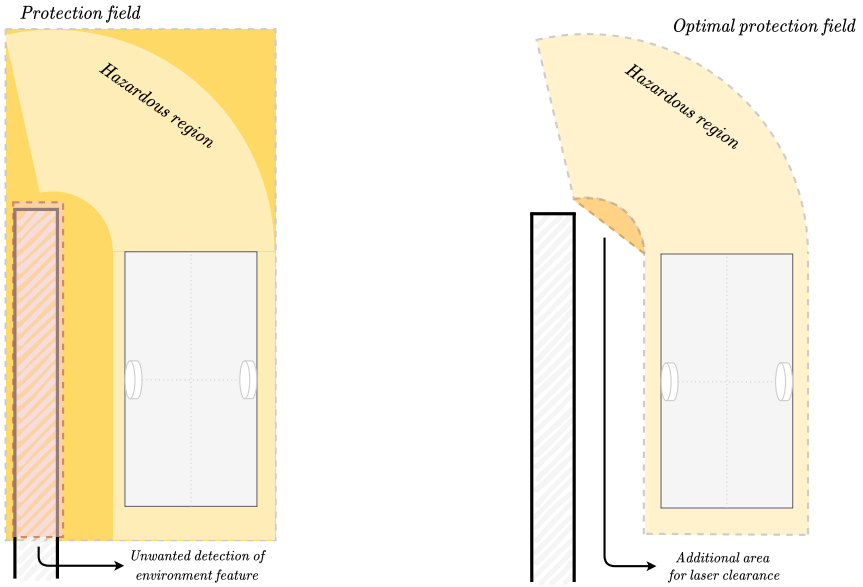

(a) Creel AGVS protection field. (b) Minimum required protection field

Figure 6.10: Limitations of the protection fields format.

Improving the flexibility of the AGVS by reducing the protection field sizes to the hazardous area would potentiate its compatibility with other applications than the creel system. An application-agnostic AGVS would increase its value by saving redundant development efforts such as implementing the personnel detection system. In turn, the decrease in development costs would encourage more complex approaches such as the "optimal" protection field format and simulation models that better predict the kinematic behaviour of the AGV.

Controlled Safe Stop

The available drive-based safety functions present flaws for mobile and multi-drive machines where the application requires not only robust but also strict speed control.

The safe controlled stops configured in Subsection 5.1.1 are based on a stop ramp that ascertains a decrease in drive speed. However, should the drive decrease at a faster rate than the ramp, the safety system does not react. Furthermore, the drive speed goes unmonitored during the reaction time (t_r).[10]

In both presented scenarios, the braking duration will not be extended as the SS0 function would otherwise intervene. However, such as in the case of a differential drive architecture, a varying drive speed might alter the vehicle motion to exceed the predicted hazardous area.

[10]Given the unmonitored drive speed during t_r, the simulation model was oversimplified by considering a constant speed for both wheels.

The safe stop ramp proposal described in Figure 6.11 aims to address the presented hazardous conditions by complementing SS1 and SS2.

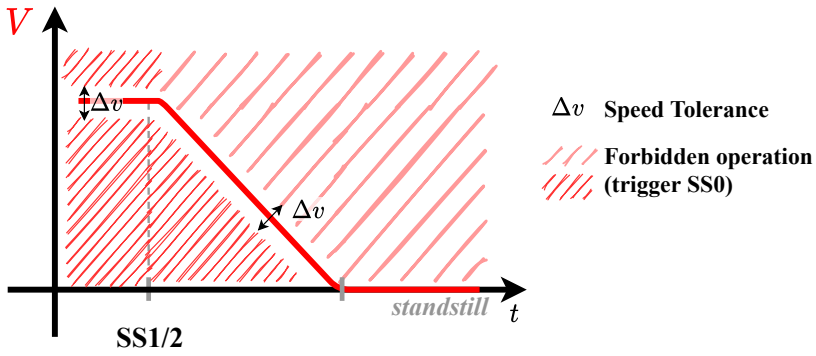

Figure 6.11: Safe Stop Ramp function proposal.

The safe stop ramp would monitor the drive speed during both t_r and braking. The function would verify if the speed remained within the bounds of the controlled stop, escalating to SS0 otherwise.[11] The Δv tolerance delimiting the speed bounds would then be considered in the simulation of the hazardous area.

Limitations of the Kinematic Model

The effectiveness of the personnel detection system relies on the accuracy of the modelled braking kinematics. The implemented simulation depicts an ideal kinematic model, assuming a linear behaviour for the differential drive system. However, an AGVS entails non-linear elements that might alter the vehicle's trajectory during braking. The wheels' traction, rigidity or possible slippage might result in exposed hazardous conditions. Considering the non-linear factors in the kinematic simulation would improve the reliability of the created model and thereby further decrease the risk of a hazardous incident.

6.3 Review of the State of the Art in AGV Safety

Throughout the undergone project in the context of this thesis, the considered bibliographic references such as standards and manufacturer's documentation presented some inconsistencies with the reviewed machine safety concepts in Chapter 3. These instances raise concerns about the available methodology for tackling functional safety in AGVS applications.

[11] Until the ESPE device triggers a safe stop, the drive monitor is not able to detect the v_i changing. Therefore, the function must account for the drive speed data before the hazard detection.

6.3.1 Faults with the Handbook Approach

The MicroScan3 operating instructions [80] provide an over-simplistic and misleading solution for addressing the mobile hazards of AGVS applications.

The proposed method to calculate the protection fields only applies to an AGV operation in an absolute straightforward motion. The field width considers the braking space exclusively in the vehicle's direction of travel and spans only across the width of the structure.[12]

It is impractical to restrict an AGV operation to exclusively navigate in a straight line. Nonetheless, the solution is pointless for non-ideal speed control systems, incapable of ensuring such a straight motion. These aspects are not only present in discrete drive monitoring. In continuous linear speed monitoring, the error tolerances in the measurements would require a consideration of turning, even if minimal. In the particular cased of differential drive systems, the slightest speed difference between the wheels results in a turning motion.

Therefore, in the author's opinion, the approach proposed by the MicroScan3 manufacturer cannot be appropriate for an AGVS safety system as, given the presented characteristics, the resulting protection fields would not comprise the entirety of the hazardous region.

Evaluating Heuristics for Determining Protection Fields.

From the attained results of the simulation in Table 6.4, it is possible to assess the shortcoming of proposed heuristics that aim to simplify the process of determining the protection field areas.

Table 6.7 presents the results for the motion category E1 of the creel AGVS calculated using the handbook approach ("SICK heuristic") and the "Extremes heuristic". The Extremes heuristic is also based on the braking kinematics model and proposes to only simulate arrangements of the boundary speeds of the motion category.[13] Moreover, the table presents the error difference between the heuristics results and the adopted full simulation approach for the creel AGVS.

Table 6.7: Determining category E1 field with different approaches

Field side	Full Simulation Field (m)	SICK heuristic		Extremes heuristic	
		Field (m)	Error (m)	Field (m)	Error (m)
ΔX_{max}	1.083	0.773	0.31	1.083	0
ΔX_{min}	−1.083	−0.773	0.31	−1.083	0
ΔY_{max}	2.146	2.141	0.005	2.141	0.005
ΔY_{min}[14]	−1.183	−1.183	0	−1.183	0

[12] In addition to the protection supplements presented in Subsection 5.2.2.

[13] Within the Speed ID ranges of a motion category, the Extremes heuristic assesses only the top wheel speeds for the y axis and the maximum differential speeds for the x axis reach.

The SICK heuristic presents significant errors from underestimating the hazardous area. Namely, as the heuristic only considers the protection supplements at the sides of the vehicle (x axis), the unprotected region extends 0.310 m. This considerable area potentiates a dangerous accident for entrapping or colliding with a person.

The Extremes heuristic presents minor errors in comparison with the full Simulation. However, as argued in Section 6.2, this does not apply to all AGVS, and in the case of the system modelled in Figure 6.9, the heuristic could significantly underestimate the hazardous area.

The reviewed heuristics further corroborate the conclusion of Section 6.2. Ultimately, the comparison results evidence that in order to determine the full coverage of the hazardous region of an AGV, the complete analysis of the structure's kinematics is required.

6.3.2 Standardization Shortcomings

The current state of the standard for safety requirements and verification of AGVS (ISO 3691-4), particularly regarding the personnel detection system, does not ensure functional safety for the machine.

The standard defines under "Detection of persons in the intended path in automatic mode", the following requirements pertaining to the protection fields:

- "b) Personnel detection means shall operate at least over the maximum width of the truck and its load in the direction(s) of travel."
- "c) Personnel detection means shall be so designed that trucks shall stop before contact between the rigid parts of the truck or load and a stationary person (not a person stepping into the truck path or moving toward it) (...). In turning direction and in pivoting direction, for the truck side protection measures, compliance with 5.2 Test B is sufficient."[15]

Based on the same argument made against the handbook approach, a protection field sizing the width of the structure is irrelevant in a real AGVS application. Setting such requirements, despite defining only the minimum width of the fields, could be misinterpreted to follow an approach such as the SICK heuristic.[16] Most significantly, requirement c) supersedes the previous requirement. In order for the

[14]The E1 category does not extend the hazardous region in the direction of ΔY_{min}, therefore the deviation errors are null. However, both heuristics present a 6 mm underestimation error for the A1 motion category as the structure rotation impacts the reach behind the vehicle.

[15]Test B refers to the test depicted in Figure 6.12 using the "test piece (B)" object.

[16]The standard requirements and validation procedures are addressed to both Electro-Sensitive Protective Equipment (ESPE) and Pressure-Sensitive Protective Equipment (PSPE) systems. Although they ensure coverage for the hazardous areas of PSPE enabled AGVS, as discussed, they are not the best suited for ESPE personnel detection systems.

truck to stop before contact with a stationary person (ensuring the set PL_r d), the personnel detection system requires the full coverage of the hazardous area, which implies a field width larger than the vehicle.

Moreover, the standardized verification methodology for the personnel detection system requirements does not ensure proper coverage of hazardous areas. The "Tests for detection of persons" depicted in Figure 6.12 only validate the fields to extend the projected width of the structure in the direction of travel. This is due to the detection test pieces only being placed within the width of the structure. Furthermore, as per the presented requirement c), validating the turning and pivot protection directions does not consider the rotation of the structure nor the structure reach outside the "intended path". This requirement opens a possibility for the hazard presented in Figure 6.8.

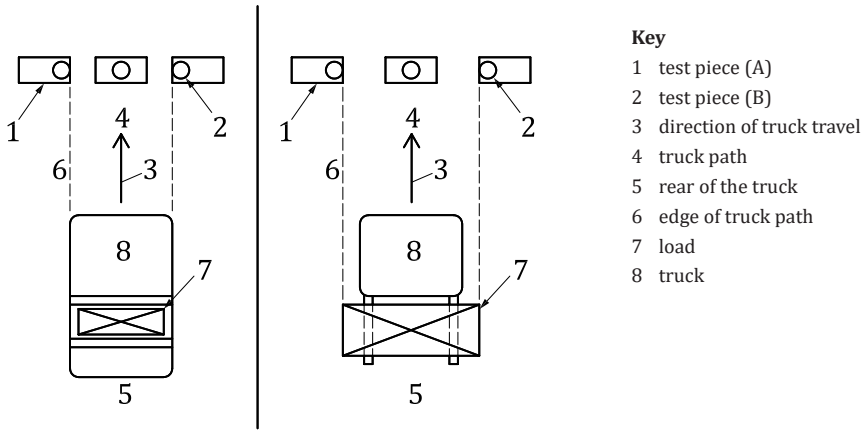

Figure 6.12: Example of tests in certain direction of travel [50].

The testing methodology does not address the challenge of validating the personnel detection system raised in Subsection 6.1.1 as the tests do not validate that the protection fields contain the entire hazardous region. Therefore, the tests are only able to validate the control logic of the personnel detection system.

Given the showcased shortcomings of standard regarding personnel detection system requirements and their respective validation, the standard does not accurately delineate a safe AGVS. An ill-designed personnel detection system, such as one following the proposed SICK heuristic, would be certified according to ISO, and yet, the resulting AGVS would not comply with the EU Machinery directive.

In summary, an AGV compliant and validated by the current safety standard does not ensure that an AGV is safe. Based on these findings, the assessment performed by Marvel and Bostelma [8] prevails, and further standardization efforts are required.

Proposals on Improving Standardization

To address the identified challenges with AGVS safety standardization, the encountered gaps suggest the need to replace the cited requirements with clear, objective and unambiguous guidelines defining, in particular, ESPE based personnel detection systems.

As showcased by the results of this thesis, the hazardous region extends beyond the width of the AGV and requires a thorough review of the structure's kinematics during braking. These established principles prompted the following requirements:

- Personnel detection means shall be so designed that vehicles shall stop before contact between the rigid parts of the structure or load and a stationary person (not a person stepping into the vehicle path or moving toward it).
- Personnel detection means shall rely exclusively on safe rated drive monitoring functions and consider the full range of manoeuvres within drive speeds.

Moreover, as argued in Chapter 3, drive-based functional safety is pivotal for achieving functional safety in mobile autonomous machines. However, the complex kinematics of AGVS and mobile robots would benefit from new standardized drive-based safety functions such as the theorised safe stop ramp in Subsection 6.2.1.

6.4 Conclusions

The purpose of the presented chapter was to review the resulting AGVS in the context of this thesis. In particular, the chapter focused on evaluating the personnel detection system and raising research findings on the safety function, paramount for providing functional safety to AGVS in the cooperative setting.

The first section tested the different elements defining the personnel detection system, namely the braking kinematics model, the resulting protection fields and the implemented braking system. Subsequently, the system was tried in the context of the creel layout navigation. The performed tests then served to verify the effectiveness of the personnel detection system.

Following the validation, the chapter reviewed the resulting safety system, concluding that the system would enable functional safety for the devised AGVS.

Furthermore, the review of the implemented personnel detection system, namely the simulation of the hazardous region, raised a pivotal finding in the thesis: Devising the personnel detection system of an AGVS requires a complete analysis of the structure kinematics throughout braking and the protection field must comprise all permissible motions; Additionally, the safety system review identified some limitations with the chosen approach and proposed future improvements.

Moreover, the chapter identified the shortcomings of the proposed methodology by the ESPE and drive-based safety equipment manufacturer. Based on the complete simulation approach for the creel AGVS, the manufacturer's heuristic and the proposed "Extremes" heuristic were deemed flawed. Lastly, considering the thesis findings, a retrospective of the standard on AGV safety revealed the need for further standardization efforts.

Chapter 7

Concluding Remarks

This study aimed to research and address the challenges of devising safety systems for AGVS in the context of industrial applications. Towards this goal, the thesis pursued an empirical approach with the implementation of a safety system for a creel AGVS application. In the context of a real industrial application, it was possible to validate the feasibility of the safety architecture and, in particular, address the challenges set for conciliating navigation and safety. The envisaged safety system accommodated and achieved functional safety for the creel application with a natural navigation solution.

7.1 Overview

A review of the current state of the art in safe machinery and AGVS and the norms that regulate these systems established the requirements for the envisaged safety architecture. Namely, the study identified drive-based safety functions and personnel detection systems as the cornerstone elements for enabling functional safety in AGVS applications.

Subsequently, the thesis outlined an AGVS architecture for the creel application to be considered by the ensuing safety system, specifically for accommodating the natural navigation solution of a differential drive system.

To achieve functional safety for the creel application and fulfil the requirements set by the standard, the safety system's implementation oversaw the configuration of the control program under the FlexiSoft PLC. This safety program integrated the

required drive-based safety functions for drive monitoring and safe stop procedures, as well as an ESPE based personnel detection system specifically tailored for the differential drive architecture. For designing the personnel detection system, namely, for determining the protection field sizes, the thesis modelled the braking kinematics of the AGV and simulated the structure reach for the set of possible manoeuvres. In addition, with the integration of the natural navigation system, it was possible to validate the AGVS safety in the context of the creel application.

7.2 Contributions of the Thesis

The research was able to pinpoint the main challenge in AGVS safety as the design of the personnel detection system. Namely, reliably identifying the mobile hazardous area prompted by autonomous navigation requires a complex and thorough analysis of the AGV's braking space.

The thesis then proposed and detailed a methodology to address the challenge. The approach was to simulate all permissible speed arrangements and their respective braking kinematics. The furthest registered reach of the structure then defined the protection fields that reliably allow the vehicle to avoid a collision. The solution was implemented and validated for a creel system that demonstrated the methodology's feasibility and effectiveness in real industrial applications.

On the same topic, the thesis also evaluated and dismissed alternative heuristics that aimed to simplify the process of calculating the hazardous area, including one proposed by the ESPE manufacturer, proving both inaccurate.

Furthermore, based on the AGVS implementation results, the thesis identified shortcomings in the standardization of AGV safety, namely for the requirements defining and validating the personnel detection system. In addition, the thesis raised the need for new drive-based safety functions that better accommodate the multi-drive complex systems such as AGVS.

7.3 Future Developments

Throughout the document, several limitations with the approach and available methodology were pointed out as possible future improvements.

In the context of Gislotica's creel system, for finalizing the creel AGVS application, the effective PL of the safety functions must be reassessed to meet their respective PL_r. Likewise, the validation procedures must again be performed with the full AGV load. The resulting AGVS was also missing the warning system, of argued importance, as well as other safety functions non-related to navigation but required by the creel aplication. In prospect, the contemplated flexibility improvements would enable Gislotica to port the AGVS to other industrial applications.

The thesis showcased the benefits of optimized protection fields and increased monitoring granularity for the presented flexibility limitations of the implemented AGVS. Furthermore, the proposed standardization improvements aim to decrease development efforts of AGVS and avoid flawed functional safety for applications.

However, one particular challenge for developing AGVS safety systems remained unheeded. This thesis reveals the need for further research for devising a better methodology for validating personnel detection systems.

Building upon the work of this thesis, in line with the proposed improvements, the aim is to mature the methodology of AGVS safety systems, improving their flexibility and compatibility with further industrial applications. The long-term goal of this thesis is to tackle the cooperative setting and strive towards a full collaborative industrial process with stringent AGVS safety.

References

[1] R. Horatiu, A. Dan, B. Lidia-Cristina, and B. N. George, "Cooperative cheap automated guided vehicles," in *20th International Carpathian Control Conference*, pp. 1–6, IEEE, May 2019. [Cited on pages 1, 2, and 8]

[2] H. Berg, P. Bendix, M. Jansen, K. L. Blévennec, P. Bottermann, M. Magnus-Melgar, E. Pohjalainen, and M. Wahlström, "Unlocking the potential of Industry 4.0 to reduce the environmental impact of production," tech. rep., European Environment Agency, June 2021. [Cited on page 1]

[3] A. Brems, E. Steele, and A. Papadamou, "Library of typical energy audit recommendations, costs and savings," tech. rep., European Commission, Oct. 2015. [Cited on page 1]

[4] UNEP, "The Six-sector solution to the climate crisis," tech. rep., United Nations, Dec. 2020. Available: `https://www.unep.org/interactive/six-sector-solution-climate-change/industry/index.php`. Accessed: 09-01-2022. [Cited on page 1]

[5] R. Kumar, A. Haleem, S. Garg, and R. Singh, "Automated guided vehicle configurations in flexible manufacturing systems: A comparative study," *International Journal of Industrial and Systems Engineering*, vol. 21, p. 207, Jan. 2015. [Cited on pages 1 and 8]

[6] G. Ullrich, "Modern areas of application," in *Automated Guided Vehicle Systems: A Primer with Practical Applications*, pp. 15–96, Berlin, Heidelberg: Springer Berlin Heidelberg, 2015. [Cited on pages 1, 9, and 24]

[7] E. A. Oyekanlu, A. C. Smith, W. P. Thomas, G. Mulroy, D. Hitesh, M. Ramsey, D. J. Kuhn, J. D. Mcghinnis, S. C. Buonavita, N. A. Looper, M. Ng, A. Ng'oma, W. Liu, P. G. Mcbride, M. G. Shultz, C. Cerasi, and D. Sun, "A review of recent advances in automated guided vehicle technologies: Integration challenges and research areas for 5g-based smart manufacturing applications," *IEEE Access*, vol. 8, 2020. [Cited on pages 2 and 7]

[8] J. Marvel and R. Bostelman, "Towards mobile manipulator safety standards," in *2013 IEEE International Symposium on Robotic and Sensors Environments (ROSE)*, pp. 31–36, Oct. 2013. [Cited on pages 2, 27, and 104]

[9] F. Platbrood and O. Görnemann, "Safe robotics – safety in collaborative robot systems," White Paper 8020621, SICK AG, June 2018. [Cited on pages 2, 15, and 23]

[10] European Commission, "Evaluation of the Machinery Directive 2006/42/EC," Tech. Rep. SWD(2018) 160, European Union, Brussels, May 2018. [Cited on pages 2 and 16]

[11] European Commission, "Impact assessment - Accompanying: Proposal for a Regulation of the European Parliament and of the Council on machinery products," Tech. Rep. SWD(2021) 82, European Union, Brussels, Apr. 2021. [Cited on page 2]

[12] European Commission, "Eurostat dataset on 3D printing and robotics." Available: `https://ec.europa.eu/eurostat`, 2018. Accessed: 10-04-2021. [Cited on pages 2 and 3]

[13] LogisticsIQ, "AGV-AMR Market, Summary description," Tech. Rep. 5232383, LogisticsIQ, Jan. 2021. Available: `https://www.thelogisticsiq.com/research/automated-guided-vehicles-agv-market/`. Accessed: 10-04-2021. [Cited on page 2]

[14] Gislotica, "Quem é a Gislotica." Available: `http://www.gislotica.pt/pt/`. Accessed: 11-01-2021. [Cited on page 3]

[15] B. Borges, "Desenvolvimento de um AGV para Tarefas Industriais," Master's thesis, Instituto Superior de Engenharia do Porto, July 2020. [Cited on pages 3 and 37]

[16] G. Ullrich, "Technological standards," in *Automated Guided Vehicle Systems: A Primer with Practical Applications*, pp. 97–163, Berlin, Heidelberg: Springer Berlin Heidelberg, 2015. [Cited on pages 4, 8, 10, 11, 12, 13, and 35]

[17] H. Fazlollahtabar and M. Saidi-Mehrabad, "Reliability model for agv," in *Autonomous Guided Vehicles: Methods and Models for Optimal Path Planning*, pp. 41–56, Springer International Publishing, 2015. [Cited on page 8]

[18] B. R. Sarker and S. S. Gurav, "Route planning for automated guided vehicles in a manufacturing facility," *International Journal of Production Research*, vol. 43, pp. 4659–4683, Feb. 2005. [Cited on page 8]

[19] J. D. Lee and B. D. Seppelt, "Human factors in automation design," in *Springer Handbook of Automation* (S. Y. Nof, ed.), pp. 417–436, Berlin, Heidelberg: Springer Berlin Heidelberg, 2009. [Cited on page 8]

[20] M. N. Tamara, A. Darmawan, N. Tamami, C. sugianto, S. Kuswadi, and B. Pramujati, "Electronics system design for low cost agv type forklift," in *2018 International Conference on Applied Science and Technology (iCAST)*, pp. 464–469, 2018. [Cited on page 8]

[21] H. Christensen and A. Trevor, "Automated guided vehicle survey," tech. rep., Georgia Institute of Technology, Office of Sponsored Programs Research Reports, May 2009. [Cited on pages 8, 10, and 12]

[22] L. Schulze and A. Wullner, "The approach of automated guided vehicle systems," in *2006 IEEE International Conference on Service Operations and Logistics, and Informatics*, pp. 522–527, July 2006. [Cited on page 8]

[23] M. Boehning, "Improving safety and efficiency of agvs at warehouse black spots," in *2014 IEEE 10th International Conference on Intelligent Computer Communication and Processing (ICCP)*, pp. 245–249, Sept. 2014. [Cited on page 8]

[24] G. Ullrich, "The history of automated guided vehicle systems," in *Automated Guided Vehicle Systems: A Primer with Practical Applications*, pp. 1–14, Berlin, Heidelberg: Springer Berlin Heidelberg, 2015. [Cited on page 9]

[25] J. Lyne and G. Hudson, "'No-hands' for materials handling," *Railway Age*, vol. 143, p. 24, Sept. 1957. [Cited on page 9]

[26] L. Garner Jr., ""No-hands" train," *Railway Age*, vol. 8, p. 59, June 1958. [Cited on page 9]

[27] J. Taalbi, "Origins and pathways of innovation in the third industrial revolution," *Industrial and Corporate Change*, vol. 28, pp. 1125–1148, Sept. 2018. [Cited on page 9]

[28] C. Feledy and M. S. Luttenberger, "A state of the art map of the agvs technology and a guideline for how and where to use it," Master's thesis, Lund University, May 2017. [Cited on pages 9, 10, 11, 12, 24, and 27]

[29] M. Martins, "Implementatation and testing of planing and scheduling algorithms of an AGV fleet," Master's thesis, Instituto Superior de Engenharia do Porto, July 2018. [Cited on page 10]

[30] L. Li, Y. Liu, M. Fang, Z. Zheng, and H. Tang, "Vision-based intelligent forklift automatic guided vehicle (AGV)," in *2015 IEEE International Conference on Automation Science and Engineering (CASE)*, pp. 264–265, Aug. 2015. [Cited on page 10]

[31] L. Sabattini, V. Digani, C. Secchi, G. Cotena, D. Ronzoni, M. Foppoli, and F. Oleari, "Technological roadmap to boost the introduction of agvs in industrial applications," in *2013 IEEE 9th International Conference on Intelligent Computer Communication and Processing (ICCP)*, pp. 203–208, 2013. [Cited on page 10]

[32] ASTI Mobile Robotics, "Product: Tractor line." Available: `http://astimobilerobotics.com/tractor`. Accessed: 10-04-2021. [Cited on page 10]

[33] Transbotics, "Product: Transbotics AGV Tugger." Available: `https://www.astimobilerobotics.com/tractor`. Accessed: 10-04-2021. [Cited on page 10]

[34] G.-C. Vosniakos and A. Mamalis, "Automated guided vehicle system design for fms applications," *International Journal of Machine Tools and Manufacture*, vol. 30, no. 1, pp. 85–97, 1990. [Cited on page 10]

[35] Roboteq, "Building a Magnetic Track Guided AGV," White Paper AN1326, Roboteq Inc., Nov. 2013. "Accessed: 21-05-2021". [Cited on page 11]

[36] S. Sabikan, M. Sulaiman, S. Najib, S. N. Sy Salim, and M. F. Bin Miskon, "Vision-based automated guided vehicle for navigation and obstacle avoidance," in *2nd International Conference on Engineering and ICT*, pp. 18–20, Feb. 2010. [Cited on page 11]

[37] P. Neto and L. Vilaça, "Low cost AGV navigation using Image Processing," dissertation, Instituto Superior de Engenharia do Porto, Jan. 2021. [Cited on page 12]

[38] H. Durrant-whyte and T. Bailey, "Simultaneous localization and mapping: part I," *IEEE Robotics & Automation Magazine*, vol. 13, pp. 99–110, June 2006. [Cited on page 13]

[39] A. Söderberg, J. Hedberg, P. Folkesson, and J. Jacobson, "Safety-related machine control systems using standard en iso 13849-1," White Paper 978-91-88695-33-8, RISE Research Institutes of Sweden, Jan. 2018. [Cited on pages 16 and 19]

[40] M. Dietrich, R. Schumacher, and D. Lilienthal, "Guide for safe machinery - Six steps," Manual 8007988, SICK AG, July 2015. [Cited on pages 16, 17, 19, 20, 24, 25, and 27]

[41] Rockwell Automation, *Safety related control systems for machinery Principles, standards and implementation*, Nov. 2016. Machinery Safebook 5, SAFEBK-RM002C-EN-P. [Cited on page 17]

[42] ABB, "Safety in control systems according to EN ISO 13849-1 - Machine Safety - Jokab Safety products," White Paper 2TLC172003B02002, ABB AB, `https://library.abb.com/en`, 2011. "Accessed: 21-05-2021". [Cited on pages 17, 18, and 19]

[43] Z. Vujanic, I. Kastelan, and P. TapavickiDejan, "Safety Certified Controllers with PL c and PL d Performance Levels - A Survey," in *2018 26th Telecommunications Forum (TELFOR)*, pp. 1–4, Nov. 2018. [Cited on page 17]

[44] ISO, "Safety of machinery — Safety-related parts of control systems — Part 1: General principles for design," Standard ISO 13849-1:2015, 3rd ed., International Organization for Standardization, Geneva, CH, Dec. 2015. [Cited on page 18]

[45] S. Robinson, "New Standards for Machinery Safety-Related Control Systems – BS EN ISO 13849-1 & BS EN 62061," *Measurement and Control*, vol. 41, pp. 272–275, Nov. 2008. [Cited on page 19]

[46] IEC, "Safety of machinery - Electrical equipment of machines - Part 1: General requirements," Standard IEC 60204-1:2016, 6th ed., International Electrotechnical Commission, Geneva, CH, Oct. 2016. [Cited on page 19]

[47] ABB, "Technical guide no. 10 functional safety," White Paper 3AUA0000048753, ABB AB, `https://library.abb.com/en`, Nov. 2017. "Accessed: 21-05-2021". [Cited on pages 20 and 36]

[48] IEC, "Adjustable speed electrical power drive systems - Part 5-2: Safety requirements - Functional ," Standard 61800-5-2:2016, 2nd ed., International Electrotechnical Commission, Geneva, CH, Apr. 2016. [Cited on page 20]

[49] ABB, "Drive-based functional safety, 3rd ed.," White Paper 3AUA0000181817, ABB AB, `https://library.abb.com/en`, Dec. 2017. "Accessed: 11-06-2021". [Cited on page 20]

[50] ISO, "Industrial trucks — Safety requirements and verification — Part 4: Driverless industrial trucks and their systems," Standard 3691-4:2020, 1st ed., International Organization for Standardization, Geneva, CH, Feb. 2020. [Cited on pages 24, 25, 27, 29, 47, 64, 83, 97, and 104]

[51] GREIN, "Product: Agv bumper." Available: `https://grein.it/Bumper-en.html`. Accessed: 22-06-2021. [Cited on page 25]

[52] R. Norcross, R. Bostelman, and J. Falco, "Automated guided vehicle bumper test method development," tech. rep., National Institute of Standards and Technology, Gaithersburg, MD, June 2015. [Cited on page 25]

[53] SICK, "Safe EFI-pro System - MICS3-CBAZ90ZA1P01," Product datasheet 1094465, SICK AG, July 2020. [Cited on pages 25, 35, and 51]

[54] R. Yan, S. J. Dunnett, and L. M. Jackson, "Reliability modelling of automated guided vehicles by the use of failure modes effects and criticality analysis, and fault tree analysis," in *5th Student Conference on Operational Research (SCOR 2016)*, vol. 50, pp. 1–10, Nov. 2016. [Cited on page 26]

[55] M. J. Nunney, "Tyres, road wheels and hubs," in *Light and Heavy Vehicle Technology*, ch. 22, pp. 442–460, Burlington, MA: Elsevier Ltd., 4 ed., 2007. [Cited on page 31]

[56] N. Mullineux, "Light vehicle tyres," market report, Rapra Technology Limited, Shawbury, SY4, Sept. 2004. [Cited on page 31]

[57] Henan Hengxing Technology Co., Ltd., "Steel cord for radial tire." Available: `en.hengxingchinese.com/product/Steel-Cord-for-Radial-Tire-3.html`. Accessed: 15-08-2021. [Cited on page 32]

[58] RJS Corporation, "Complete creel systems." Available: `https://rjscorp.com/creel-systems`. Accessed: 15-08-2021. [Cited on page 32]

[59] Rockwell Automation, "CompactLogix 5380, Compact GuardLogix 5380, and CompactLogix 5480 Controllers Specifications," Technical Data 5069-TD002J-EN-P, Rockwell Automation, Inc., Aug. 2020. [Cited on pages 35 and 36]

[60] Wittenstein, *Simco drive SIM2050D - Operating manual*. Wittenstein SE, 4 ed., June 2019. [Cited on pages 35, 39, 45, 46, and 80]

[61] Wittenstein, *TAS drive actuator for automated guided vehicles - Operating manual*. Wittenstein SE, 3 ed., May 2019. [Cited on pages 35 and 39]

[62] BlueBotics, *ANT lite+ User manual*. BlueBotics SA, Mar. 2021. [Cited on pages 35, 37, 38, 60, 82, and 83]

[63] SICK, "EFI-pro Safe device communication via the network," Tech. Rep. 8022345, SICK AG, July 2019. [Cited on page 36]

[64] Wittenstein, "iTAS servo drive system for automated guided vehicles," catalogue, Wittenstein, 2017. "Accessed: 22-09-2021". [Cited on pages 38, 39, and 45]

[65] H. Gürocak, "Electric motors - AC servo motors," in *Industrial Motion Control: Motor Selection, Drives, Controller Tuning, Applications*, pp. 107–147, Vancouver, WA: Wiley, Oct. 2015. [Cited on page 39]

[66] T. Hellström, "Kinematics equations for differential drive and articulated steering," White Paper UMINF-11.19, Department of Computing Science Umeå University, Dec. 2011. [Cited on page 40]

[67] W. Chung and G. Campion, "Wheeled robots," in *Springer Handbook of Robotics* (B. Siciliano and O. Khatib, eds.), pp. 391–410, Cham: Springer International Publishing, 1 ed., 2008. [Cited on page 40]

[68] G. Dudek and M. Jenkin, "Mobile robot hardware - locomotion," in *Computational Principles of Mobile Robotics*, pp. 31–70, Cambridge University Press, 2010. [Cited on pages 40 and 70]

[69] SICK, "Safe EFI-pro System - FX3-MOC100000 ," Product datasheet 1057833, SICK AG, Sept. 2021. [Cited on pages 42, 44, and 61]

[70] SICK, "Safe EFI-pro System - FX3-GEPR00000 ," Product datasheet 1069070, SICK AG, July 2020. [Cited on pages 42 and 43]

[71] SICK, "Safe EFI-pro System - FX3-CPU000000 ," Product datasheet 1043783, SICK AG, July 2020. [Cited on pages 42, 43, and 61]

[72] SICK, "Safe EFI-pro System - FX3-XTIO84002 ," Product datasheet 1044125, SICK AG, July 2020. [Cited on pages 42 and 44]

[73] Farnell, "Pushbuttons and Indicating Lights," Product datasheet FAK-R-V-KC12-IY, Premier Farnell Ltd, Mar. 2009. [Cited on pages 42 and 44]

[74] SICK, "DFS60 - Incremental encoders," Product datasheet 1062177, SICK AG, Aug. 2020. [Cited on pages 42 and 46]

[75] T. Seiki, "Smartsyn - Brushless resolvers," Product datasheet TS2620N21E11, Tamagawa Seiki Co., Ltd., Aug. 2020. [Cited on pages 42 and 46]

[76] SICK, "Flexi Soft in the Safety Designer," Operating instructions 8014519/15UG, SICK AG, Nov. 2019. [Cited on pages 42, 43, 46, 57, 58, and 121]

[77] SICK, "Flexi Soft Gateways - Hardware," Operating instructions 8012664/1BPI, SICK AG, May 2021. [Cited on page 43]

[78] SICK, "Flexi Soft Gateways in Flexi Soft Designer - Configuration Software," Operating instructions 8018172/19YF, SICK AG, Dec. 2020. [Cited on page 43]

[79] SICK, "Drive Monitor FX3-MOC - Motion Control," Operating instructions 8017009, SICK AG, Feb. 2014. [Cited on page 44]

[80] SICK, "Safety laser scanner MicroScan3 EFI-pro," Operating instructions 8021913/15ZW, SICK AG, Nov. 2019. [Cited on pages 51, 52, 75, 76, 78, and 102]

[81] R. Wolfson, "Rotational motion," in *Essential University Physics*, vol. 1, ch. 10, pp. 175–187, Pearson Education, 4 ed., jan 2019. [Cited on pages 56, 59, and 71]

[82] Wittenstein, "TAS 025x-031x-2xx-094W-xxx-000," product datasheet, Wittenstein SE, Mar. 2016. [Cited on page 59]

[83] H. Gürocak, "Drive-Train Design - Torque–Speed Curves for AC Servomotors," in *Industrial Motion Control: Motor Selection, Drives, Controller Tuning, Applications*, pp. 62–67, Vancouver, WA: Wiley, Oct. 2015. [Cited on page 60]

[84] H. Willer, "COMBISTOP N 023811N-4071," Product datasheet 20141780, Karl E. Brinkmann GmbH, Nov. 2016. [Cited on page 60]

[85] R. Wolfson, "Motion in a straight line," in *Essential University Physics*, vol. 1, ch. 2, pp. 16–33, Pearson Education, 4 ed., jan 2019. [Cited on pages 70 and 72]

[86] P. Walls, "Numerical integration." Available: `https://personal.math.ubc.ca/~pwalls/math-python/`, Dec. 2019. Accessed: 10-07-2021. [Cited on page 74]

Appendix A

Differential Drive Kinematics Formulas

A.1 Angular Velocity

$$\begin{cases} \omega = \frac{v_r}{R_{ICC}+\frac{l}{2}} \\ \omega = \frac{v_l}{R_{ICC}-\frac{l}{2}} \end{cases} \quad (=) \quad \begin{cases} R_{ICC} = \frac{v_r}{\omega} - \frac{l}{2} \\ R_{ICC} = \frac{v_l}{\omega} + \frac{l}{2} \end{cases} \quad (=)$$

$$\frac{v_r}{\omega} - \frac{l}{2} = \frac{v_l}{\omega} + \frac{l}{2} \quad (=) \quad \frac{v_r - v_l}{w} = l \quad (=)$$

$$\omega = \frac{v_r - v_l}{l} \quad // \tag{A.1}$$

A.2 Turning Radius

$$\begin{cases} \omega = \frac{v_r}{R_{ICC}+\frac{l}{2}} \\ \omega = \frac{v_l}{R_{ICC}-\frac{l}{2}} \end{cases} \quad (=) \quad \frac{v_r}{R_{ICC}+\frac{l}{2}} = \frac{v_l}{R_{ICC}-\frac{l}{2}} \quad (=)$$

$$v_r(R_{ICC}-\tfrac{l}{2}) = v_l(R_{ICC}+\tfrac{l}{2}) \quad (=) \quad R_{ICC}(v_r-v_l) = \tfrac{l}{2}(v_r+v_l) \quad (=)$$

$$R_{ICC} = \frac{l}{2}\frac{v_r+v_l}{v_r-v_l} \quad // \tag{A.2}$$

Appendix B

Safety Program Logic in Safety Designer

The following figures were extracted from the logic configuration of the implemented safety program in the Flexi Soft system, via the Safety Designer tool.

As a note for reviewing the presented configurations, the safety control logic follows a norm of “normally closed” state for error indicators and controlling safe outputs (1 for "OK" and 0 for "Errors/Failures/Emergency"), for the event of a power or connection loss the safety system interprets the state as a failure by default [76]. This convention presents direct implications for the design of the safety program and respective logic operators.

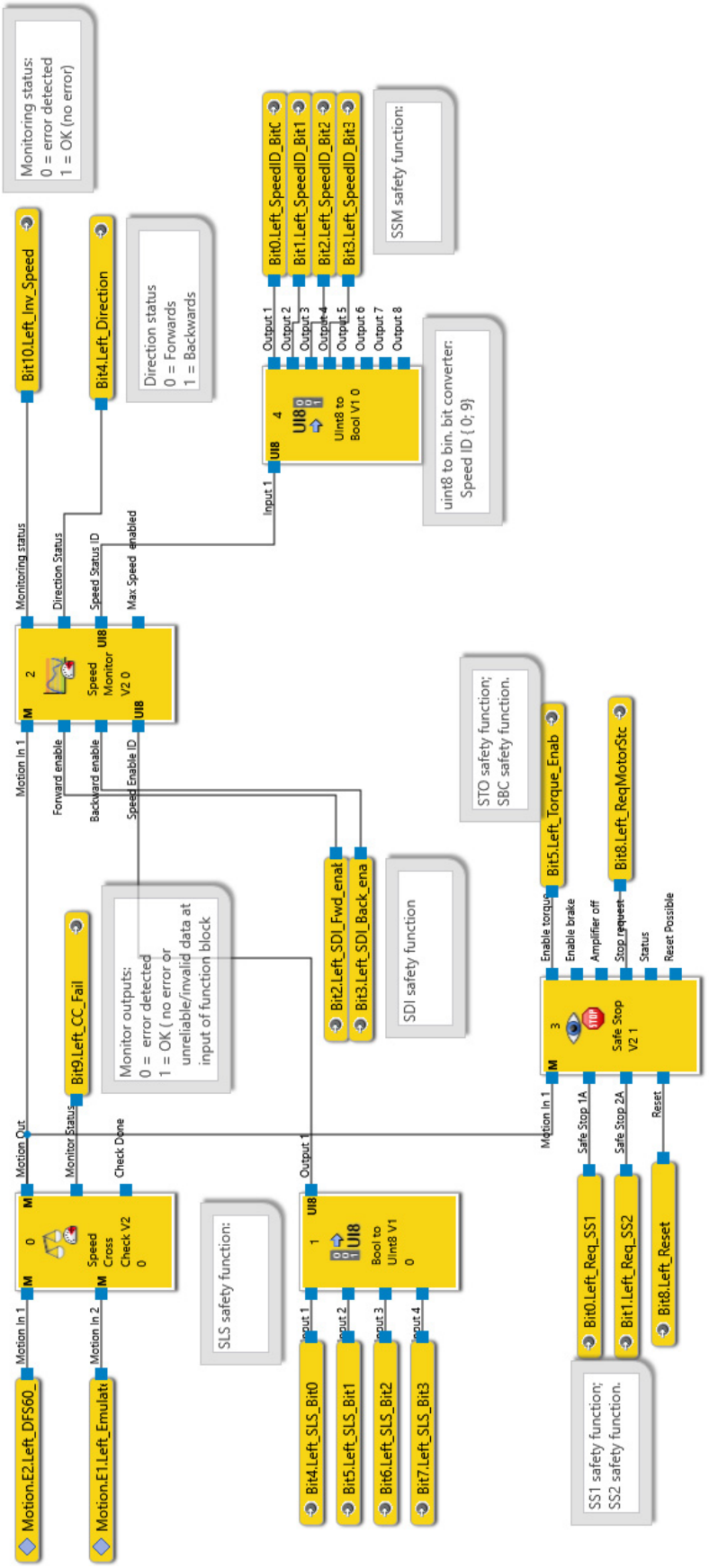

Figure B.1: Drive monitor logic (MOC1).

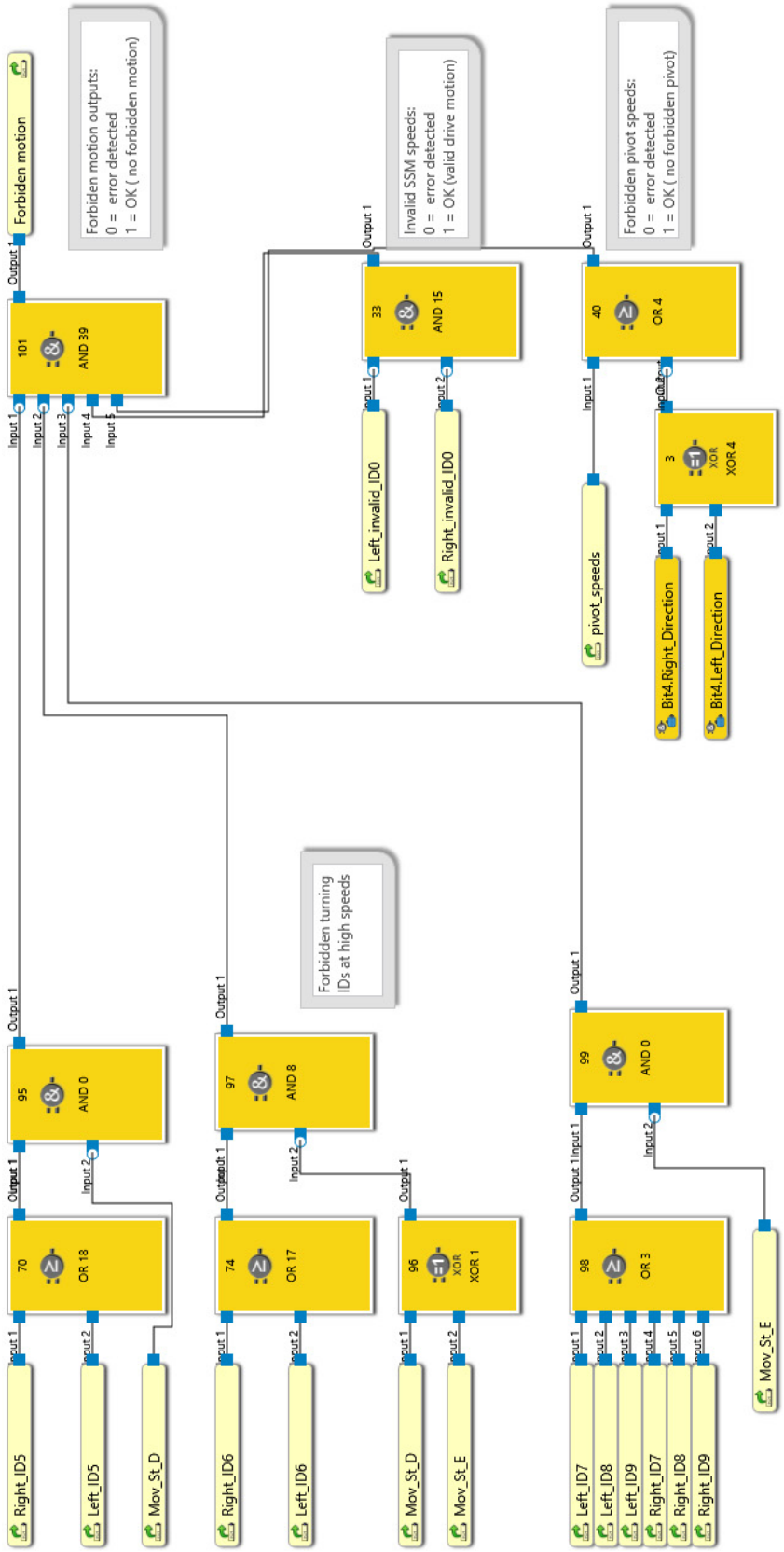

Figure B.2: Forbidden motion detection (CPU0).

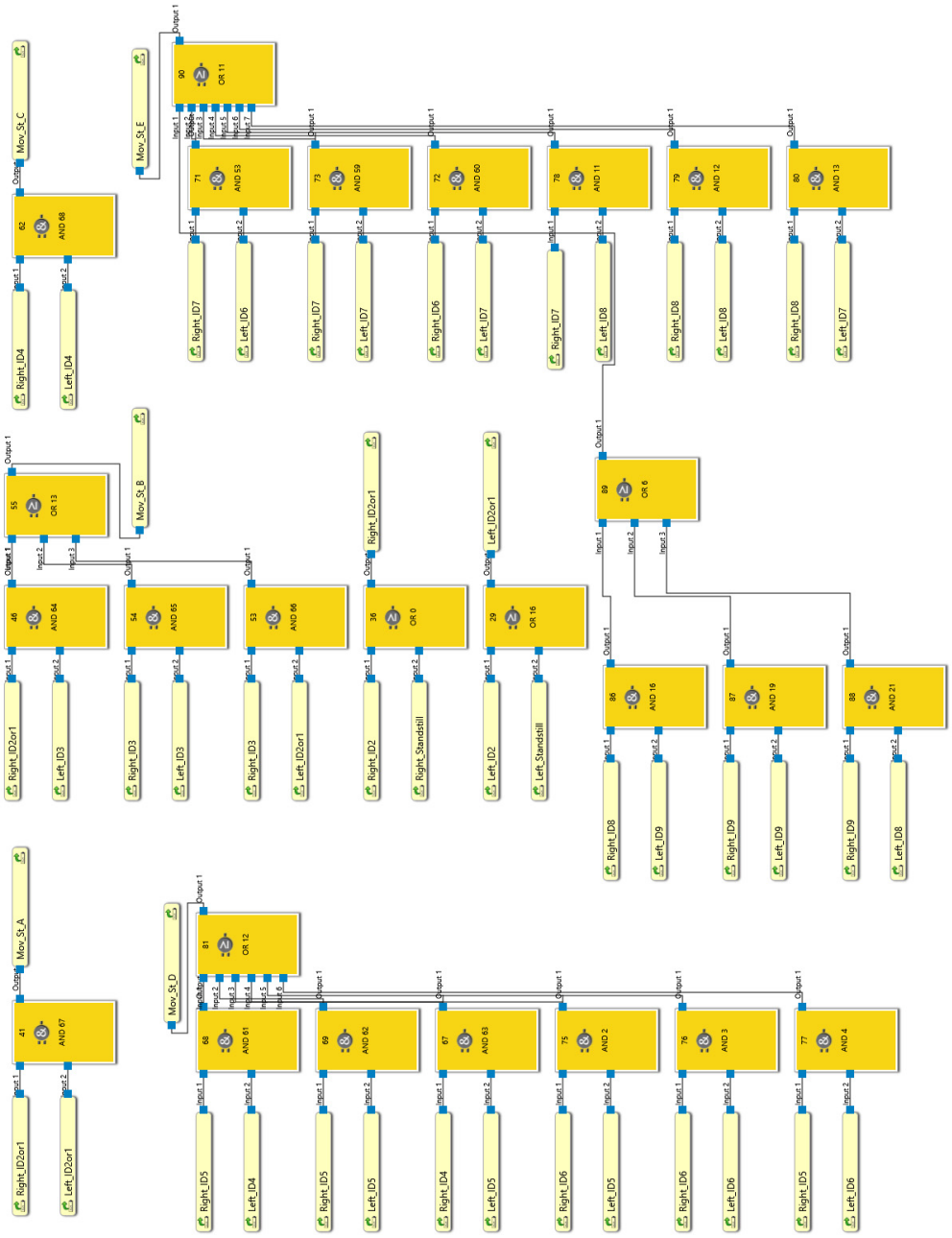

Figure B.3: Straight motion detection (CPU0).

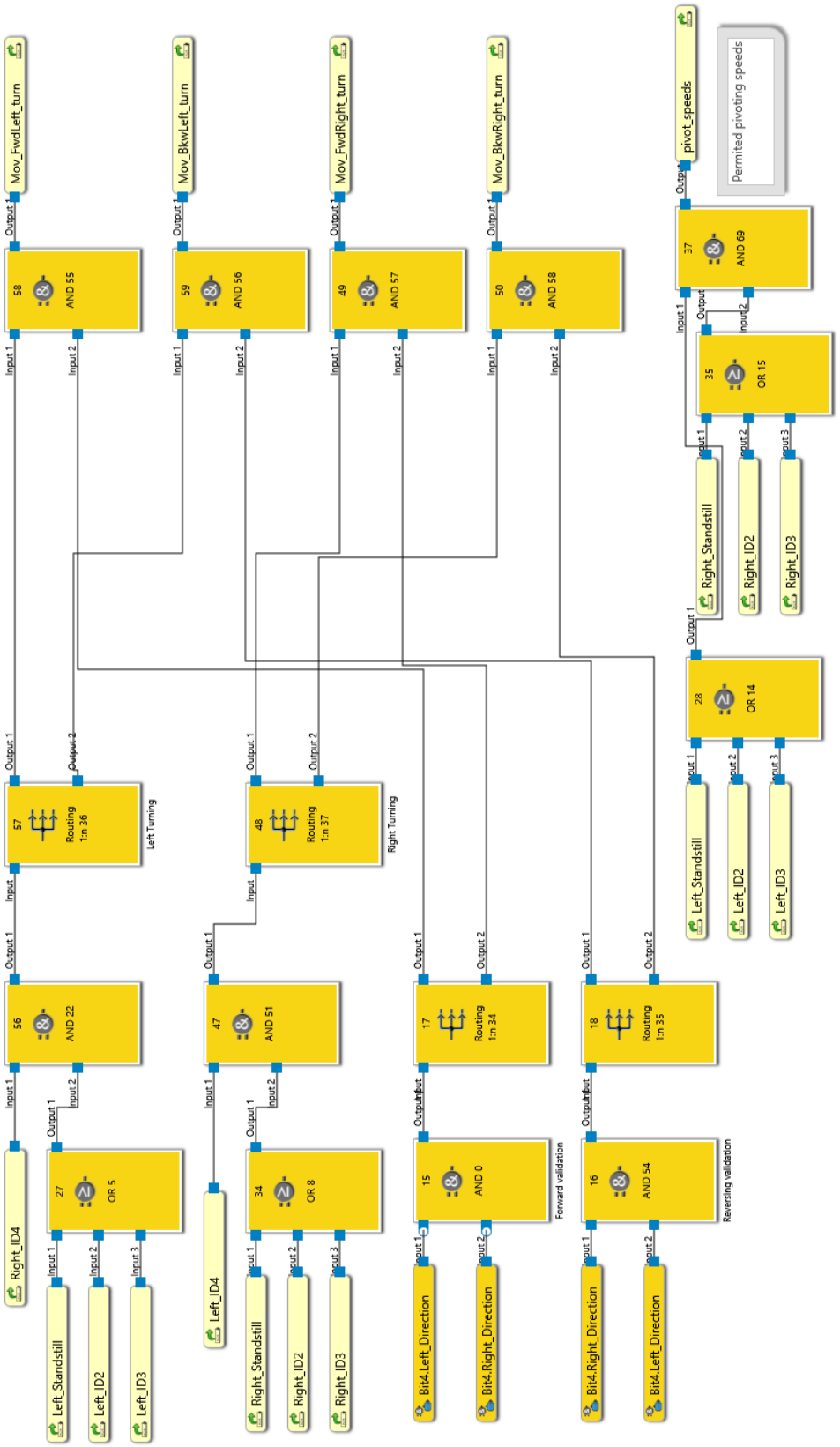

Figure B.4: Turn motion detection (CPU0).

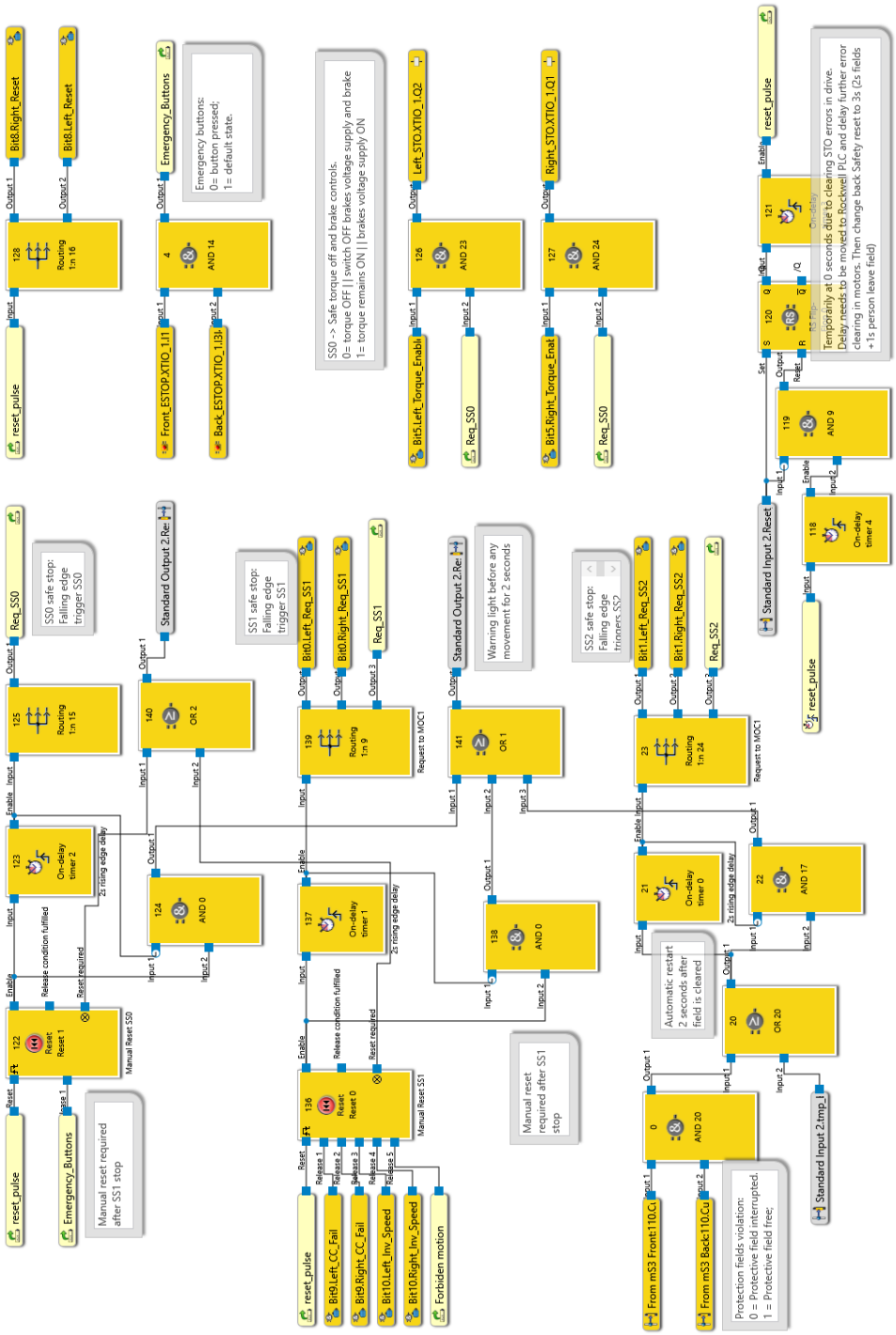

Figure B.5: Safe stops control (CPU0).

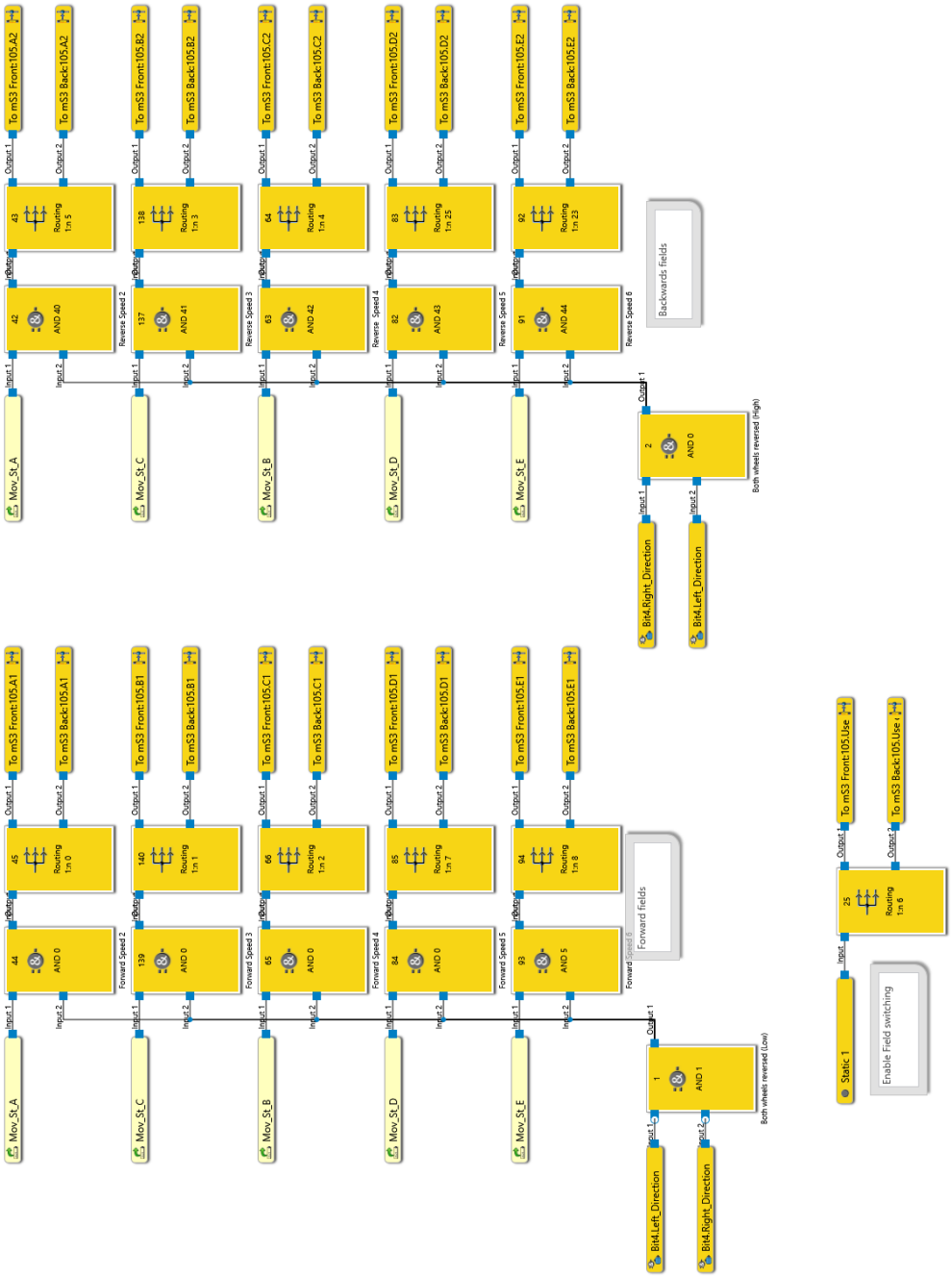

Figure B.6: Straight fields switching (CPU0).

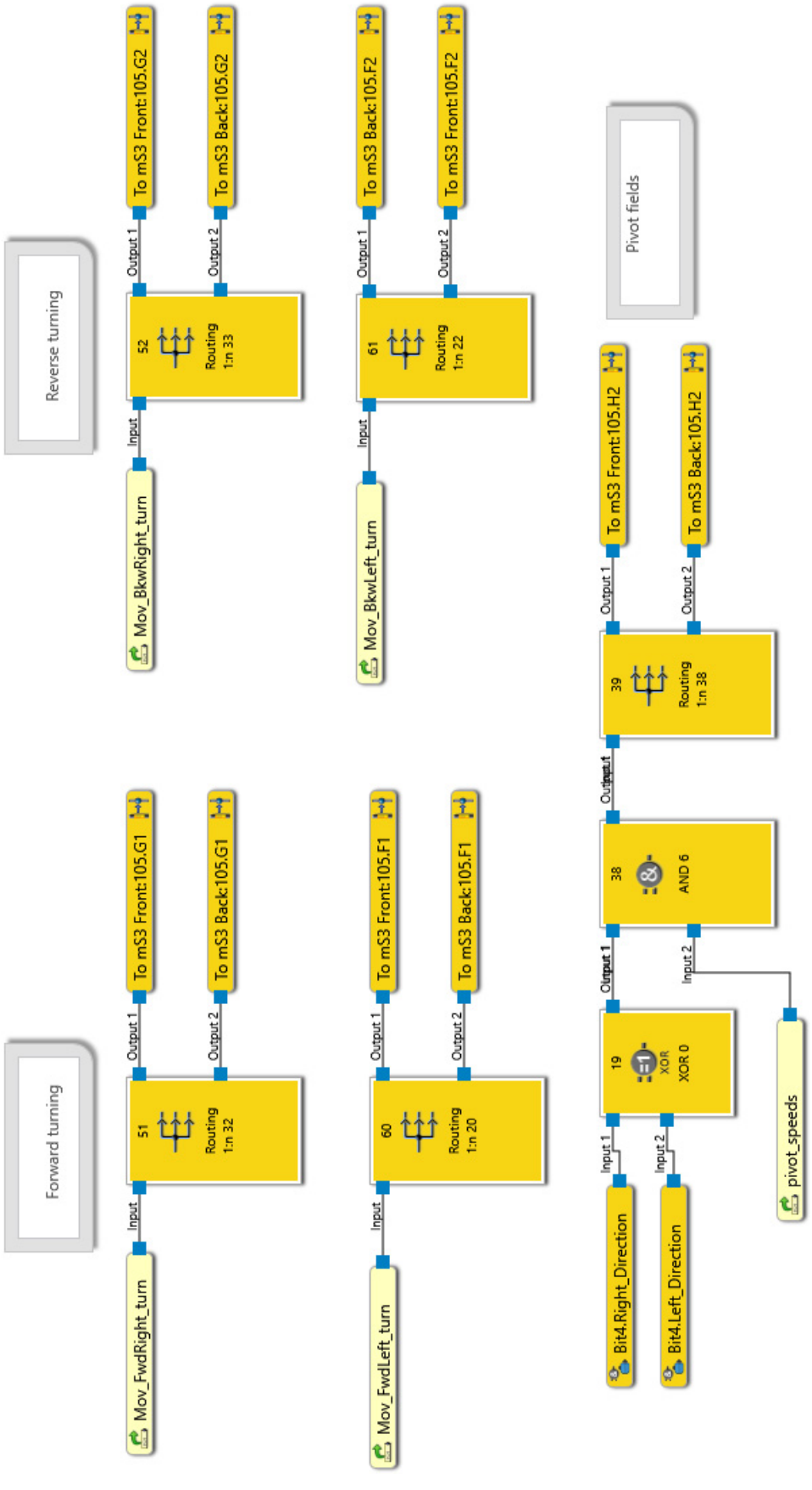

Figure B.7: Turning fields switching (CPU0).

Appendix C

Hazardous Area Simulation Code

C.1 Differential Drive Braking Kinematics

```
# -*- coding: utf-8 -*-
"""
Created on Thu May 17 13:10:52 2021
@author: pedro neto
"""

#Libraries
import numpy as np                  #Numerical calculus library
import matplotlib.pyplot as plt     #Plotting lib
#import scipy.integrate as spi      #Symbolic calculus library

import diff_ploting as k_plt        # Differential Plotting code


# ---- ---- ---- Settings AGV constants ---- ---- ---- #
#Numerical computation settings
t_res=180       #numerical calc. resolution


#AGV parameters
h=1.936         #AGV length (m)
w=1.116         #AGV width (m)
axle_l=0.903    #distance between wheels
a=-1.3          #Wheel deceleration for braking (m/s2)
#a=0            #for tracing constant differential kinematics (m/s2)
#a=-0.6         #for braking kinematics example
tr=0.337        #Reaction time (s)

#Structure corner parameters
diag=np.sqrt((w/2)**2+(h/2)**2)
th_diag=np.arctan(w/h)


def structure_reach(t, th_t, x_t, y_t, vil, vir):

    #Calculate instant angle for each corner in function fo theta
    th_a = th_t +th_diag +np.pi/2
    th_b = th_t -th_diag +np.pi/2
    th_c = th_t+np.pi -th_diag +np.pi/2
    th_d = th_t+np.pi +th_diag +np.pi/2

    #Determine
    #... in x
    ax_t= x_t+diag*np.cos(th_a)
    bx_t= x_t+diag*np.cos(th_b)
    cx_t= x_t+diag*np.cos(th_c)
    dx_t= x_t+diag*np.cos(th_d)
    #... in y
    ay_t= y_t+diag*np.sin(th_a)
    by_t= y_t+diag*np.sin(th_b)
    cy_t= y_t+diag*np.sin(th_c)
    dy_t= y_t+diag*np.sin(th_d)

```

```
54      #Global maximums and minimums reached by the structure
55      #... in x
56      x_max=np.amax([ax_t,bx_t,cx_t,dx_t])
57      x_min=np.amin([ax_t,bx_t,cx_t,dx_t])
58      #... in y
59      y_max=np.amax([ay_t,by_t,cy_t,dy_t])
60      y_min=np.amin([ay_t,by_t,cy_t,dy_t])
61
62      #Debug
63      #print(f'x_max={x_max:.3f}, x_min={x_min:.3f}, y_max={y_max:.3f}, y_min={
            y_min:.3f}')
64      #print(f'Max: ax={np.amax(ax_t):.3f},bx={np.amax(bx_t):.3f},cx={np.amax(
            cx_t):.3f},dx={np.amax(dx_t):.3f}')
65      #print(f'Min: ax={np.amin(ax_t):.3f},bx={np.amin(bx_t):.3f},cx={np.amin(
            cx_t):.3f},dx={np.amin(dx_t):.3f}')
66
67      #Plot structure reach (disable to calculate motion table)
68      k_plt.edge_kin(t,th_t, x_t,ax_t,bx_t,cx_t,dx_t, y_t,ay_t,by_t,cy_t,dy_t,
            vil,vir, a)
69
70      return x_min, x_max, y_min, y_max
71
72
73  #Midpoint Riemann sum
74  def Midpoint_Riemann_t(f, t):
75
76      #initialize variables
77      mid_f=np.linspace(0, 0, t.size)
78      mid_rie=np.linspace(0, 0, t.size)
79
80      #calculate midpoints
81      for n in range(0,t.size-1):
82          mid_f[n]=(f[n]+f[n+1])/2
83
84      #Numerical integration
85      for n in range(1,t.size):
86          mid_rie[n]=np.sum(mid_f[0:n])*t[n]/n
87
88      return mid_rie
89
90
91  #Calculate diff vehicle braking kinematics for a configuration
92  def brake_diff_kin(vi_l, vi_r):
93      #avoid indeterminate form
94      vi_l+=1E-10;vi_r+=2E-10
95
96      #deceleration to be contrary to initial speed
97      a_l=np.sign(vi_l)*a;    a_r=np.sign(vi_r)*a
98
99      #Time scale adjusted to stop time
100     if a==0: #for constant speed analysis in the unit circle
101         t_brake=2*np.pi/(np.abs(vi_l-vi_r)/axle_l); #Time to stop t=2*pi/w_0
102     else: #Time to stop t=vi/(-a) *1.01(extended)
103         t_brake=(np.max([ vi_l/(-a_l) , vi_r/(-a_r) ])+tr)*1.01
104         #initialize t variable to scale
105
106     t=np.linspace(0, t_brake, t_res)
```

```
107
108     #wheels speed
109     vl=np.piecewise(t, [t<=tr,t>tr], [vi_l, lambda t: vi_l+a_l*(t-tr)])
110     vr=np.piecewise(t, [t<=tr,t>tr], [vi_r, lambda t: vi_r+a_r*(t-tr)])
111
112     #null speed after braking (v!=vi_sig) (don't invert speed)
113     vl[np.where( np.sign(vl)!=np.sign(vi_l) )] = 0
114     vr[np.where( np.sign(vr)!=np.sign(vi_r) )] = 0
115
116     #R_icc - Radius of differential drive
117     Ricc_t=(axle_l/2)*(vr+vl)/(vl-vr)
118     Ricc_t=np.nan_to_num(Ricc_t) #'nan' to 0 for null speeds
119
120     #W_i - Angular speed of differential drive
121     w_t=(vr-vl)/axle_l #Reference of direction as anti-clock wise (v2>v1)
122
123     #Integrate theta_t
124     theta_t=Midpoint_Riemann_t(w_t,t)
125
126     #Instantaneous linear and vectorial velocity of the AGV centre
127     #V_t=w_t*Ricc_t #resulting signal is necessary
128     V_t=(vl+vr)/2
129     Vx_t=V_t*np.cos(theta_t+np.pi/2)
130     Vy_t=V_t*np.sin(theta_t+np.pi/2)
131
132     # ---- Calculate displacement in X axis ---- #
133     x_t=Midpoint_Riemann_t(Vx_t,t) #integrate vx to determine delta_x_t
134
135     # ---- Calculate displacement in Y axis ---- #
136     y_t=Midpoint_Riemann_t(Vy_t,t) #integrate vy to determine delta_y_t
137
138     #Plots (disable to calculate config table)
139     k_plt.diff_kin(t, theta_t, Ricc_t, vi_l,vi_r, vl,vr, w_t, V_t,Vx_t,Vy_t,
            x_t,y_t, a)
140
141     x_min, x_max, y_min, y_max = structure_reach(t,theta_t, x_t,y_t, vi_l,vi_r)
142
143     #Retrieve final theta at last position (stop orientation):
144     delta_theta=theta_t[-1]
145
146     return delta_theta, x_min, x_max, y_min, y_max
```

C.2 Protection Field Areas for Motion Categories

```
# -*- coding: utf-8 -*-
"""
Created on Thu Jul 15 15:31:08 2021
@author: pedro neto
"""

#Libraries
import numpy as np                 #Numerical calculus library
import matplotlib.pyplot as plt    #Plotting lib

#Differential AGV libraries
import braking_kinematics as agv_kin  #Modelled AGV braking kinematics
import diff_ploting as k_plt          #Differential Plotting code

# ---- ---- ---- Settings constants ---- ---- ---- #
#Numerical computation settings
v_res=121    #Possible configurations resolution (1,2/0,01 +1=120 +1)


def calc_in_range(v1_start, v1_end, v2_start, v2_end):

    #wheels configuration speed
    vl_i = np.linspace(v1_start, v1_end, v_res)
    vr_i = np.linspace(v2_start, v2_end, v_res)

    #initialize variables with 2D dimensions
    theta=np.zeros((v_res,v_res))
    X_min=np.zeros((v_res,v_res))
    X_max=np.zeros((v_res,v_res))
    Y_min=np.zeros((v_res,v_res))
    Y_max=np.zeros((v_res,v_res))

    #Calculate all maximum values in v_i range
    for i in range(0,v_res):
        for n in range(0,v_res):
            theta[i,n],X_min[i,n],X_max[i,n],Y_min[i,n],Y_max[i,n]= agv_kin.
                break_diff_kin(vl_i[i],vr_i[n])

    return theta, X_min, X_max, Y_min, Y_max, vl_i, vr_i


# ---------- ---------- Table for profiles max delta_x ---------- ---------- #
def generate_conf_table():

    #Configure speed profiles
    #ID range max     ID1   ID2   ID3   ID4  ID5   ID6  ID7   ID8  ID9
    s_id= np.array( [ 0.00, 0.2, 0.3, 0.6, 0.75, 0.9, 1.00, 1.1, 1.20] )

    #perform calculations in diff_conf
    d_theta, d_xmin, d_xmax, d_ymin, d_ymax, vl, vr = calc_in_range(
        s_id[0],s_id[-1],s_id[0],s_id[-1])

    #Plot 3D of global maximums for different initial speeds
```

```
53      k_plt.diff_3d(d_theta, d_xmax, d_xmin, d_ymax, d_ymin ,vl ,vr)
54
55      #Generate Table
56      print(f' Right turning analysis:\n {"-"*42}')
57      #print(f' v2  v1  |d_theta | max_x | Max_x (v1,v2) | {" "*7} vi1 ---- vi2')
58      print(' vl  vr  |  MIN_x | MAX_x |  MIN_y  | MAX_y  | Point Max_X | Point
            Max_Y |theta ')
59      for i in range(0,s_id.size-1): #Right turning possibility analysis (v2<=v1)
60          for n in range(i,s_id.size-1):
61
62              if n>4-2 and (n-i)>1: #filter high speed turning
63                  #print(f'skipped ID{n+2} ID{i+2}')
64                  break
65
66              else:
67                  #Find index of nearest velocity values in v range (start to end)
68                  vl_s_idx=(np.abs(vl - s_id[n])).argmin()
69                  vl_e_idx=(np.abs(vl - s_id[n+1])).argmin()
70                  vr_s_idx=(np.abs(vr - s_id[i])).argmin()
71                  vr_e_idx=(np.abs(vr - s_id[i+1])).argmin()
72
73                  #Find maximum values for speed configuration ranges
74                  MAX_th=np.amax(np.abs(d_theta[vl_s_idx:vl_e_idx+1,vr_s_idx:
                        vr_e_idx+1]))
75                  MIN_x=np.amin((d_xmin[vl_s_idx:vl_e_idx+1,vr_s_idx:vr_e_idx+1]))
76                  MAX_x=np.amax((d_xmax[vl_s_idx:vl_e_idx+1,vr_s_idx:vr_e_idx+1]))
77                  MIN_y=np.amin((d_ymin[vl_s_idx:vl_e_idx+1,vr_s_idx:vr_e_idx+1]))
78                  MAX_y=np.amax((d_ymax[vl_s_idx:vl_e_idx+1,vr_s_idx:vr_e_idx+1]))
79
80                  #Retrieve speed configuration for min_x
81                  #min_x_coord = np.where(d_xmin == MIN_x)
82                  #min_x_vl = vl[min_x_coord[0]].item()
83                  #min_x_vr = vr[min_x_coord[1]].item()
84                  #Retrieve speed configuration for max_x
85                  max_x_coord=np.where(d_xmax == MAX_x)
86                  max_x_vl = vl[max_x_coord[0]].item()
87                  max_x_vr = vr[max_x_coord[1]].item()
88
89                  #Retrieve speed configuration for min_y
90                  #min_y_coord=np.where(d_ymin == MIN_y)
91                  #min_y_vl = vl[min_y_coord[0]].item()
92                  #min_y_vr = vr[min_y_coord[1]].item()
93                  #Retrieve speed configuration for max_y
94                  max_y_coord=np.where(d_ymax == MAX_y)
95                  max_y_vl = vl[max_y_coord[0]].item()
96                  max_y_vr = vr[max_y_coord[1]].item()
97
98                  #print table line values
99                  print(f' ID{n+2} ID{i+2} ',end='')
100                 print(f'| {MIN_x: .4f}',end='')
101                 print(f'|{MAX_x: .4f}',end='')
102                 print(f'| {MIN_y: .4f} ',end='')
103                 print(f'| {MAX_y: .4f}|',end='')
104                 print(f'  {max_x_vl:.2f};{max_x_vr:.2f}  |',end='')
105                 print(f'  {max_y_vl:.2f};{max_y_vr:.2f}',end='')
106                 print(f'  |{MAX_th: .2f} \n',end='')
107     return
```

```
108
109
110 #Pivot mode analysis
111 def calc_pivot():
112
113     # Velocity range to pivot right (start to end)
114     vl_s=-0.2;      vl_e=0.2
115     vr_s=-0.2;      vr_e=0.2
116
117     # Calculate x shift from pivot motion
118     #theta,  xmin, xmax, ymin, ymax, vl, vr= calc_in_range(vl_s,vl_e,vr_s,vr_e)
119     d_theta, d_xmin, d_xmax, d_ymin, d_ymax, vl, vr = calc_in_range(vl_s,vl_e,
            vr_s,vr_e)
120
121     min_theta=np.amin(d_theta) #only for theta<0
122     MIN_x=np.amin(d_xmin)
123     MAX_x=np.amax(d_xmax)
124     MIN_y=np.amin(d_ymin)
125     MAX_y=np.amax(d_ymax)
126
127     #Plot 3D of absolute extrema
128     #k_plt.diff_3d(d_theta, d_xmax, d_xmin, d_ymax, d_ymin ,vl ,vr)
129
130     #Retrieve speed configuration for max_x
131     max_x_coord=np.where(d_xmax == MAX_x)
132     max_x_vl = vl[max_x_coord[0]].item()
133     max_x_vr = vr[max_x_coord[1]].item()
134
135     #Retrieve speed configuration for max_y
136     max_y_coord=np.where(d_ymax == MAX_y)
137     max_y_vl = vl[max_y_coord[0]].item()
138     max_y_vr = vr[max_y_coord[1]].item()
139
140
141     print( "\nPivot analysis:\n|  theta  |  MIN_x  |  MAX_x  |  MIN_y  |  MAX_y
            |  Point Max_X  |  Point Max_Y ")
142     print(f'| {min_theta: .4f} | {MIN_x: .4f} | {MAX_x: .4f} | {MIN_y: .4f} | {
            MAX_y: .4f} | ({max_x_vl: .2f};{max_x_vr: .2f}) | ({max_y_vl: .2f};{
            max_y_vr: .2f})')
143     return
144
145
146 generate_conf_table()
147 calc_pivot()
```

C.3 Plotting AGV Pose and Structure Reach

```
# -*- coding: utf-8 -*-
"""
Created on Thu Jul 15 15:27:10 2021
@author: pedro neto
"""

#Libraries
import numpy as np                  #Numerical calculus library
import matplotlib.pyplot as plt     #Plotting lib

#plot sizes and padding configuration
plt.rcParams.update({
    "axes.labelsize":   20,
    "xtick.labelsize":  18,
    "ytick.labelsize":  18,
    "lines.linewidth":  2.2,
    "font.size":16,
})

#AGV parameters
h=1.936         #AGV height (m)
w=1.116         #AGV width (m)

# ---------- ---------- 2D Plots ---------- ---------- #
def diff_kin(t, theta_t, Ricc, vil, vir, vl, vr, w_t, V_t, Vx_t, Vy_t,
             delta_x_t, delta_y_t,a):

    #Plot velocities
    fig = plt.figure(2)
    if a==0: #Theta based
        #plt.plot(theta_t, w_t, '-', label=r'$w$')
        plt.plot(theta_t, V_t, '-', label='$V$')
        plt.plot(theta_t, Vx_t, '-', label='$V_x$')
        plt.plot(theta_t, Vy_t, '-', label='$V_y$')
        plt.plot(theta_t, delta_x_t, '-', label='$\Delta x$')
        plt.plot(theta_t, delta_y_t, '-', label='$\Delta y$')
        plt.yticks([0, V_t[0], -V_t[0], Ricc[0], -Ricc[0], 2*Ricc[0]],
                   [0,'$V$','$-V$','$R_{icc}$','$-R_{icc}$','$2 R_{icc}$'])
        theta_range_method(vil,vir)
        plt.legend()

    else: #Time based
        #plt.plot(t, w_t, '-', label=r'$w(t)$')
        plt.plot(t, V_t, '-', label='$V(t)$')
        plt.plot(t, vl, '-', label='$v_l(t)$')
        plt.plot(t, vr, '-', label='$v_r(t)$')
        plt.plot(t, Vx_t, '-', label='$V_x(t)$')
        plt.plot(t, Vy_t, '-', label='$V_y(t)$')
        plt.plot(t, delta_x_t, '-', label='$\Delta x(t)$')
        plt.xlabel("$t(s)$");        plt.legend()

    plt.show()
    return
```

```
53 def edge_kin(t,theta_t, x_t,ax,bx,cx,dx, y_t,ay,by,cy,dy, vil,vir, a):
54
55     if a==0: #Theta based
56         #Plot reach x(theta)
57         fig = plt.figure(4)
58         plt.plot(theta_t, ax, '—', label=r'$a_x(\Delta\theta)$')
59         plt.plot(theta_t, bx, '—', label=r'$b_x(\Delta\theta)$')
60         plt.plot(theta_t, cx, '—', label=r'$c_x(\Delta\theta)$')
61         plt.plot(theta_t, dx, '—', label=r'$d_x(\Delta\theta)$')
62         #plt.plot(theta_t, x_t, '—', label=r'$debug\Delta X(\Delta\theta)$')
63         theta_range_method(vil,vir)
64         plt.yticks([0, np.amax([ax, bx, cx, dx]), np.amin([ax, bx, cx, dx])],
65                    [0, "Max x" , 'Min x'])
66         plt.legend()
67
68         #Plot reach y(theta)
69         fig = plt.figure(5)
70         plt.plot(theta_t, ay, '—', label=r'$a_y(\Delta\theta)$')
71         plt.plot(theta_t, by, '—', label=r'$b_y(\Delta\theta)$')
72         plt.plot(theta_t, cy, '—', label=r'$c_y(\Delta\theta)$')
73         plt.plot(theta_t, dy, '—', label=r'$d_y(\Delta\theta)$')
74         #plt.plot(theta_t, y_t, '—', label=r'$debug\Delta Y(\Delta\theta)$')
75         theta_range_method(vil,vir)
76         plt.yticks([0, np.amax([ay, by, cy, dy]), np.amin([ay, by, cy, dy])],
77                    [0, "Max y" , 'Min y'])
78         plt.legend()
79
80     else: #Time based
81         #Plot reach x(t)
82         fig = plt.figure(4)
83         #plt.plot(t, x, '—', label=r'$x(t)$')
84         plt.plot(t, ax, '—', label=r'$a_x(t)$')
85         plt.plot(t, bx, '—', label=r'$b_x(t)$')
86         plt.plot(t, cx, '—', label=r'$c_x(t)$')
87         plt.plot(t, dx, '—', label=r'$d_x(t)$')
88         #plt.plot(theta_t, x_t, '—', label=r'$debug\Delta X(\Delta\theta)$')
89         plt.yticks([0, np.amax([ax, bx, cx, dx]), np.amin([ax, bx, cx, dx])],
90                    [0, "Max x" , 'Min x'])
91         plt.xlabel("$t(s)$")
92         plt.legend()
93
94         #Plot reach y(t)
95         fig = plt.figure(5)
96         plt.plot(t, ay, '—', label=r'$a_y(t)$')
97         plt.plot(t, by, '—', label=r'$b_y(t)$')
98         plt.plot(t, cy, '—', label=r'$c_y(t)$')
99         plt.plot(t, dy, '—', label=r'$d_y(t)$')
100        #plt.plot(theta_t, y_t, '—', label=r'$debug\Delta Y(\Delta\theta)$')
101        plt.yticks([0, np.amax([ay, by, cy, dy]), np.amin([ay, by, cy, dy])],
102                   [0, "Max y" , 'Min y'])
103        plt.xlabel("$t(s)$")
104        plt.legend()
105
106    plt.show()
107    return
108
109
```

```
110 def theta_range_method(vi1,vi2):
111     if(vi1 < vi2):
112         #plt.xlim(0,2*np.pi)
113         plt.xticks( [ 0, np.pi/2, np.pi, 3*np.pi/2, 2*np.pi] ,
114                [0, "$\pi/2$", '$\pi$', r'$3\frac{\pi}{2}$','$2\pi$'] )
115     else:
116         plt.xlim(0, -2*np.pi) #invert axis
117         plt.xticks( [ 0, -np.pi/2, -np.pi, -3*np.pi/2, -2*np.pi] ,
118                [0, "$-\pi/2$", '$-\pi$', r'$-3\pi/2$','$-2\pi$'] )
119     plt.xlabel(r'$\Delta \theta$')
120     return
121
122
123 # ---------- ---------- 3D Plots ---------- ---------- #
124 def diff_3d(theta_3d, d_xmax_3d, d_xmin_3d, d_ymax_3d, d_ymin_3d, vl_1d,vr_1d):
125
126     vl, vr = np.meshgrid(vl_1d, vr_1d)    #Convert wheels speed to 2D data
127
128     # ----- ----- Plot theta ----- -----#
129     fig2 = plt.figure(6)
130     theta_plt = fig2.add_subplot(projection='3d')
131     theta_plt.plot_surface(vr, vl, theta_3d, cmap='viridis')
132     theta_plt.set_xlabel(r' $vl \:(ms^{-2})$', fontsize=10,labelpad=8)
133     theta_plt.set_ylabel(r' $vr \:(ms^{-2})$', fontsize=10,labelpad=8)
134     theta_plt.set_zlabel(r' $\Delta \theta\:(rad)$', fontsize=12,labelpad=8)
135     theta_plt.invert_xaxis()
136     theta_plt.set_zticks([-np.pi/4, -np.pi/2, -3*np.pi/4, -np.pi ,0
137                           , np.pi/4, np.pi/2, 3*np.pi/4, np.pi])
138     theta_plt.set_zticklabels(["", "$-\pi/2$","", '$-\pi$'
139                           , "0", "", "$\pi/2$","", '$\pi$'])
140
141     print('\nPloting global maximums and minimums for all wheel speeds:')
142
143     # ----- ----- Plot MAX x ----- ----- #
144     fig3 = plt.figure(8)
145     d_xt_plt = fig3.add_subplot(projection='3d')
146     d_xt_plt.plot_surface(vr, vl, d_xmax_3d, cmap='Spectral_r')
147     d_xt_plt.set_xlabel(r' $vl \:(ms^{-2})$', fontsize=10,labelpad=8)
148     d_xt_plt.set_ylabel(r' $vr \:(ms^{-2})$', fontsize=10,labelpad=8)
149     d_xt_plt.set_zlabel(r'$ \Delta x_{max} (m)$', fontsize=12,labelpad=8)
150     d_xt_plt.invert_xaxis()
151
152     # ----- ----- Plot MIN x ----- ----- #
153     fig3 = plt.figure(9)
154     d_xt_plt = fig3.add_subplot(projection='3d')
155     d_xt_plt.plot_surface(vr, vl, d_xmin_3d, cmap='Spectral_r')
156     d_xt_plt.set_xlabel(r' $vl \:(ms^{-2})$', fontsize=10,labelpad=8)
157     d_xt_plt.set_ylabel(r' $vr \:(ms^{-2})$', fontsize=10,labelpad=8)
158     d_xt_plt.set_zlabel(r'$ \Delta x_{min} (m)$', fontsize=12,labelpad=8)
159     d_xt_plt.invert_xaxis()
160     d_xt_plt.invert_zaxis()
161
162     # ----- ----- Plot MAX y ----- ----- #
163     fig3 = plt.figure(10)
164     d_xt_plt = fig3.add_subplot(projection='3d')
165     d_xt_plt.plot_surface(vr, vl, d_ymax_3d, cmap='Spectral_r')
166     d_xt_plt.set_xlabel(r' $vl \:(ms^{-2})$', fontsize=10,labelpad=8)
```

```
167     d_xt_plt.set_ylabel(r' $vr \:(ms^{-2})$', fontsize=10,labelpad=8)
168     d_xt_plt.set_zlabel(r'$ \Delta Y_{max} (m)$', fontsize=12,labelpad=8)
169     d_xt_plt.invert_xaxis()
170 
171     # ----- ----- Plot MIN y ----- ----- #
172     fig3 = plt.figure(11)
173     d_xt_plt = fig3.add_subplot(projection='3d')
174     d_xt_plt.plot_surface(vr, vl, d_ymin_3d, vmin=-0.974, vmax=-0.96, cmap='
            Spectral_r')
175     d_xt_plt.set_xlabel(r' $vl \:(ms^{-2})$', fontsize=10,labelpad=8)
176     d_xt_plt.set_ylabel(r' $vr \:(ms^{-2})$', fontsize=10,labelpad=8)
177     d_xt_plt.set_zlabel(r'$ \Delta y_{min} (m)$', fontsize=12,labelpad=8)
178     d_xt_plt.invert_xaxis()
179     d_xt_plt.set_zticks([-1.5, -1, -0.9])# force scale to compare with Max y
180     d_xt_plt.invert_zaxis()
181 
182     plt.show()
183 
184     return
```

Appendix D

Validation of the Modelled AGV Turning Movements

Following the AGV motion referential established in Figure D.1, the four distinct turning movements defined in Subsection 5.2.1 were simulated with a constant vehicle velocity.

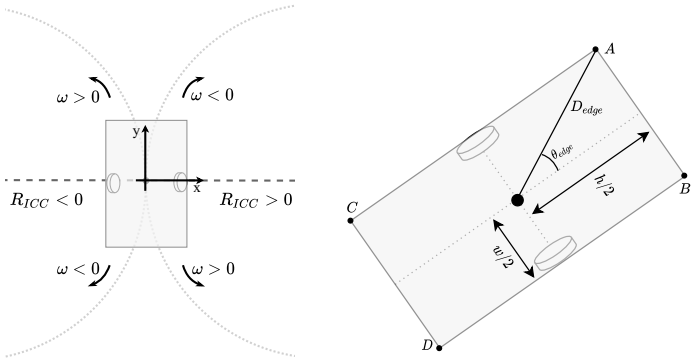

Figure D.1: Structure motion referential of the AGV.

The resulting plots are presented below and outline the vehicle pose, velocities and structure edges kinematics throughout the differential circle.

The resulting kinematic variables match the predicted outline for each respective turning movement. Therefore, the data is able to validate the kinematic model of the AGV structure.

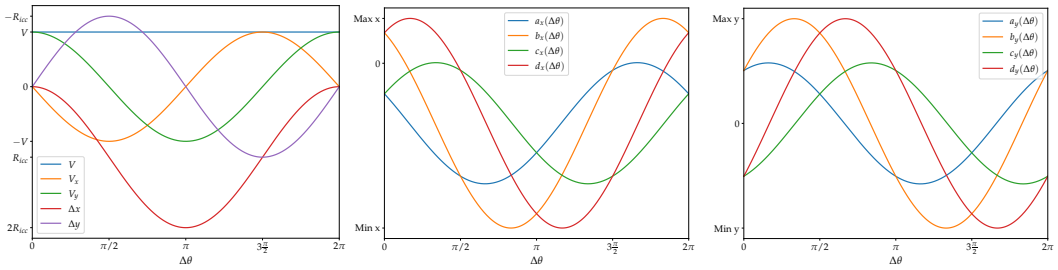

(a) Vel. and AGV pose (b) Edges displacement in x (c) Edges displacement in y

Figure D.2: Forward left ($\omega > 0$ and $R_{ICC} < 0$)

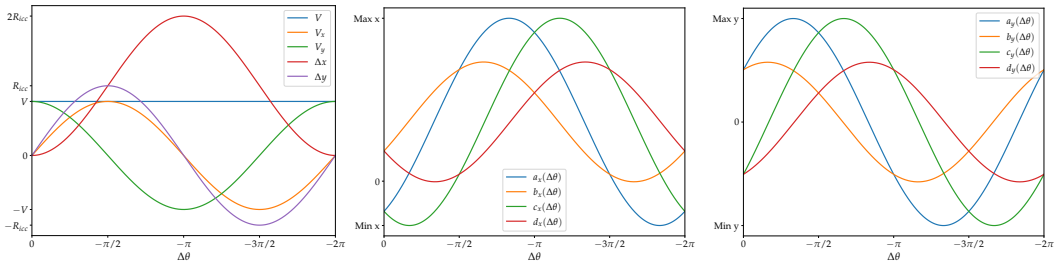

(a) Vel. and AGV pose (b) Edges displacement in x (c) Edges displacement in y

Figure D.3: Forward right ($\omega < 0$ and $R_{ICC} > 0$)

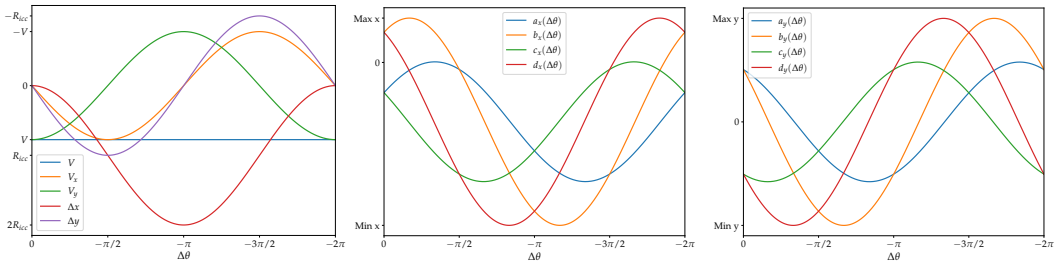

(a) Vel. and AGV pose (b) Edges displacement in x (c) Edges displacement in y

Figure D.4: Backward left ($\omega < 0$ and $R_{ICC} < 0$)

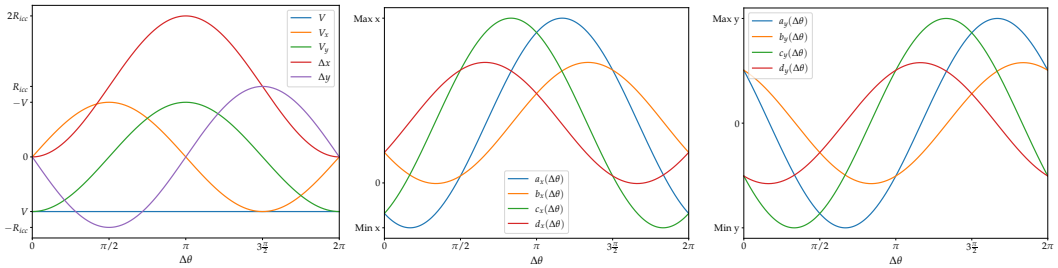

(a) Vel. and AGV pose (b) Edges displacement in x (c) Edges displacement in y

Figure D.5: Backward right ($\omega > 0$ and $R_{ICC} > 0$)